



Master Thesis

Leading Logarithmic 3-loop Corrections to $(g - 2)_\mu$ in the Two-Higgs-Doublet Model

Kilian Möhling

Born on: 3rd August 1999 in Berlin

to achieve the academic degree

Master of Science (M.Sc.)

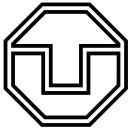
First referee

Prof. Dr. Dominik Stöckinger

Second referee

Dr. Massimo Passera

Submitted on: 4th October 2022



Abstract

The persistent deviation Δa_μ of the measured value of the anomalous magnetic moment of the muon from the prediction in the Standard Model is currently one of the most tantalizing hints at new physics. Extensions to the Standard Model are strongly constrained by this observable, which motivates more precise calculations in the new models. This thesis focuses on the Two-Higgs-Doublet Model as one of the promising possible explanations of the deviation. Here, the dominant contributions to Δa_μ arise through two-loop Barr-Zee diagrams with large Yukawa couplings to heavy fermion loops. However, these diagrams bring with them significant uncertainties from QCD corrections at higher orders. The goal of this thesis is to calculate the leading logarithmic 3-loop corrections to these Barr-Zee diagrams and in this way specify a parametrization of the two-loop result which reduces the higher order uncertainties. The corrections are obtained using the renormalization group equations of appropriate effective field theories.

Zusammenfassung

Die bestehende Abweichung Δa_μ zwischen dem Messwert des anomalen magnetischen Momentes des Myons und der Vorhersage im Standardmodell ist zurzeit einer der aussichtsreichsten Hinweise auf neue Physik. Erweiterungen des Standardmodells sind durch diese Observable stark eingeschränkt, was präzisere Rechnungen in den neuen Modellen motiviert. Die vorliegende Arbeit konzentriert sich auf das Zwei-Higgs-Dublett-Modell als eine der vielversprechendsten möglichen Erklärungen für die Abweichung. Die dominanten Beiträge zu Δa_μ entstehen hier durch Barr-Zee-Zweischleifendiagramme mit großen Yukawa Kopplungen an schwere Fermionenschleifen. Diese Diagramme führen jedoch zu signifikanten Unsicherheiten durch QCD Korrekturen in höheren Ordnungen. Das Ziel dieser Arbeit ist es, die führenden logarithmischen Dreischleifenkorrekturen zu diesen Barr-Zee-Diagrammen zu berechnen und daraus eine Parametrisierung des Zweischleifenergebnisses zu erhalten, welche die Unsicherheiten höherer Ordnung reduziert. Die Korrekturen werden mithilfe der Renormierungsgruppengleichungen von geeigneten effektiven Feldtheorien berechnet.

Contents

1	Introduction	7
2	The Magnetic Moment of the Muon	9
2.1	Relativistic Spin Motion	9
2.2	Experimental Measurement	10
2.3	The Magnetic Moment in Quantum Field Theory	12
2.3.1	Vertex Function and Form Factors	13
2.3.2	Relation to the Classical Definition	14
2.3.3	Renormalization with External Background Field	15
2.3.4	Prediction of the Standard Model	16
3	The Two-Higgs-Doublet Model	18
3.1	Definition and Parameters	18
3.2	One-loop Contribution to a_μ	21
3.3	Two-Loop Barr-Zee Diagram	22
3.3.1	Subgraph Vertex Function	22
3.3.2	Two-loop Amplitude	24
3.3.3	Parametrization Uncertainty	25
3.3.4	Asymptotic Expansion of the Loop Functions	26
4	Effective Field Theory	28
4.1	Large Mass Expansion	28
4.1.1	One-Loop Examples	30
4.1.2	Constructing the EFT	32
4.2	Renormalization	34
4.2.1	Counterterm Structure	35
4.2.2	Renormalized Lagrangian	36
4.3	Logarithms, Poles and the Renormalization Scale	37
4.3.1	Strategy I: $\mu = M$	37
4.3.2	Strategy II: $\mu = m$	39
4.4	The EFT Renormalization Group Equation	39
4.4.1	General Renormalization Group Equations	39
4.4.2	The Anomalous Dimension Matrix	41
4.4.3	Change of Operator Basis	44
5	Corrections for Heavy Fermion Loop	46
5.1	Operators and Matching Conditions	46
5.1.1	One-Loop Matching Diagrams	46
5.1.2	Two-Loop Matching Diagrams	47
5.2	Operator Mixing	53
5.3	Running Wilson Coefficients	55
6	Corrections for Light Fermion Loop	59
6.1	Operators and Matching Condition	59
6.2	Operator Mixing	60
6.3	Running Wilson Coefficients	62

7 Summary	68
A Conventions	70
B Loop Integral Techniques	71
B.1 Feynman Parametrization	71
B.2 Master Formula	71
C Operators and Feynman Rules	72
C.1 Dim-4 Operators	72
C.2 Dim-5 Operators	73
C.3 Dim-6 Operators	73
Bibliography	75

1 Introduction

Ever since its conception in the 1970s the Standard Model (SM) of particle physics has withstood experimental scrutiny incredibly well. The vast majority of collider and other high precision experiments confirm the theoretical predictions of the Standard Model with great accuracy and after the detection of the final missing particle, the Higgs boson, in 2012 the SM seems to provide us with an excellent description of the fundamental building blocks of nature.

And yet, we know that the Standard Model must be incomplete. For one it does not contain a description of the, arguably, oldest known force - gravity. But there is also good reason to believe that the SM does not yet capture the full particle content of our universe either. None of the SM particles, for example, can explain dark matter which however makes up roughly 85%, i.e. the vast majority, of the total matter density. There are also several other open questions regarding baryon asymmetry, the strong CP problem, the hierarchy problem and so on. All of these questions motivate the search for physics beyond the Standard Model on both the theory and experimental side. The progress in constructing the SM was in large parts driven by the discovery of countless numbers of new particles in collider experiments. Unfortunately, since then, and despite many upgrades, these colliders have not produced any of the new particles physicists were hoping for. Our best alternative, therefore, might be to study indirect evidence of new physics by looking for small deviations of measurements from the SM prediction.

Thankfully, we have already found several hints of such deviations, for example and perhaps most notably (certainly most relevant to this thesis) the recent confirmation by the FNAL E989 experiment at Fermilab of the Brookhaven National Laboratory (BNL) E821 measurement of the *anomalous magnetic moment* of the muon $a_\mu = (g - 2)_\mu/2$, which now deviates from the current theoretical value in the SM by 4.2σ [1–3].

$$a_\mu^{\text{Ex}} = 116\,592\,061(41) \times 10^{-11}, \quad (1.1)$$

$$a_\mu^{\text{SM}} = 116\,591\,810(43) \times 10^{-11} \quad (1.2)$$

It is, of course, very tempting to try and explain this deviation with additional contributions from new particles, which are not included in the SM calculation. As a result, many of the simple extensions of the SM have been tested for a possible explanation of the anomaly while simultaneously evading existing constraints and were subsequently excluded [4]. Some however, in particular the Two-Higgs-Doublet Model (2HDM), certain Leptoquark models and Supersymmetric extensions, remain very much viable. In this thesis we focus on the 2HDM, which has already been studied extensively even before the BNL measurement, for instance in the context of baryogenesis due to its introduction of additional sources of CP violation. A large part of its popularity also comes from supersymmetric models like the MSSM which require an extended Higgs sector. Here we are interested in its contributions to a_μ , in particular from the new pseudoscalar Higgs with a mass of around $m_A \sim 20\ldots 100$ GeV, for which the 2HDM could potentially explain the full discrepancy between the measurement and theoretical value [5].

From a technical standpoint, the new contributions to a_μ in the 2HDM are somewhat unusual, as the dominant correction first enters at the two-loop level through Barr-Zee diagrams with large Yukawa couplings to heavy fermion loops. The results of these diagrams together with the constraints on the parameter space have already been known for a while [6–10] and

more recently, similar studies for the full two-loop calculation have been presented [5, 11]. Besides the strong Yukawa couplings a second reason the Barr-Zee diagrams give such large contributions is, that the chirality flip required by a_μ now brings with it a factor of the heavy fermion mass m_f . In comparison to the one-loop results in the 2HDM, the Barr-Zee diagrams are thus additionally enhanced by a factor $m_f/m_\mu \sim 10 \dots 1000$. However, especially for quarks, the running of m_f brings with it a large uncertainty and it is not clear which renormalization scale should be chosen in order to reduce these uncertainties as much as possible.

The goal of this thesis, therefore, is to estimate the 3-loop corrections to these Barr-Zee diagrams and determine which parametrization of the known 2-loop contribution results in the smallest uncertainty. We will do so by calculating leading logarithms (LL) of large mass ratios like m_t/m_μ which make up a substantial proportion of the 3-loop result. Surprisingly, although these logarithmic terms are quite complicated to extract from the full calculation, they are resummed in a rather simple way by the renormalization group equation (RGE) of an appropriate effective field theory (EFT). Such methods were already used in the early 1990s in calculations of QCD corrections to hadronic decays [12–15] and later to compute electroweak contributions to a_μ [16, 17]. Now we will use it to calculate corrections to new physics contributions to a_μ in the 2HDM.

To start off this thesis we should clarify some of the points mentioned thus far. We begin with the anomalous magnetic moment a_μ as an observable both in the context of the experimental measurement as well as in Quantum Field Theory in chapter 2. The goal will be to understand where the two numbers (1.1) and (1.2) come from and how contributions of new physics affect these results. Afterwards, in chapter 3 we introduce the Two-Higgs-Doublet model as an extension of the Standard Model and present a calculation of the important 2-loop Barr-Zee diagram. We then move on to effective field theories in chapter 4 and explain how to construct them and how the logarithms are resummed by the renormalization group equation. After this, we apply the method to our particular question, first in the case of $m_f \gg m_A$ in chapter 5 and then for $m_f \ll m_A$ in chapter 6, where we also combine the calculations and present the full result for the 3-loop leading logarithmic corrections. Finally, in chapter 7 we give a summary and conclude the thesis.

2 The Magnetic Moment of the Muon

The muon was among the first elementary particles discovered and quite quickly proved very useful in testing new physics. For example, muons produced by cosmic radiation in the upper atmosphere gave the first direct evidence for time dilation as predicted by special relativity. Another important experiment was the observation of the pion decay chain $\pi \rightarrow \mu \rightarrow e$ by Garwin, Lederman and Weinrich [18], which together with the Wu experiment [19] provided the first evidence for the parity violation of the Weak interaction predicted by Lee and Yang [20]. In the same experiment Garwin et al. were also able to measure the muon magnetic moment for the first time. The pion decay and short lifespan of the muon still are the basis for all of the $(g - 2)_\mu$ measurements today.

In the following we want to give a precise definition of the anomalous magnetic moment of the muon, first in the context of classical electrodynamics and the Bargmann-Michel-Telegdi equation which is used to extract the value of $(g - 2)_\mu$ from the measurement and afterwards in the context of quantum field theory (QFT) and the SM where the magnetic moment is no longer a free parameter, but a prediction of the theory.

2.1 Relativistic Spin Motion

In classical electrodynamics, the magnetic moment $\boldsymbol{\mu}$ of a particle with mass m , charge q and spin angular momentum \mathbf{s} is given by

$$\boldsymbol{\mu} = g \frac{q}{2m} \mathbf{s} \quad (2.1)$$

Here, the Landé g -factor is a free parameter and has to be determined experimentally. In an external magnetic field \mathbf{B} , the magnetic moment results in a torque on the particle. The corresponding equation of motion in its rest frame is [21]

$$\left(\frac{d\mathbf{s}}{dt} \right)_{\text{rest frame}} = \boldsymbol{\mu} \times \mathbf{B}_{\text{rest frame}} \quad (2.2)$$

Since we want to describe the spin motion of particles at high energies in the laboratory frame, we need a Lorentz covariant generalization of this equation. In special relativity, spin is naturally described by the angular momentum tensor $J^{\mu\nu}$ which can be decomposed as

$$J^{\mu\nu} = x^\mu p^\nu - x^\nu p^\mu + S^{\mu\nu} \quad (2.3)$$

where p^μ is the 4-momentum. $S^{\mu\nu}$ is invariant under translation and therefore corresponds to the intrinsic angular momentum of the particle. The spin 3-vector \mathbf{s} is related to $S^{\mu\nu}$ by

$$s_i = \frac{1}{2} \epsilon_{ijk} S^{jk} \quad (2.4)$$

However, it is more convenient to work with the Pauli-Lubanski pseudovector W^μ and define a spin 4-vector S_μ as

$$S_\mu := \frac{W_\mu}{m} = \frac{1}{2} \epsilon_{\mu\nu\alpha\beta} u^\nu J^{\alpha\beta} \quad (2.5)$$

where $u^\nu = (\gamma, \gamma \mathbf{v})$ denotes the particles 4-velocity. In the rest-frame S_μ reduces to

$$S_0 = 0, \quad \mathbf{S}_i = \frac{1}{2} \epsilon_{ijk} S^{jk} = \mathbf{s}_i \quad (2.6)$$

As usual, the electric and magnetic fields are combined into the field strength tensor $F^{\mu\nu}$, such that

$$\mathbf{E}_i = F^{i0}, \quad \mathbf{B}_i = -\frac{1}{2} \epsilon_{ijk} F^{jk} \quad (2.7)$$

and the Lorentz force can be written as

$$\frac{du^\mu}{d\tau} = \frac{q}{m} F^{\mu\nu} u_\nu \quad (2.8)$$

Assuming the external force on the particle is given only by (2.8) and requiring that the equation of spin motion reduces to (2.2) in the rest frame leads to [21, 22]

$$\boxed{\frac{dS^\mu}{d\tau} = g \frac{q}{2m} F^{\mu\nu} S_\nu + (g - 2) \frac{q}{2m} F^{\alpha\beta} S_\alpha u_\beta u^\mu} \quad (2.9)$$

This is called the Bargmann-Michel-Telegdi (BMT) equation [22] and gives a relativistic, but purely classical description of the spin motion. The BMT equation can also be derived in the semi-classical limit of the Dirac equation if an effective dipole term is included [23, 24], however, it has not yet been derived directly from the coupled QED (or SM) field equations. We will show in section 2.3 how to nevertheless connect the QFT result with the classical definition of g .

2.2 Experimental Measurement

In this section we want to briefly discuss the principle of the most recent measurement at Fermilab [2] and its predecessors at Brookhaven [1] and CERN [25]. An overview of the complete history of the $(g - 2)_\mu$ experiments can be found in [26].

The main idea behind the experiment at Fermilab becomes clearest if we rewrite the BMT equation (2.9) in a slightly different form. Specifically, we can obtain an analogous equation to (2.2) in the laboratory frame by relating \mathbf{s} to the spatial component of S^μ with use of the appropriate Lorentz transformation. After some algebraic manipulation one finds [27, 28]

$$\frac{d\mathbf{s}}{dt} = \boldsymbol{\omega}_s \times \mathbf{s} \quad (2.10)$$

This equation describes a rotation of the spin with frequency $|\boldsymbol{\omega}_s|$. Explicitly,

$$\boldsymbol{\omega}_s = -\frac{q}{m} \left[\left(\frac{g-2}{2} + \frac{1}{\gamma} \right) \mathbf{B} - \frac{g-2}{2} \frac{\gamma}{\gamma+1} (\mathbf{v} \cdot \mathbf{B}) \mathbf{v} - \left(\frac{g}{2} - \frac{\gamma}{\gamma+1} \right) \mathbf{v} \times \mathbf{E} \right] \quad (2.11)$$

where \mathbf{B} , \mathbf{E} and \mathbf{v} (and t) are now measured in the laboratory frame and γ denotes the Lorentz factor. On the other hand, from (2.8) we have

$$\frac{d\mathbf{v}}{dt} = \boldsymbol{\omega}_c \times \mathbf{v} + \frac{q}{\gamma m} \frac{1}{\gamma^2 - 1} (\mathbf{v} \cdot \mathbf{E}) \mathbf{v} \quad (2.12)$$

with the cyclotron frequency

$$\boldsymbol{\omega}_c = -\frac{q}{m} \left[\frac{1}{\gamma} \mathbf{B} - \frac{\gamma}{\gamma^2 - 1} \mathbf{v} \times \mathbf{E} \right] \quad (2.13)$$

Ideally, no electric fields are present and the magnetic field is uniform and transversal $\mathbf{v} \cdot \mathbf{B} = 0$. Then, (2.13) reduces to $\omega_c = -\frac{q}{\gamma m} \mathbf{B}$ and the muon rotates in a circle with radius $r = \frac{|\mathbf{v}|}{|\omega_c|}$ and constant $|\mathbf{v}|$. According to (2.10) the spin also rotates, however with a slightly different frequency such that

$$\omega_a = \omega_s - \omega_c = -a_\mu \frac{q}{m} \mathbf{B} \quad (2.14)$$

If we measure this relative precession frequency by tracking the spin polarization along the circular trajectory, we can directly obtain the value of the anomalous magnetic moment $a_\mu = (g - 2)/2$ of the muon.

The experimental realization (illustrated in Fig.2.1) is, however, much more involved. First, pions are produced by an accelerator which then decay into the beam of polarized muons. The beam has to be injected into the storage ring and placed onto a central orbit by fast pulsed dipole magnets (kicker magnets). In order to maintain the beam inside the storage ring, additional vertical focusing is required. This is provided by electrostatic quadrupoles positioned along the circumference of the ring. These additional electric fields as well as corrections from the complicated beam dynamics [29] have to be taken into account when calculating the anomalous spin precession frequency, such that

$$\omega_a = -\frac{q}{m} \left[a_\mu \mathbf{B} - a_\mu \frac{\gamma}{\gamma + 1} (\mathbf{v} \cdot \mathbf{B}) \mathbf{v} - \left(a_\mu - \frac{1}{\gamma^2 - 1} \right) \mathbf{v} \times \mathbf{E} \right] \quad (2.15)$$

In order to suppress the additional contribution from the electric quadrupole field as much as possible, the muons are produced and stored with momentum $|\mathbf{p}| = 3.094 \text{ GeV}$. This gives $\gamma \sim 29.3$ and the terms in the round brackets approximately cancel.

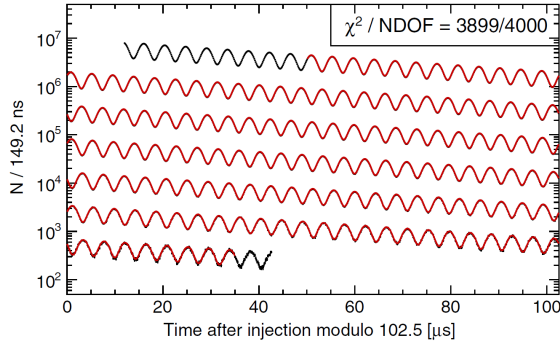


Figure 2.2: Time distribution of positron counts around the storage ring from the FNAL E989 Run-1d data. Taken from [30]

track the polarization of the muon. In the Fermilab experiment this is done by a total of 24 calorimeters spread evenly around the storage ring which detect and count the emitted positrons. The number of measured positrons with energy above a given threshold E_{th} varies with time as [30]

$$N(t) = N_0 e^{-t/\gamma\tau_\mu} [1 + A(E_{th}) \cos(|\omega_a|t + \phi_0)] \quad (2.16)$$

where N_0 is the initial beam density, $A(E_{th})$ is an energy dependent asymmetry factor and ϕ_0 denotes the average initial angle of the muon spins relative to the beam direction. The

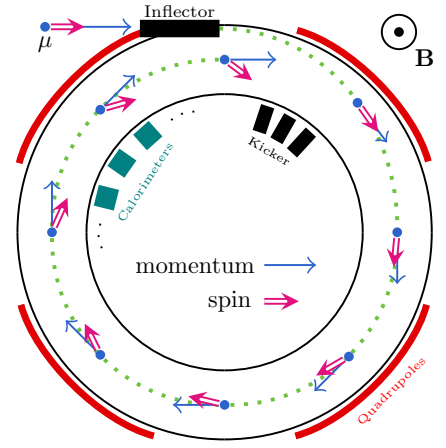


Figure 2.1: Schematic of the spin precession in a storage ring.

Since the magnitude of the magnetic field is chosen to be $|\mathbf{B}| \approx 1.45 \text{ T}$, the muons travel in a circle with a mean radius $r = 7.112 \text{ m}$ and with the cyclotron frequency $|\omega_c|/(2\pi) = 6.7 \text{ MHz}$. The average lifetime of the muons is dilated to $\gamma\tau_\mu \approx 64 \mu\text{s}$ allowing them to circle the ring many times before decaying into a positron and two neutrinos $\mu^+ \rightarrow e^+ + \nu_e + \bar{\nu}_\mu$. Like the pion decay, the decay of the muon is maximally parity violating and the direction of emission of the positron is strongly correlated with the spin direction of the muon. Measuring these positrons therefore allows us to

value of the observed precession frequency can thus be extracted from fits (see Fig.2.2) to the calorimeter data [30] and after including the corrections from above and together with a precise measurement of the magnetic field [31], the value of a_μ can be determined. The complete details of the experimental setup can be found in the technical design report of the experiment at Fermilab [32]. Combined with the BNL E821 measurement [1], the current experimental average for the anomalous magnetic moment of the muon a_μ is [2]

$$\boxed{a_\mu^{\text{Ex}} = 116\,592\,061(41) \times 10^{-11}} \quad (2.17)$$

In the near future this result will be further improved by better statistics from Run-2 through Run-6 data as well as reduced systematic uncertainties [33]. Lastly, we should mention that a new Muon $g - 2$ experiment at J-PARC is in construction [34, 35], which will serve as an independent confirmation of the current measured value. The goal is to eliminate the need for electric beam focusing by using ultra cold muons with very low transverse momentum. This allows for measurement of both a_μ as well as, if present, the muon electric dipole moment (EDM) d_μ and provides a test for possible unaccounted systematic effects.

2.3 The Magnetic Moment in Quantum Field Theory

Classical electrodynamics, while applicable in the context of macroscopic processes like the beam polarization in the experiment, breaks down in the description of individual elementary particles and fundamental interactions. Instead, it has to be replaced by the much more general framework of quantum field theory. In this section we want to discuss in detail how the magnetic moment is defined in QFT and how this definition relates to the classical results from section 2.1 as well as give an overview of the current calculation of the SM prediction.

In QFT the basic interaction between leptons and the photon field is determined by the following term in the Lagrangian density

$$-eQ\bar{\psi}(x)\gamma^\mu\psi(x)A_\mu(x) \subset \mathcal{L}(x) \quad (2.18)$$

where ψ is the lepton field, A_μ is the photon field, Q is the charge of the lepton and e is the electromagnetic coupling strength. In order to include the external background field, we should expand the photon field around the classical gauge potential A_μ^{cl}

$$A_\mu(x) \rightarrow A_\mu^{\text{cl}}(x) + A_\mu(x) \quad (2.19)$$

As a consequence, we obtain a new interaction vertex with the following Feynman rule¹

$$\text{---}\overrightarrow{p}\text{---}\otimes\text{---}\overrightarrow{p'}\text{---} = -ieQ\gamma^\mu\tilde{A}_\mu^{\text{cl}}(q) \quad (2.20)$$

where $\tilde{A}_\mu^{\text{cl}}$ denotes the Fourier transform of the gauge potential and $q = p' - p$. To extract the classical definition of the magnetic moment from this description, we first calculate the amplitude of a muon scattering in the external background field

$${}_{out}\langle p', r | p, s \rangle_{in} \equiv i\mathcal{M} \approx -ieQ\bar{u}_r(p')\Gamma^\mu(p, p')u_s(p)\tilde{A}_\mu^{\text{cl}}(q) + \mathcal{O}\left((\tilde{A}^{\text{cl}})^2\right) \quad (2.21)$$

where $u_s(p)$ denotes a spinor at momentum p and spin state s and Γ^μ denotes the quantum corrected vertex function. Terms of higher order in the classical field are strongly suppressed in a weak background and can be neglected. In the static limit, this amplitude can be related to the known classical scattering potential $V(x)$ using the Born approximation [36]

$$\mathcal{M} = -2m(2\pi)\delta(p'_0 - p_0)\tilde{V}(\mathbf{q}) \quad (2.22)$$

where m denotes the lepton mass. From this, the classical values can be read off by comparison. The first step, therefore, is to determine the form of the vertex function Γ^μ

¹In Feynman diagrams we will denote this insertion by an external photon line.

2.3.1 Vertex Function and Form Factors

We now want to consider the full quantum corrections to the tree-level vertex (2.20). The corresponding on-shell amplitude can be expanded as

$$-ieQ \bar{u}_s(p') \Gamma^\mu(p, p') u_s(p) \tilde{A}_\mu^{cl}(q) = \text{diagram with blob} = \text{diagram with cross} + \text{diagram with wavy line} + \dots \quad (2.23)$$

Depending on the specific model different particles and interactions will contribute to these quantum corrections. In general, since the amplitude is Lorentz invariant, $\bar{u}_s(p') \Gamma^\mu(p, p') u_s(p)$ must transform as a 4-vector and therefore has the following covariant decomposition (suppressing the spinors) [28]

$$\Gamma^\mu = \gamma^\mu A_1(q^2) + P^\mu A_2(q^2) + q^\mu A_3(q^2) + \gamma^\mu \gamma^5 A_4(q^2) + P^\mu \gamma^5 A_5(q^2) + q^\mu \gamma^5 A_6(q^2) \quad (2.24)$$

where $q^\mu = p'^\mu - p^\mu$ and $P^\mu = q'^\mu + q^\mu$. The prefactors A_i , as functions of the external momenta, can depend only on Lorentz invariant scalar products of the external momenta. Since the lepton is on-shell, these can all be written in terms of m^2 and q^2 . Therefore, the prefactors depend only on a single kinematic variable q^2 and the parameters of the theory. We can further simplify (2.24) by using the Ward identity² [37]

$$0 = q_\mu \bar{u}_s(p') \Gamma^\mu(p, p') u_s(p) \quad (2.25)$$

as well as the Gordon identities, which follow from the Dirac equation $(\not{p} - m)u_s(p) = 0$ and its conjugate $\bar{u}_s(p')(\not{p}' - m) = 0$ and hold in between the spinors

Gordon Identities

For $q = p' - p$ and $P = p' + p$ we have

$$\begin{aligned} \bar{u}_r(p') i\sigma^{\mu\nu} q_\nu u_s(p) &= \bar{u}_r(p') (2m\gamma^\mu - P^\mu) u_s(p) \\ \bar{u}_r(p') i\sigma^{\mu\nu} P_\nu u_s(p) &= -\bar{u}_r(p') q^\mu u_s(p) \\ \bar{u}_r(p') i\sigma^{\mu\nu} q_\nu \gamma^5 u_s(p) &= -\bar{u}_r(p') P^\mu \gamma^5 u_s(p) \\ \bar{u}_r(p') i\sigma^{\mu\nu} P_\nu \gamma^5 u_s(p) &= \bar{u}_r(p') (2m\gamma^\mu \gamma^5 - q^\mu \gamma^5) u_s(p) \end{aligned} \quad (2.26)$$

where $\sigma^{\mu\nu} = \frac{i}{2}[\gamma^\mu, \gamma^\nu]$

Using $P^\mu q_\mu = 0$ together with the Gordon identities, the Ward identity (2.25) implies

$$A_3(q^2) = 0, \quad q^2 A_6(q^2) = 2m A_4(q^2) \quad (2.27)$$

With this, we can bring the on-shell vertex function into the following form

$$\Gamma^\mu = \gamma^\mu F_E(q^2) + \frac{i\sigma^{\mu\nu} q_\nu}{2m} F_M(q^2) + \frac{\sigma^{\mu\nu} q_\nu}{2m} \gamma^5 F_D(q^2) + \frac{q^2 \gamma^\mu - \not{q} q^\mu}{(2m)^2} \gamma^5 F_A(q^2) \quad (2.28)$$

The dimensionless prefactors $F_E(q^2)$, $F_M(q^2)$, $F_D(q^2)$ and $F_A(q^2)$ are called the electric charge, magnetic and electric dipole and anapole form factors. As we will see in section 2.3.2, the classical quantities, such as the electric charge and the magnetic moment, are related to the form factors evaluated at $q^2 = 0$. The CP violating electric dipole moment and the P violating anapole moment arise in the Standard Model only via the weak interaction and are consequently extremely tiny [38–40], although, if there are additional sources of CP violation from contributions beyond the SM, the EDM could be within reach of the J-PARC experiment [35].

²The Ward identity holds even for $q^2 \neq 0$, as is the case in momentum transfer from the external field.

2.3.2 Relation to the Classical Definition

We now want to determine the connection between the scattering amplitude (2.21) and the classical notion of a magnetic moment. The non-relativistic interaction potential of a particle with electric charge q , magnetic moment $\boldsymbol{\mu}$, electric dipole moment \mathbf{d} and anapole moment $\boldsymbol{\alpha}$ in a static external magnetic field \mathbf{B} and static electric field \mathbf{E} is given by

$$V(\mathbf{x}) = q\phi(\mathbf{x}) - \boldsymbol{\mu} \cdot \mathbf{B}(\mathbf{x}) - \mathbf{d} \cdot \mathbf{E}(\mathbf{x}) - \boldsymbol{\alpha} \cdot \nabla \times \mathbf{B}(\mathbf{x}) \quad (2.29)$$

In order to recover this scattering potential from the amplitude (2.28), we need to take the non-relativistic limit $|\mathbf{p}|, |\mathbf{p}'| \ll m$. This is possible, since for static and slowly varying fields the Fourier transform of the external vector potential $\tilde{A}_\mu^d(q) = (2\pi)\delta(q_0)(\tilde{\phi}(\mathbf{q}), -\tilde{\mathbf{A}}(\mathbf{q}))$ is strongly concentrated about $\mathbf{q} = 0$. Using the explicit form of the Dirac spinors in the Weyl representation we can expand to first order in the external momenta [41]

$$u_s(p) = \begin{pmatrix} \sqrt{p \cdot \bar{\sigma}} \xi_s \\ \sqrt{p \cdot \sigma} \xi_s \end{pmatrix} \approx \sqrt{m} \begin{pmatrix} (1 - \frac{\mathbf{p} \cdot \boldsymbol{\sigma}}{2m}) \xi_s \\ (1 + \frac{\mathbf{p} \cdot \boldsymbol{\sigma}}{2m}) \xi_s \end{pmatrix} \quad (2.30)$$

where $\sigma^\mu = (\sigma^0, \boldsymbol{\sigma})$ and $\bar{\sigma}^\mu = (\sigma^0, -\boldsymbol{\sigma})$. With this,

$$\begin{aligned} \bar{u}_r(p') \gamma^0 u_s(p) &\approx 2m \xi_r^\dagger \xi_s, & \bar{u}_r(p') \gamma^k u_s(p) &\approx \mathbf{P}^k \xi_r^\dagger \xi_s - 2i\epsilon^{kij} \mathbf{q}_i \xi_r^\dagger \frac{\boldsymbol{\sigma}^j}{2} \xi_s \\ \bar{u}_r(p') \gamma^0 \gamma^5 u_s(p) &\approx 2\mathbf{P}^k \xi_r^\dagger \frac{\boldsymbol{\sigma}^k}{2} \xi_s, & \bar{u}_r(p') \gamma^k \gamma^5 u_s(p) &\approx 4m \xi_r^\dagger \frac{\boldsymbol{\sigma}^k}{2} \xi_s \end{aligned} \quad (2.31)$$

Further, since we work to linear order in \mathbf{q}

$$\begin{aligned} \bar{u}_r(p') \frac{i\sigma^{0\nu} q_\nu}{2m} u_s(p) &\approx 0, & \bar{u}_r(p') \frac{i\sigma^{k\nu} q_\nu}{2m} u_s(p) &\approx -2i\epsilon^{kij} \mathbf{q}_i \xi_r^\dagger \frac{\boldsymbol{\sigma}^j}{2} \xi_s \\ \bar{u}_r(p') \frac{\sigma^{0\nu} q_\nu}{2m} \gamma^5 u_s(p) &\approx 2i\mathbf{q}_k \xi_r^\dagger \frac{\boldsymbol{\sigma}^k}{2} \xi_s, & \bar{u}_r(p') \frac{\sigma^{k\nu} q_\nu}{2m} \gamma^5 u_s(p) &\approx 0 \end{aligned} \quad (2.32)$$

with this, we have all necessary terms to evaluate the non-relativistic expansion of $i\mathcal{M}$

$$\begin{aligned} i\mathcal{M} \approx -ieQ(2\pi)\delta(q_0) &\left(2mF_E(0)\tilde{\phi}(\mathbf{q})\xi_r^\dagger \xi_s + 2[F_E(0) + F_M(0)]i\epsilon^{kij} \mathbf{q}_i \tilde{\mathbf{A}}_k(\mathbf{q}) \xi_r^\dagger \frac{\boldsymbol{\sigma}^j}{2} \xi_s \right. \\ &\left. + 2F_D(0)i\tilde{\phi}(\mathbf{q})\mathbf{q}_k \xi_r^\dagger \frac{\boldsymbol{\sigma}^k}{2} \xi_s + \dots \right) \end{aligned} \quad (2.33)$$

On the other hand, the Fourier transform of the scattering potential (2.29) is

$$\tilde{V}(\mathbf{q}) = q\tilde{\phi}(\mathbf{q}) + i\boldsymbol{\mu} \cdot \mathbf{q} \times \tilde{\mathbf{A}}(\mathbf{q}) + i\mathbf{d} \cdot \mathbf{q} \tilde{\phi}(\mathbf{q}) + \boldsymbol{\alpha} \cdot \mathbf{q} \times (\mathbf{q} \times \tilde{\mathbf{A}}(\mathbf{q})) \quad (2.34)$$

from which we can now directly read off the definitions of the classical quantities. Note, that (2.33) does not contain the anapole term, since we only expanded to first order in \mathbf{q} .

$$q = F_E(0)eQ \quad (2.35)$$

$$\boldsymbol{\mu} = 2[F_E(0) + F_M(0)] \frac{eQ}{2m} \langle \mathbf{S} \rangle \quad (2.36)$$

$$\mathbf{d} = 2F_D(0) \frac{eQ}{2m} \langle \mathbf{S} \rangle \quad (2.37)$$

where $\langle \mathbf{S} \rangle = \xi_r^\dagger \frac{\boldsymbol{\sigma}}{2} \xi_s$ is the expectation value of the spin operator. It corresponds to the classical definition of the spin vector \mathbf{s} in (2.1) in the sense that, if we prepare a beam of muons in the same initial spin state and then track $\langle \mathbf{S} \rangle$ along the trajectory through individual scattering (or decay) events, we obtain \mathbf{s} as the time dependent average. Since $q = Qe$ we must have $F_E(0) = 1$ and the anomalous magnetic moment is therefore given by $a_\mu = F_M(0)$.

2.3.3 Renormalization with External Background Field

Before we move on to the SM prediction, let us address a few subtleties regarding renormalization. Of course, in order to calculate finite predictions in QFT, we need to regulate divergent integrals and chose an appropriate subtraction scheme to cancel the divergences. For all explicit calculations, we will choose dimensional regularization and the minimal subtraction (MS) scheme, however, the formal discussions will be mostly scheme independent. Following the conventions in [42], we introduce the renormalization scale μ and write the bare fields and parameters in the Lagrangian as

$$\psi^0 = \sqrt{Z(\mu)}\psi(\mu), \quad A_\mu^0 = \sqrt{Z_\gamma(\mu)}A_\mu(\mu), \quad e^0 = \mu^\epsilon Z_e(\mu)e(\mu), \quad \dots \quad (2.38)$$

The renormalized fields and parameters are finite, but μ dependent and all divergences are contained in the renormalization factors Z_i . We also explicitly factor out powers of μ such that the renormalized parameters have integer mass dimension³. If there is no external background field, the exact form of the 2-point function is given by the Källén-Lehman spectral representation and can be compared with the resummed perturbative expansion [37, 41]

$$\int d^4x e^{ipx} \langle \Omega | T \{ \psi(x; \mu) \bar{\psi}(0; \mu) \} | \Omega \rangle \simeq \frac{iR(\mu)}{\not{p} - m} = \frac{i}{\not{p} - m^R(\mu) + \Sigma(\not{p}; \mu)} \quad (2.39)$$

$$\int d^4x e^{ipx} \langle \Omega | T \{ A^\mu(x; \mu) A^\nu(0; \mu) \} | \Omega \rangle \simeq \frac{-iR_A(\mu)}{p^2} p^{\mu\nu} = \frac{-ip^{\mu\nu}}{p^2(1 + \Pi(p^2; \mu))} \quad (2.40)$$

where $p^{\mu\nu} = \eta^{\mu\nu} - \frac{p^\mu p^\nu}{p^2}$, $\Sigma(\not{p})$ and $\Pi(p^2)$ denote the renormalized self energy of the lepton and photon and m denotes the physical pole mass of the lepton. The residues of the propagators R and R_A are called the field strength normalization of the lepton and photon field and are given by [37]

$$R(\mu) = \left(1 + \frac{d\Sigma}{d\not{p}} \Big|_{\not{p}=m} \right)^{-1}, \quad R_A(\mu) = \frac{1}{1 + \Pi(0; \mu)} \quad (2.41)$$

Let us first look at the photon vertex function, which has the same exact structure as (2.28), except that the form factors now depend on μ . To see how the μ dependence cancels from physical predictions, consider the corresponding amplitude given by the LSZ formula [41, 43]

$$\begin{aligned} {}_{out} \langle p' | p; q \rangle_{in} &= \int d^4x \frac{ie^{-ipx}}{\sqrt{R(\mu)}} [(i\not{\partial}_x + m) u_s(p)]_\alpha \int d^4y \frac{-ie^{ip'y}}{\sqrt{R(\mu)}} [\bar{u}_r(p') (i\not{\partial}_y - m)]_\beta \\ &\quad \int d^4z \frac{ie^{-iqz}}{\sqrt{R_A(\mu)}} [\epsilon_\lambda^{\nu*}(q) \square_z] \langle \Omega | T \{ \psi_\beta(y; \mu) \bar{\psi}_\alpha(x; \mu) A_\nu(z; \mu) \} | \Omega \rangle \\ &= (2\pi)^4 \delta^{(4)}(q + p - p') R(\mu) \sqrt{R_A(\mu)} \bar{u}_r(p') (-iQe(\mu) \Gamma^\mu(p, p'; \mu)) u_s(p) \epsilon_\lambda^{\nu*}(q) \end{aligned} \quad (2.42)$$

We can now use (2.28) together with the Ward-Takahashi identity [37]

$$q_\mu \Gamma^\mu(q, p, p'; \mu) = \not{q} + \Sigma(\not{p} + \not{q}; \mu) - \Sigma(\not{p}; \mu) \quad (2.43)$$

and take the on-shell limit to find

$$F_E(0; \mu) = 1 + \frac{d\Sigma}{d\not{p}} \Big|_{\not{p}=m} = \frac{1}{R(\mu)} \quad (2.44)$$

³For the bare quantities in D dimensions we have $[\phi^0] = \frac{D-2}{2}$, $[\psi^0] = \frac{D-1}{2}$, $[A_\mu^0] = \frac{D-2}{2}$, $[m_\mu^0] = 1$ and $[e^0] = \frac{4-D}{2}$

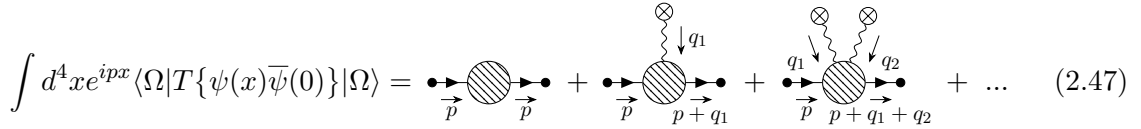
The renormalized coupling parameter and μ dependent Form factors are therefore related to the physical elementary charge and anomalous magnetic moment by

$$e^{phys} = \frac{e(\mu)}{\sqrt{1 + \Pi(0; \mu)}}, \quad a_\mu^{phys} = \frac{F_M(0; \mu)}{F_E(0; \mu)} \quad (2.45)$$

If we want to include a physical background field we must first think about how to expand the photon field. A_μ^0 is not physical and neither is $A_\mu(\mu)$, instead we must write A_μ^0 in terms of the on-shell renormalized field and only then expand around A_μ^{cl}

$$A_\mu^0 = \sqrt{Z_A(\mu)} A_\mu(\mu) = \sqrt{Z_A(\mu)} \sqrt{R_A(\mu)} A_\mu^{OS} \rightarrow \sqrt{Z_A(\mu)} \left(\sqrt{R_A(\mu)} A_\mu^{cl} + A_\mu(\mu) \right) \quad (2.46)$$

Unfortunately, (2.39) and (2.40) no longer hold, since we need to include the additional interaction with the external field. For example, the perturbative expansion of the fermion 2-point function can be written diagrammatically as



$$\int d^4x e^{ipx} \langle \Omega | T \{ \psi(x) \bar{\psi}(0) \} | \Omega \rangle = \text{diagram 1} + \text{diagram 2} + \text{diagram 3} + \dots \quad (2.47)$$

where the crossed dots stand for insertions of $-ieQ\gamma^\mu \tilde{A}_\mu^{cl}(q_i)$ and the transferred momenta q_i are integrated over. These terms hint at important non-perturbative effects which need to be taken into account in the treatment of intense background fields [44]. However, since we are only interested in weak background fields we may treat (2.47) as an $\mathcal{O}(A^{cl})$ correction to (2.41) which, in turn, contributes only to the $\mathcal{O}((A^{cl})^2)$ correction in (2.21) and can therefore be ignored. We can then use the LSZ formula

$$\begin{aligned} {}_{out} \langle p'; r | p; s \rangle_{in} &= \int d^4x \frac{ie^{-ipx}}{\sqrt{R(\mu)}} [(i\partial_x + m_\mu) u_s(p)]_\alpha \int d^4y \frac{-ie^{ip'y}}{\sqrt{R(\mu)}} \\ &\quad [\bar{u}_r(p') (i\partial_y - m_\mu)]_\beta \langle \Omega | T \{ \psi_\beta(y; \mu) \bar{\psi}_\alpha(x; \mu) \} | \Omega \rangle \\ &= R(\mu) \bar{u}_r(p') (-iQe(\mu) \Gamma^\mu(p, p'; \mu)) u_s(p) \sqrt{R_A(\mu)} \tilde{A}_\mu^{cl}(q) \end{aligned} \quad (2.48)$$

which again leads to the same expressions for the physical coupling and anomalous magnetic moment as in (2.45), except that the factor $\sqrt{R_A(\mu)}$ now comes from the expansion of the 2-point function rather than the normalization factor in the LSZ formula.

2.3.4 Prediction of the Standard Model

Lastly, let us briefly discuss the value of a_μ in the Standard Model. The full summary of the current theory prediction can be found in [3]. The calculation can be split into 4 parts

$$a_\mu^{SM} = a_\mu^{QED} + a_\mu^{EW} + a_\mu^{HVP} + a_\mu^{HLbL} \quad (2.49)$$

By far the largest contribution to the SM prediction is given by the QED correction a_μ^{QED} . It is known up to 5-loop order and depends on the input used for the fine structure constant α as well as the ratios of the lepton masses m_μ/m_e and m_μ/m_τ . Its value is [45, 46]

$$a_\mu^{QED} = 116\,584\,718.931(104) \times 10^{-11} \quad (2.50)$$

The electroweak contribution a_μ^{EW} , on the other hand, is strongly suppressed by the masses of the heavy EW bosons and is, therefore, even smaller than the discrepancy between theory and experiment. The complete results are currently known up to two-loop order including

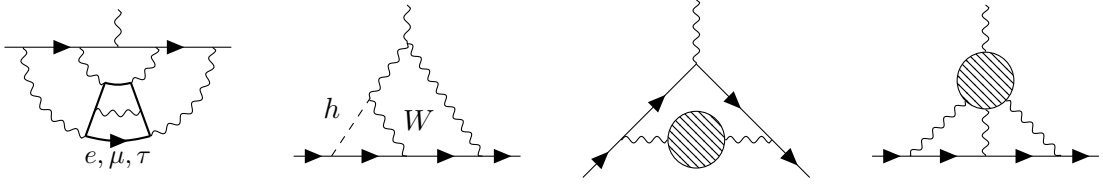


Figure 2.3: Sample diagrams contributing to a_μ^{QED} , a_μ^{EW} , a_μ^{HVP} and a_μ^{HLbL} . All diagrams in this thesis are generated using TikZ-Feynman [48].

estimates of higher order leading logarithms. The uncertainty mainly results from the hadronic loops at the two-loop level and could be improved by a non-perturbative treatment. The value is [17, 47]

$$a_\mu^{\text{EW}} = 153.6(1.0) \times 10^{-11} \quad (2.51)$$

The largest uncertainty, however, comes from the hadronic contributions a_μ^{HVP} and a_μ^{HLbL} . Both have to be calculated non-perturbatively using either lattice QCD or data driven evaluation of dispersive integrals, and while both methods are in excellent agreement for the hadronic light by light scattering, there are significant tensions in the evaluation of the contribution from the hadronic vacuum polarization [3, 49]. Due to the smaller uncertainty, the current value of a_μ^{HVP} is taken from the data driven evaluation based on [50–56]

$$a_\mu^{\text{HVP}} = 6845(40) \times 10^{-11} \quad (2.52)$$

The value of a_μ^{HLbL} is based on a weighted average of the lattice and dispersive calculation and is given by [57–65]

$$a_\mu^{\text{HLbL}} = 92(18) \times 10^{-11} \quad (2.53)$$

With this, the current theoretical prediction for a_μ in the Standard Model is

$$a_\mu^{\text{SM}} = 116\,591\,810(43) \times 10^{-11} \quad (2.54)$$

which deviates from the experimental value (2.17) by

$$\Delta a_\mu = a_\mu^{\text{Ex}} - a_\mu^{\text{SM}} = 251(59) \times 10^{-11} \quad (2.55)$$

with a significance of 4.2σ . The efforts on the theory side are now focused on improving the accuracy of this prediction by reducing the uncertainties of the hadronic contributions as well as exploring extensions to the SM for an explanation of the hopefully persistent discrepancy between the SM and experiment. In the following chapter we will discuss in detail one particular extension, the Two-Higgs-Doublet Model, which will be the main focus of this thesis.

3 The Two-Higgs-Doublet Model

In comparison with its rich matter content comprised of three generations of fermions with distinct properties and interactions governed by the gauge group $SU(3)_C \times SU(2)_L \times U(1)_Y$ and mixing matrices, the scalar sector of the Standard Model is remarkably simple. It contains just a single Higgs-doublet used to break the $SU(2)_L \times U(1)_Y$ subgroup down to the $U(1)_{EM}$ group of electromagnetism and explain the masses of the W and Z boson. Together with the elusive nature of the corresponding Higgs boson, this raises the question whether there exist other Higgs-like fields which thus far have evaded detection in our experiments. This question has, of course, been studied extensively both experimentally and theoretically. A major constraint on extensions to the Higgs sector of the SM comes from the ρ parameter which is given at tree-level by [66]

$$\rho = \frac{m_W^2}{m_Z^2 \cos^2 \theta_W} = \frac{\sum_{i=1}^n [I_i(I_i + 1) - \frac{1}{4}Y_i^2]v_i^2}{\sum_{i=1}^n \frac{1}{2}Y_i^2v_i^2} \quad (3.1)$$

where the sum runs over all scalar multiplets ϕ_i and I_i , Y_i and v_i are the corresponding weak isospin, weak hypercharge and vacuum expectation value (vev) of the neutral component. The current experimental value for ρ is very close to one [67]

$$\rho = 1.0038(20) \quad (3.2)$$

The simplest extensions to the SM therefore consist of additional $SU(2)$ singlets with $Y = 0$ and doublets with $I = \frac{1}{2}$ and $Y = \pm 1$ which give $\rho = 1$ at tree-level. In particular, the Two-Higgs-Doublet Model (2HDM) results from adding just a single $SU(2)$ doublet to the SM.

Another strong constraint on the scalar sector comes from the limits on flavor changing neutral currents (FCNC) [68, 69]. In the SM such FCNC's are absent at tree-level, because the mass matrix and Higgs-fermion couplings are diagonalized simultaneously. However, in models with an extended Higgs sector fermions generically couple to all additional scalars and such a simultaneous diagonalization is therefore no longer possible. The easiest way to circumvent this issue is to require that all fermions with the same electric charge couple only to one Higgs doublet. Different types of models can then be classified by a choice of these couplings (see for example table 3.1).

In the following, we will discuss in more detail the aligned 2HDM [70] which avoids tree-level FCNC and contains several interesting types as special cases. A much more general review of the 2HDM including models with tree-level FCNC is given in [71].

3.1 Definition and Parameters

The 2HDM is given by the SM with an extended Higgs sector consisting of two $SU(2)$ doublets with $Y_i = 1$

$$\Phi_1 = \begin{pmatrix} \phi_1^+ \\ \phi_1^0 \end{pmatrix}, \quad \Phi_2 = \begin{pmatrix} \phi_2^+ \\ \phi_2^0 \end{pmatrix} \quad (3.3)$$

In total the two doublets contain 8 real degrees of freedom, 3 of which are used to spontaneously break $SU(2)_L \times U(1)_Y$ down to the $U(1)_{EM}$ electromagnetism leaving us with 5 physical

Higgs bosons. The most general Higgs Lagrangian is given by

$$\mathcal{L}_{Higgs} = \sum_i (D_\mu \Phi_i)^\dagger (D_\mu \Phi_i) - V(\Phi_1, \Phi_2) \quad (3.4)$$

where $D_\mu = \partial_\mu + ig_2 t^a W_\mu^a + ig_1 \frac{Y}{2} B_\mu$ (with $t^a = \frac{\sigma^a}{2}$) is the $SU(2)_L \times U(1)_Y$ covariant derivative. The most general Higgs potential $V(\Phi_1, \Phi_2)$ has 14 parameters and a complicated vacuum structure. For simplicity we assume that CP is conserved and impose a discrete \mathbb{Z}_2 symmetry used to eliminate terms odd in either doublet¹. Under these assumptions, the Higgs potential can be written as [71]

$$\begin{aligned} V(\Phi_1, \Phi_2) = & m_{11}^2 \Phi_1^\dagger \Phi_1 + m_{22}^2 \Phi_2^\dagger \Phi_2 + \frac{\lambda_1}{2} (\Phi_1^\dagger \Phi_1)^2 + \frac{\lambda_2}{2} (\Phi_2^\dagger \Phi_2)^2 \\ & + \lambda_3 (\Phi_1^\dagger \Phi_1) (\Phi_2^\dagger \Phi_2) + \lambda_4 (\Phi_1^\dagger \Phi_2) (\Phi_2^\dagger \Phi_1) \\ & + \frac{\lambda_5}{2} [(\Phi_1^\dagger \Phi_2)^2 + (\Phi_2^\dagger \Phi_1)^2] \end{aligned} \quad (3.5)$$

In minimizing this potential both neutral components of the doublets acquire a vacuum expectation value v_i . Before expanding the fields around their respective vev's it is convenient to change basis through a rotation with angle $\tan \beta = \frac{v_2}{v_1}$ (following the notation in [11])

$$\begin{pmatrix} \Phi_v \\ \Phi_\perp \end{pmatrix} = \begin{pmatrix} \cos \beta & \sin \beta \\ -\sin \beta & \cos \beta \end{pmatrix} \begin{pmatrix} \Phi_1 \\ \Phi_2 \end{pmatrix} \quad (3.6)$$

This is usually referred to as the Higgs basis. Expanding around the minimum we find the explicit components

$$\Phi_v = \begin{pmatrix} G^+ \\ \frac{1}{\sqrt{2}}(v + S_1 + iG^0) \end{pmatrix}, \quad \Phi_\perp = \begin{pmatrix} H^+ \\ \frac{1}{\sqrt{2}}(S_2 + iA) \end{pmatrix} \quad (3.7)$$

where the doublet Φ_v now contains the SM vev $v = \sqrt{v_1^2 + v_2^2}$ and the Goldstone bosons G^+ and G^0 . While H^+ and A already correspond to the mass eigenstate of the charged and the neutral CP-odd Higgs boson, S_1 and S_2 have to be rotated again to obtain the CP-even mass eigenstates h and H

$$\begin{pmatrix} H \\ h \end{pmatrix} = \begin{pmatrix} \cos(\beta - \alpha) & -\sin(\beta - \alpha) \\ \sin(\beta - \alpha) & \cos(\beta - \alpha) \end{pmatrix} \begin{pmatrix} S_1 \\ S_2 \end{pmatrix} \quad (3.8)$$

We identify h with the SM Higgs field and do not include its contributions in any of the calculations. In this basis we can rewrite the potential (3.5) in terms of the boson masses m_h, m_H, m_A, m_{H^\pm} , the mixing angles β and α and the vev v . Like in the SM, after a rotation by the angle θ_W into the appropriate mass eigenstates

$$\begin{pmatrix} W_\mu^+ \\ W_\mu^- \end{pmatrix} = \begin{pmatrix} \frac{1}{\sqrt{2}} & -\frac{i}{\sqrt{2}} \\ \frac{1}{\sqrt{2}} & \frac{i}{\sqrt{2}} \end{pmatrix} \begin{pmatrix} W_\mu^1 \\ W_\mu^2 \end{pmatrix}, \quad \begin{pmatrix} A_\mu \\ Z_\mu \end{pmatrix} = \begin{pmatrix} \cos \theta_W & \sin \theta_W \\ -\sin \theta_W & \cos \theta_W \end{pmatrix} \begin{pmatrix} B_\mu \\ W_\mu^3 \end{pmatrix} \quad (3.9)$$

we obtain the gauge boson masses

$$m_{W^\pm}^2 = \frac{v^2}{4} g_2^2, \quad m_Z^2 = \frac{v^2}{4} (g_1^2 + g_2^2), \quad m_\gamma^2 = 0 \quad (3.10)$$

The $SU(2)_L \times U(1)_Y$ covariant derivative can be rewritten in terms of these mass eigenstates

$$D_\mu = \partial_\mu + ig_2(t^+ W_\mu^+ + t^- W_\mu^-) + i \frac{g_2}{\cos \theta_W} (t^3 - Q \sin^2 \theta_W) Z_\mu + ie Q A_\mu \quad (3.11)$$

where $t^\pm = t^1 \pm it^2$, $Q = t^3 + \frac{Y}{2}$ and $e = g_1 \cos \theta_W = g_2 \sin \theta_W$. The Higgs-gauge interaction vertices then follow from the kinetic term in (3.4) and can be found for example in [72].

¹Such a discrete symmetry under which $\Phi_1 \rightarrow -\Phi_1$ and $\Phi_2 \rightarrow +\Phi_2$ (or vice versa) together with a choice for the transformation of the right-handed fermions is motivated by the fact that it automatically eliminates all terms coupling fermions of the same charge to more than one Higgs doublet.

Fermion Sector and Yukawa Couplings The Higgs mechanism not only generates masses of the gauge bosons, but also of chiral fermions via (model dependent) Yukawa couplings. The most general Yukawa Lagrangian is given by [70]

$$\begin{aligned} \mathcal{L}_Y = & -\bar{Q}_L^i \left(\Phi_1 \Upsilon_{1,d}^{ij} + \Phi_2 \Upsilon_{2,d}^{ij} \right) d_R'^j - \bar{Q}_L^i \left(\tilde{\Phi}_1 \Upsilon_{1,u}^{ij} + \tilde{\Phi}_2 \Upsilon_{2,u}^{ij} \right) u_R'^j \\ & - \bar{L}_L^i \left(\Phi_1 \Upsilon_{1,l}^{ij} + \Phi_2 \Upsilon_{2,l}^{ij} \right) l_R'^j + \text{h.c.} \end{aligned} \quad (3.12)$$

where Q_L^i and L_L^i denote left-handed quark and lepton doublets with generation index i in the flavor basis, $d_R'^j, u_R'^j$ and $l_R'^j$ denote the right-handed singlets, $\Upsilon_{k,f}^{ij}$ the corresponding Yukawa coupling matrices and $\tilde{\Phi}_j = i\sigma^2 \Phi_j^*$ the charge conjugate Higgs fields. In order to avoid tree-level FCNC the fermion mass matrices and Yukawa couplings must be simultaneously diagonalizable. In general, this is not possible and one must further restrict the couplings. This can be done either by imposing a \mathbb{Z}_2 symmetry which eliminates terms coupling fermions of the same charge to more than one of the Higgs doublets or by requiring that the Yukawa matrices are proportional to each other, that is

$$\Upsilon_{2,f} \propto \Upsilon_{1,f}, \quad f \in \{u, d, l\} \quad (3.13)$$

Here, we will use the second approach, also called the aligned 2HDM [70], since it is less restrictive. In the Higgs basis (3.12) becomes

$$\begin{aligned} \mathcal{L}_Y = & -\bar{Q}_L^i \left(\Phi_v Y_{v,d}^{ij} + \Phi_\perp Y_{\perp,d}^{ij} \right) d_R'^j - \bar{Q}_L^i \left(\tilde{\Phi}_v Y_{v,u}^{ij} + \tilde{\Phi}_\perp Y_{\perp,u}^{ij} \right) u_R'^j \\ & - \bar{L}_L^i \left(\Phi_v Y_{v,l}^{ij} + \Phi_\perp Y_{\perp,l}^{ij} \right) l_R'^j + \text{h.c.} \end{aligned} \quad (3.14)$$

Note, that the proportionality between Yukawa couplings survives the unitary transformation, such that

$$Y_{\perp,f}' = \zeta_f Y_{v,f}' \quad (3.15)$$

for some arbitrary constant ζ_f . The fermion mass terms are generated by the vev of the neutral component of Φ_v , but are not yet diagonal. In order to obtain the fermion mass eigenstates, we introduce unitary matrices $V_{L/R}^{u/d/l}$, such that the fermion mass matrices

$$M_f = \frac{v}{\sqrt{2}} V_L^f Y_{v,f}' V_R^{f\dagger} \quad (3.16)$$

are diagonal. The Yukawa alignment ensures that the same operation also diagonalizes $Y_{\perp,f}$. The mass eigenstates are thus given by

$$\bar{q}_L = \bar{q}_L' V_L^{q\dagger}, \quad q_R = V_R^q q_R', \quad \bar{e}_L = \bar{e}_L' V_L^{e\dagger}, \quad e_R = V_R^e e_R', \quad \bar{\nu}_L = \bar{\nu}_L' V_L^{\nu\dagger} \quad (3.17)$$

Since, like in the SM, neutrinos are massless in the 2HDM the neutrino mass matrix is diagonal in any basis and $V_L^{\nu\dagger}$ is, therefore, arbitrary. In particular, we can choose $V_L^{\nu\dagger} = V_L^{e\dagger}$ and in this way absorb the leptonic mixing matrix into the definition of the neutrino fields. For quarks this is not possible and we need to introduce the CKM mixing matrix

$$V_{\text{CKM}} = V_L^u V_L^{d\dagger} \quad (3.18)$$

With this we can express the Yukawa Lagrangian in terms of the mass eigenstates for both the Higgs doublets as well as the fermions [11]

$$\mathcal{L}_Y = -\sqrt{2}H^+ \left(\bar{u} [V_{\text{CKM}} y_d^A P_R + y_u^A V_{\text{CKM}} P_L] d + \bar{\nu} y_l^A P_R l \right) - \sum_{S,f} \mathcal{S} \bar{f} y_f^S P_R f + \text{h.c.} \quad (3.19)$$

	u_R	d_R	e_R	ζ_u	ζ_d	ζ_e	\mathbb{Z}_2
Type I	Φ_2	Φ_2	Φ_2	$\cot \beta$	$\cot \beta$	$\cot \beta$	$\Phi_1 \rightarrow -\Phi_1$
Type II	Φ_2	Φ_1	Φ_1	$\cot \beta$	$-\tan \beta$	$-\tan \beta$	$(\Phi_1, d_R, e_R) \rightarrow -(\Phi_1, d_R, e_R)$
Type X	Φ_2	Φ_2	Φ_1	$\cot \beta$	$\cot \beta$	$-\tan \beta$	$(\Phi_1, e_R) \rightarrow -(\Phi_1, e_R)$
Type Y	Φ_2	Φ_1	Φ_2	$\cot \beta$	$-\tan \beta$	$\cot \beta$	$(\Phi_1, d_R) \rightarrow -(\Phi_1, d_R)$

Table 3.1: Choices of the Higgs-fermion coupling for different types of the 2HDM.

where the sum runs over $\mathcal{S} \in \{h, H, iA\}$, $P_{R/L} = \frac{1}{2}(1 \pm \gamma^5)$ and the diagonal Yukawa matrices are defined as

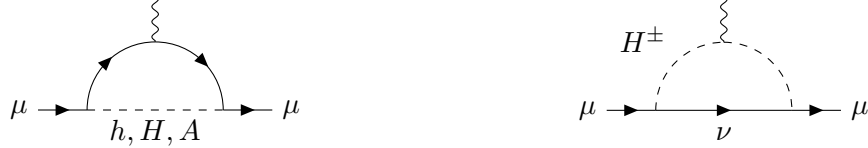
$$y_f^{\mathcal{S}} = \frac{1}{v} Y_f^{\mathcal{S}} M_f \quad (3.20)$$

with coefficients $Y_f^{\mathcal{S}}$ given by

$$\begin{aligned} Y_{d,l}^A &= \zeta_{d,l}, & Y_u^A &= -\zeta_u \\ Y_f^h &= \sin(\beta - \alpha) + \cos(\beta - \alpha)\zeta_f \\ Y_f^H &= \cos(\beta - \alpha) - \sin(\beta - \alpha)\zeta_f \end{aligned} \quad (3.21)$$

The usual Type I, II, X and Y 2HDM follow from particular choices of ζ_f (see table 3.1) in the following calculations we will, however, keep them arbitrary. The relevant Feynman rules are listed in Appendix C.

3.2 One-loop Contribution to a_μ

**Figure 3.1:** One-Loop contributions to a_μ in the 2HDM.

All new scalars contribute to a_μ at one-loop through the diagrams in Fig.3.1. The result can be written in a compact form as [10, 11, 73]

$$\Delta a_\mu^{2\text{HDM},1} = \frac{1}{8\pi^2} \sum_{\mathcal{S}} (y_\mu^{\mathcal{S}})^2 \frac{m_\mu^2}{m_{\mathcal{S}}^2} \mathcal{F}_{\mathcal{S}}^{(1)} \left(\frac{m_\mu^2}{m_{\mathcal{S}}^2} \right) \quad (3.22)$$

where the sum runs over $\mathcal{S} \in \{H, A, H^\pm\}$ and the loop functions $\mathcal{F}_{\mathcal{S}}$ are given by

$$\begin{aligned} \mathcal{F}_H^{(1)}(x) &= \int_0^1 du \frac{u^2(2-u)}{xu^2 + 1 - u} \underset{x \rightarrow 0}{\simeq} -\ln(x) - \frac{7}{6} + \mathcal{O}(x) \\ \mathcal{F}_A^{(1)}(x) &= \int_0^1 du \frac{-u^3}{xu^2 + 1 - u} \underset{x \rightarrow 0}{\simeq} +\ln(x) + \frac{11}{6} + \mathcal{O}(x) \\ \mathcal{F}_{H^\pm}^{(1)}(x) &= \int_0^1 du \frac{-u(1-u)}{1 - (1-u)x} \underset{x \rightarrow 0}{\simeq} -\frac{1}{6} + \mathcal{O}(x) \end{aligned} \quad (3.23)$$

Due to the strong suppression by large scalar masses and small muon Yukawa couplings, the one-loop contribution on its own cannot account for the current deviation (2.55). However, additional large contributions to a_μ enter at two-loop level due to Barr-Zee diagrams with heavy fermion loops.

3.3 Two-Loop Barr-Zee Diagram

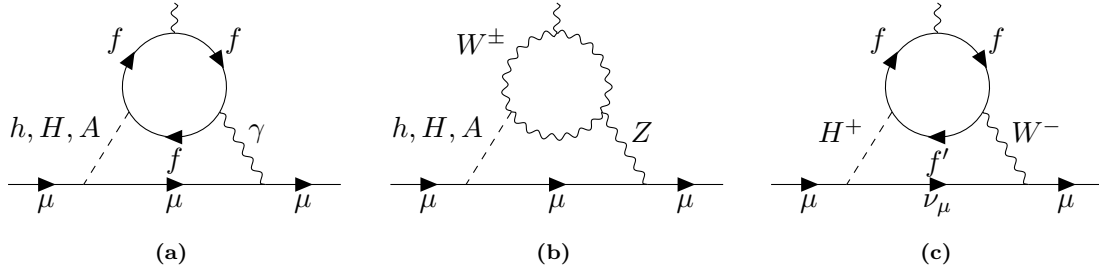


Figure 3.2: Examples of Barr-Zee diagrams contributing to a_μ in the 2HDM. In particular, the dominant contribution is given by (a) for a light pseudoscalar $m_A \sim 20 \dots 100$ GeV and with heavy fermions $f = t, \tau$ running in the loop.

Barr-Zee diagrams have, in the past, already been studied extensively in the context of the anomalous magnetic and electric dipole moments [6–10, 73–76]. In this section we want to present a calculation of the dominant 2-loop contribution to a_μ in the 2HDM, given by Fig.3.2a [5], as this provides a good starting point for evaluating the leading 3-loop corrections in chapter 5 and 6. The calculation can be split into two parts by first evaluating the inner fermion loop and then inserting the resulting vertex function into the full amplitude. Throughout this thesis we will give results both for the CP-even and CP-odd neutral scalars although, considering experimental constraints, only the latter leads to a significant correction to a_μ in the 2HDM.

3.3.1 Subgraph Vertex Function

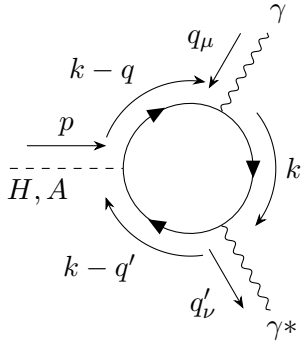


Figure 3.3: Momentum routing in the $S\gamma\gamma$ subgraph. γ^* denotes the virtual photon.

Before calculating the amplitudes, let us briefly consider the tensor structure of the resulting vertex function. We denote the momentum of the incoming external photon by q_μ and of the outgoing virtual photon by q'_ν . The vertex function then takes the following general form

$$i\Gamma^{\mu\nu} = A_1\eta^{\mu\nu} + A_2q'^\mu q^\nu + A_3q^\mu q'^\nu + A_4q'^\mu q'^\nu + A_5q^\mu q'^\nu + A_6\epsilon^{\mu\nu\alpha\beta}q_\alpha q'_\beta \quad (3.24)$$

Since we are interested in contributions to a_μ we can drop the terms proportional to q^μ from this expression. Similarly, the term $q'^\mu q'^\nu$ can also be discarded, as it results in a trivial gamma structure in the two-loop amplitude [76]. Finally, from the Ward identity $q_\mu\Gamma^{\mu\nu} = 0$ we find

$$\begin{aligned} 0 &= A_1 + A_2qq' + A_5q^2 \\ 0 &= A_3q^2 + A_4qq' \end{aligned} \quad (3.25)$$

which, to first order in q , implies the following gauge invariant form of the amplitude

$$i\Gamma_S^{\mu\nu}(q, q') = i\Gamma(q, q') [qq'\eta^{\mu\nu} - q'^\mu q^\nu] + i\Gamma^5(q, q')\epsilon^{\mu\nu\alpha\beta}q_\alpha q'_\beta \quad (3.26)$$

$H\gamma\gamma^*$ Vertex The amplitude for the CP-even external scalars (H and h) is given by

$$i\Gamma_H^{\mu\nu} = -N_c^f Q_f^2 e^2 y_f^H \mu^{2\epsilon} \int \frac{d^D k}{(2\pi)^D} \frac{\text{Tr}\left\{(\not{k} - \not{q}' + m_f)\gamma^\nu(\not{k} + m_f)\gamma^\mu(\not{k} - \not{q} + m_f)\right\}}{[(k - q')^2 - m_f^2][k^2 - m_f^2][(k - q)^2 - m_f^2]} \quad (3.27)$$

We can evaluate the trace using the following identities²

Trace Identities

$$\text{Tr}(\gamma^\mu \gamma^\nu) = 4\eta^{\mu\nu} \quad (3.28)$$

$$\text{Tr}(\gamma^\mu \gamma^\nu \gamma^\sigma \gamma^\lambda) = 4(\eta^{\nu\sigma} \eta^{\mu\lambda} - \eta^{\nu\lambda} \eta^{\mu\sigma} + \eta^{\mu\nu} \eta^{\sigma\lambda}) \quad (3.29)$$

$$\text{Tr}(\gamma^{\mu_1} \dots \gamma^{\mu_{2n+1}}) = 0 \quad (3.30)$$

$$\text{Tr}(\gamma^5 \gamma^\mu \gamma^\nu) = 0 \quad (3.31)$$

$$\text{Tr}(\gamma^5 \gamma^\mu \gamma^\nu \gamma^\alpha \gamma^\beta) = -4i\epsilon^{\mu\nu\alpha\beta} \quad (3.32)$$

which give for the trace in (3.27)

$$\text{Tr}\{\dots\} = 4m_f \left[\eta^{\mu\nu}(m_f^2 - k^2 + qq') + (2k^\mu - q^\mu)(2k^\nu - q'^\nu) - q'^\mu q^\nu \right] \quad (3.33)$$

Next, we simplify the denominator by introducing Feynman parameter (see (B.1))

$$\frac{1}{[(k - q')^2 - m_f^2][k^2 - m_f^2][(k - q)^2 - m_f^2]} = \int_0^1 dx \int_0^{1-x} dy \frac{2!}{[(k - xq' - yq)^2 - \Delta]^3} \quad (3.34)$$

where $\Delta = m_f^2 - q'^2 x(1 - x) - q^2 y(1 - y) + 2xyqq'$. The amplitude can now be written as

$$\begin{aligned} i\Gamma_H^{\mu\nu} &= -N_c^f Q_f^2 e^2 y_f^H \int_0^1 dx \int_0^{1-x} dy \int_k \frac{8m_f}{[k^2 - \Delta]^3} \left(\eta^{\mu\nu} \left[m_f^2 + \frac{4-D}{D} k^2 \right. \right. \\ &\quad \left. \left. + (1 - 2xy)qq' - x^2 q'^2 - y^2 q^2 \right] - (1 - 4xy)q'^\mu q^\nu + (2y - 1)(2x - 1)q^\mu q'^\nu \right. \\ &\quad \left. + 2x(2x - 1)q'^\mu q'^\nu + 2y(2y - 1)q^\mu q^\nu \right) \\ &= iN_c^f Q_f^2 e^2 \frac{y_f^H m_f}{4\pi^2} \int_0^1 dx \int_0^{1-x} dy \frac{1}{\Delta} \left(\eta^{\mu\nu} \left[(1 - 4xy)qq' - q'^2 x(2x - 1) \right. \right. \\ &\quad \left. \left. - q^2 y(2y - 1) \right] - (1 - 4xy)q'^\mu q^\nu + (2y - 1)(2x - 1)q^\mu q'^\nu \right. \\ &\quad \left. + 2x(2x - 1)q'^\mu q'^\nu + 2y(2y - 1)q^\mu q^\nu \right) \end{aligned} \quad (3.35)$$

where we have used (B.2) to evaluate the D -dimensional ($D := 4 - 2\epsilon$) momentum integral and afterwards took the limit $\epsilon \rightarrow 0$ as the result does not contain any divergences. Using (3.25), we can see that the Feynman integrals of the gauge variant terms evaluate to zero³ and the vertex function takes the gauge invariant form of (3.26)

$$i\Gamma_H^{\mu\nu}(q, q') = -iN_c^f Q_f^2 e^2 \frac{y_f^H m_f}{2\pi^2} \int_0^1 dx \int_0^{1-x} dy \frac{(1 - 4xy)[qq'\eta^{\mu\nu} - q'^\mu q^\nu]}{q'^2 x(1 - x) - 2xyqq' - m_f^2} \quad (3.36)$$

with an additional factor of 2 coming from the diagram with opposite fermion direction.

²In dimensional regularization, (3.32) is inconsistent with $\{\gamma^\mu, \gamma^5\} = 0$ (" γ^5 -problem"). There are several well known schemes for treating γ^5 in D dimensions. We will use the simplest approach, called Naive Dimensional Regularization (NDR), which keeps both the anticommutation relation and (3.32) in exchange for γ^5 not being well defined [77].

³This can also be explicitly checked, e.g. by expanding in q , evaluating the y -integrals and then substituting $x \rightarrow 1 - x$.

A $\gamma\gamma^*$ Vertex The amplitude for the CP-odd scalar is given by

$$i\Gamma_A^{\mu\nu} = iN_c^f Q_f^2 e^2 y_f^A \mu^{2\epsilon} \int \frac{d^D k}{(2\pi)^D} \frac{\text{Tr}\{\gamma^5(\not{k} - \not{q}' + m_f)\gamma^\nu(\not{k} + m_f)\gamma^\mu(\not{k} - \not{q} + m_f)\}}{[(k - q')^2 - m_f^2][k^2 - m_f^2][(k - q)^2 - m_f^2]} \quad (3.37)$$

The trace evaluates to

$$\text{Tr}\{\dots\} = -4im_f \epsilon^{\mu\nu\alpha\beta} q_\alpha q'_\beta \quad (3.38)$$

and is already in the correct gauge invariant form. The rest of the calculation is analogous to above and the vertex function is given by (again including a factor of 2 from the other fermion loop)

$$i\Gamma_A^{\mu\nu}(q, q') = iN_c^f Q_f^2 e^2 \frac{y_f^A m_f}{2\pi^2} \int_0^1 dx \int_0^{1-x} dy \frac{\epsilon^{\mu\nu\alpha\beta} q_\alpha q'_\beta}{q'^2 x(1-x) - 2xyqq' - m_f^2} \quad (3.39)$$

3.3.2 Two-loop Amplitude

The amplitude of Fig.3.4 can be written as

$$i\Gamma_S^\mu = y_S^\mu \int_k \frac{\gamma_\nu(\not{p}' - \not{k} + m_\mu)\gamma^\mu i\Gamma_S^{\mu\nu}(q, k)}{[(k - p')^2 - m_\mu^2][(k - q)^2 - m_S^2]k^2} \quad (3.40)$$

where $\gamma^H = i$ and $\gamma^A = \gamma^5$. After factoring $x(1-x)$ from the denominator of the integrand, $\Gamma_S^{\mu\nu}$ takes the form of a scalar propagator

$$i\Gamma_S^{\mu\nu}(q, k) \sim \frac{1}{x(1-x)} \frac{f_S(x, y)}{[k^2 - \frac{2y}{1-x}kq - m_f^2(x)]} \quad (3.41)$$

where $f_H(x, y) = 1 - 4xy$, $f_A(x, y) = 1$ and we have defined $m_f^2(x) := m_f^2/x(1-x)$. We can now introduce new Feynman parameters

$$\begin{aligned} & \frac{1}{[(k - p')^2 - m_\mu^2][(k - q)^2 - m_H^2][k^2 - 2kq\frac{y}{1-x} - m_f^2(x)]k^2} \\ &= \int_0^1 ds \int_0^{1-s} dt \int_0^{1-s-t} du \frac{3!}{[(k - sp' - (t + \frac{uy}{1-x})q)^2 - \Delta_S]^4} \end{aligned} \quad (3.42)$$

where $\Delta_S = tm_S^2 + um_f^2(x) + s^2m_\mu^2$. To simplify the gamma structure of the numerator, we use the Dirac equation which gives

$$\bar{u}(p')\not{q}\not{p}'u(p) = 0, \quad \bar{u}(p')\gamma_\nu\not{p}'\gamma^5 u(p) = \bar{u}(p')(2p'_\nu\gamma^5 - m_\mu\gamma_\nu\gamma^5)u(p) \quad (3.43)$$

We further use the relations

$$\begin{aligned} \epsilon^{\mu\nu\alpha\beta}\gamma_\nu\gamma_\beta\gamma^5 &= 2\sigma^{\mu\alpha} \\ i\epsilon^{\mu\nu\alpha\beta}\gamma_\nu\gamma^5 &= \gamma^\mu\gamma^\alpha\gamma^\beta - \eta^{\mu\alpha}\gamma^\beta + \eta^{\mu\beta}\gamma^\alpha - \eta^{\alpha\beta}\gamma^\mu \end{aligned} \quad (3.44)$$

To bring the result into the form of (2.28). Neglecting terms suppressed by m_μ^2 the amplitude can be written as

$$\begin{aligned} i\Gamma_S^\mu &= iN_c^f Q_f^2 e^2 y_S^\mu y_f^S \frac{m_f}{2\pi} \iint dx dy \iiint ds dt du \int_k \frac{f_S(x, y)}{x(1-x)} \frac{3k^2\sigma^{\mu\alpha}q_\alpha}{[k^2 - \Delta_S]^4} \\ &= N_c^f Q_f^2 e^2 \frac{y_\mu^S y_f^S}{(4\pi)^2} \frac{m_f}{2\pi^2} \iint dx dy \frac{f_S(x, y)}{x(1-x)} \iiint ds dt du \frac{\sigma^{\mu\alpha}q_\alpha}{[tm_S^2 + um_f^2(x)]} \\ &= N_c^f Q_f^2 e^2 \frac{y_\mu^S y_f^S}{(4\pi)^2} \frac{m_f}{2\pi^2} \iint dx dy \frac{f_S(x, y)}{x(1-x)} \frac{1}{2} \frac{\sigma^{\mu\alpha}q_\alpha}{m_f^2(x) - m_S^2} \ln\left(\frac{m_f^2(x)}{m_S^2}\right) \end{aligned} \quad (3.45)$$

Finally, the y -integral can be evaluated and after including a factor of 2 for the diagram with exchanged scalar and photon line the fermionic Barr-Zee contribution to a_μ can be written in a compact form as

$$\Delta a_\mu^{2\text{HDM},2} = \frac{\alpha}{\pi} \frac{1}{8\pi^2} \sum_{S,f} N_c^f Q_f^2 y_\mu^S y_f^S \frac{m_\mu m_f}{m_S^2} \mathcal{F}_S^{(2)}\left(\frac{m_f^2}{m_S^2}\right) \quad (3.46)$$

where

$$\mathcal{F}_H^{(2)}(x) = \int_0^1 du \frac{2u(1-u)-1}{x-u(1-u)} \ln\left(\frac{x}{u(1-u)}\right) \quad (3.47)$$

$$\mathcal{F}_A^{(2)}(x) = \int_0^1 du \frac{1}{x-u(1-u)} \ln\left(\frac{x}{u(1-u)}\right) \quad (3.48)$$

3.3.3 Parametrization Uncertainty

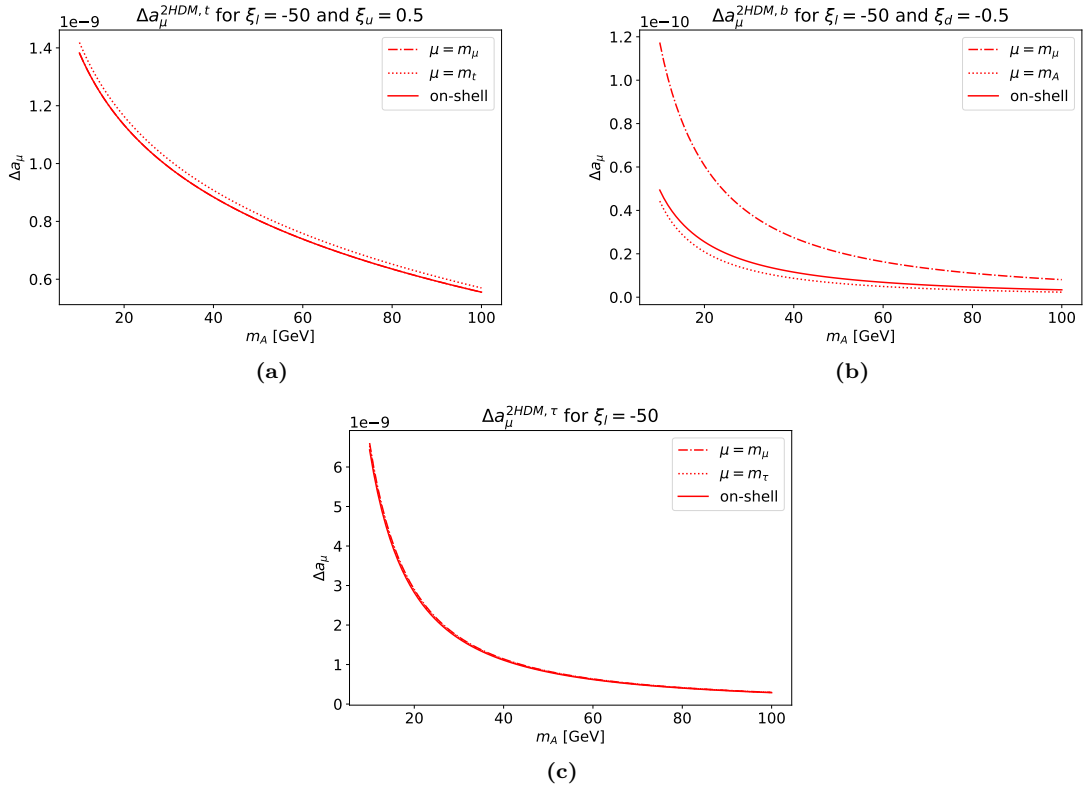


Figure 3.5: Contributions to $\Delta a_\mu^{2\text{HDM},2}$ from the Barr-Zee diagram with CP-odd Higgs and t-quark (a), b-quark (b) and tau-lepton (c) loop as a function of m_A for representative values of the alignment parameters $\xi_l = -50$, $\xi_u = 0.5$ and $\xi_d = -0.5$ and different choices of the renormalization scale μ .

Now that we have obtained results for the two-loop contributions to a_μ in the 2HDM, the important question is which values we should use for the coupling parameters and masses appearing in (3.46). One possible choice would be taking the on-shell values (found in [67]) for the parameters which (approximately) corresponds to $e^{\text{OS}} \approx e^{\text{MS}}(\mu = m_\mu)$ and $m_f^{\text{OS}} \approx m_f^{\text{MS}}(\mu = m_f)$. In principle, we are also free to choose parameters $e(\mu)$, $m_\mu(\mu)$, ... at any other renormalization scale since predictions for the physical observables must ultimately be independent of this arbitrary choice of μ . However, the unphysical μ dependence cancels only if corrections of all orders are included. For fixed order calculations, like in this case,

there will always be a residual μ dependence coming from the corrections at higher orders. In this way, the renormalization scale can potentially be used to reduce higher order uncertainties by choosing μ such that the neglected corrections become as small as possible. Fig.3.5 shows contributions to $\Delta a_\mu^{\text{2HDM},2}$ for different choices of the renormalization scale. We see quite significant differences between the different choices, in particular for the quark contributions where both QCD running and the heavy quark masses have a strong impact on the results. It is worth pointing out that in the case of the top-quark, the on-shell parametrization is essentially given by the low scale ($\mu = m_\mu$) parametrization, while for the bottom-quark it is given by the high scale ($\mu = m_b$) parametrization. This already suggests that the differences between the choice of parametrization in both contributions are of different origin. For the τ lepton the scale dependence is much smaller, which reflects the fact that in this case there won't be any large correction from QCD at 3-loop order. We will discuss the differences between these choices in detail in chapter 6 where we also present the results for the leading 3-loop logarithms. Until then it is not possible to decide which of these parametrizations best captures the higher order corrections.

3.3.4 Asymptotic Expansion of the Loop Functions

In principle, we could now move on to 3-loop order and, after tedious calculation, again obtain a similar result involving much more complicated loop functions. In practice, however, we are only interested in certain limits for the scalar masses like $m_\mu \ll m_S \ll m_t$ ($x \gg 1$). The corresponding asymptotic expansion of the loop functions will then contain powers of large logarithms $\ln x$. Precisely these logarithms can be calculated in a surprisingly simple way using the EFT methods introduced in the next chapter. Here, we want to illustrate how extracting these logarithms from the explicit loop functions can be quite complicated in comparison. This will also provide us with a nice confirmation of the later EFT calculations.

Expansion for $x \rightarrow 0$ Starting with the expansion of $\mathcal{F}_A^{(2)}(x)$, we immediately see that a simple Taylor expansion of the integrand is insufficient, as the lowest order term is already divergent. Instead, we first split the logarithm and treat the two resulting integrals separately.

$$\begin{aligned} \int_0^1 du \frac{\ln(x)}{x - u(1-u)} &= \int_0^1 du \frac{\ln(x)}{(u - \frac{1}{2})^2 - (\frac{1}{4} - x)} \approx 2 \ln(x) \int_{-1-2x}^{1+2x} \frac{dy}{y^2 - 1} \\ &= \ln(x) \ln\left(\frac{y-1}{y+1}\right) \Big|_{-1-2x}^{1+2x} = 2 \ln(x) \ln\left(\frac{x}{1+x}\right) \\ &\approx 2 \ln^2(x) + \mathcal{O}(x) \end{aligned} \quad (3.49)$$

The second integral is slightly more involved and gives

$$\begin{aligned} \int_0^1 du \frac{\ln(u(1-u))}{x - u(1-u)} &= 2 \int_0^1 \frac{\ln(u)}{x - u(1-u)} \\ &\approx 2 \left[\ln(u) \ln\left(\frac{|1-u+x|}{|u-x|}\right) - \int \frac{du}{u} \ln\left(\frac{|1-u+x|}{|u-x|}\right) \right]_0^1 \\ &= 2 \left[\ln(u) \ln\left(\frac{|1-u+x|}{|u-x|}\right) - \ln(u) \ln\left(\frac{1+x}{x}\right) + \text{Li}_2\left(\frac{u}{1+x}\right) - \text{Li}_2\left(\frac{u}{x}\right) \right]_0^1 \\ &= 2 \text{Li}_2\left(\frac{1}{1+x}\right) - 2 \text{Li}_2\left(\frac{1}{x}\right) \approx -\frac{\pi^2}{3} + \ln^2(x) + \mathcal{O}(x) \end{aligned} \quad (3.50)$$

where $\text{Li}_2(z) = -\int dz \frac{\ln(1-z)}{z}$ denotes the Dilogarithm function [78]. For the second loop function we can use

$$\mathcal{F}_H^{(2)}(x) = 4 \int_0^1 du \ln(u) - 2 \ln(x) - (1-2x) \mathcal{F}_A^{(2)}(x) \quad (3.51)$$

From this, we find the following asymptotic expansions

$$\boxed{\begin{aligned}\mathcal{F}_H^{(2)}(x) &\underset{x \rightarrow 0}{\simeq} -4 - \frac{\pi^2}{3} - 2\ln(x) - \ln^2(x) \\ \mathcal{F}_A^{(2)}(x) &\underset{x \rightarrow 0}{\simeq} \frac{\pi^2}{3} + \ln^2(x)\end{aligned}} \quad (3.52)$$

Expansion for $x \rightarrow \infty$ Again, we start with $F_A^{(2)}(x)$ and split up the logarithm. This time, however, we can simply Taylor expand the denominator

$$\begin{aligned}\int_0^1 dz \frac{\ln(x)}{x - z(1-z)} &= \ln(x) \sum_{k=0}^{\infty} \frac{1}{x^{k+1}} \int_0^1 dz [z(1-z)]^k \\ &= \ln(x) \sum_{k=0}^{\infty} \frac{(k!)^2}{(2k+1)!} \frac{1}{x^{k+1}} \approx \frac{\ln(x)}{x} + \mathcal{O}\left(\frac{1}{x^2}\right)\end{aligned} \quad (3.53)$$

and

$$\begin{aligned}\int_0^1 dz \frac{\ln(z(1-z))}{x - z(1-z)} &= 2 \sum_{k=0}^{\infty} \frac{1}{x^{k+1}} \int_0^1 [z(1-z)]^k \ln(z) \\ &= \sum_{k=0}^{\infty} \frac{2}{x^{k+1}} \sum_{n=0}^k \binom{k}{n} (-1)^n \int_0^1 dz \ln(z) z^{k+n} \\ &= \sum_{k=0}^{\infty} \frac{2}{x^{k+1}} \sum_{n=0}^k \binom{k}{n} \frac{(-1)^{n+1}}{(n+k+1)^2} \approx -\frac{2}{x} + \mathcal{O}\left(\frac{1}{x^2}\right)\end{aligned} \quad (3.54)$$

Using again (3.51), the asymptotic expansions are given by

$$\boxed{\mathcal{F}_H^{(2)}(x) \underset{x \rightarrow \infty}{\simeq} -\frac{2}{3} \frac{\ln(x)}{x} - \frac{13}{9x}, \quad \mathcal{F}_A^{(2)}(x) \underset{x \rightarrow \infty}{\simeq} \frac{\ln(x)}{x} + \frac{2}{x}} \quad (3.55)$$

Fig.3.6 illustrates the validity of the asymptotic expansions of the loop functions for the contributions of the Barr-Zee diagram with light ($x \rightarrow 0$) and heavy ($x \rightarrow \infty$) fermions. In both cases the approximations are in very good agreement with the numerical results.

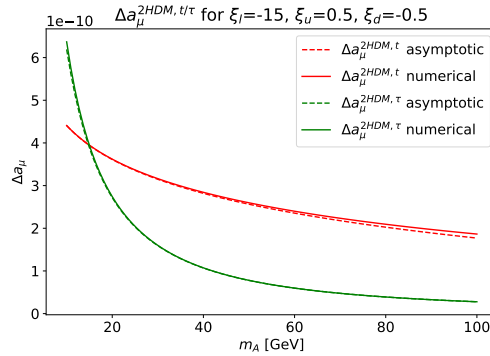


Figure 3.6: Comparison between the asymptotic (dashed) and numerical (continuous) evaluation of the loop function $\mathcal{F}_A(m_f^2/m_A^2)$ in the contribution of the Barr-Zee diagram with CP-odd Higgs and top-quark (red) and τ -lepton (green) as a function of m_A .

4 Effective Field Theory

As we have seen in the last chapter, corrections from Feynman diagrams with multiple different mass scales typically contain logarithms of ratios of these masses. If the scale differences become large, these logarithmic terms give the dominant contribution and can be used to accurately estimate the corrections. At the same time, evaluating the amplitudes of the diagrams can be quite tedious, especially at higher orders where many different diagrams contribute and the Feynman integrals become more complicated. Moreover, in order to obtain simple expressions for the results and extract the logarithmic terms, we have to expand the appearing loop functions which on its own is already not entirely straight forward. This then begs the question whether the whole process can be simplified and the logarithms extracted in a more direct way. In this chapter we will discuss a rather elegant solution to this issue which connects the physical logarithms to the renormalization group running in an appropriate effective field theory (EFT).

4.1 Large Mass Expansion

The main idea for simplifying calculations involving different mass (or momentum) scales is to already expand out the large scale in the integrand rather than the final result. The remaining integrals then contain only a single mass scale and can be evaluated much more easily. There is one subtlety however. As the loop momenta are integrated over, there are regions where they are much larger than the heavy scale. A naive expansion therefore leads to additional divergences and does not reproduce the original result. This reflects the fact that, due to logarithmic terms, the original result is non-analytic in the mass scales and Taylor expansion and integration do not commute. To see how to resolve this issue, let us consider the following simple example with $m \ll M$ [79]

$$I(m, M) = \mu^{2\epsilon} \int \frac{d^D k}{(2\pi)^D} \frac{1}{[k^2 - m^2][k^2 - M^2]} = \overset{p=0}{\text{---}\circ\text{---}} \quad (4.1)$$

For visual reference, we denote propagators of heavy particles by thick lines. The integral can be evaluated exactly using (B.2)

$$I(m, M) = \frac{i}{(4\pi)^2} \left[\frac{1}{\epsilon} + 1 + \ln \left(\frac{\bar{\mu}^2}{M^2} \right) + \underbrace{\frac{m^2}{M^2 - m^2}}_{\approx \frac{m^2}{M^2} + \frac{m^4}{M^4} + \dots} \ln \left(\frac{m^2}{M^2} \right) \right] \quad (4.2)$$

Naively expanding the integrand in powers of $\frac{k^2}{M^2}$ we obtain a second integral

$$\begin{aligned}
I^{\mathcal{T}}(m, M) &= \mu^{2\epsilon} \int \frac{d^D k}{(2\pi)^D} \frac{1}{[k^2 - m^2]} \left(\frac{1}{M^2} + \frac{k^2}{M^4} + \dots \right) \\
&= \text{diagram of a dashed circle with a small loop} \circ \mathcal{T} \left(\text{diagram of two dashed lines meeting at a vertex} \right)
\end{aligned}
\tag{4.3}$$

where $\mathcal{T}(G)$ denotes the *matching diagram* obtained from Taylor expanding the integrand of G where the external momenta and light masses are treated as small compared to M .

This expansion is then inserted into the effective vertex of the *EFT diagram*. Note that some of the external momenta of the matching diagram are loop momenta of the EFT diagram, but are nonetheless treated as small in the Taylor expansion. The integral gives

$$I^{\mathcal{T}}(m, M) = \frac{i}{(4\pi)^2} \left[-\frac{1}{\epsilon} - 1 + \ln\left(\frac{m^2}{\bar{\mu}^2}\right) \right] \cdot \left(\frac{m^2}{M^2} + \frac{m^4}{M^4} + \dots \right) \quad (4.4)$$

As expected, $I^\mathcal{T}$ is not equal to the original integral. Only the terms non-analytic in m are the same in both expressions. This observation holds in general, since expanding in the large scale only modifies the integrand at large loop momenta while the terms non-analytic in m come from the region $|k^2| \ll m^2$ where the expansion in powers of $\frac{k^2}{M^2}$ is justified and gives the correct result. Importantly, this observation implies that the difference

$$\Delta I(m, M) = I(m, M) - I^{\mathcal{T}}(m, M) \quad (4.5)$$

is analytic in m and can be computed by expanding in the light scale. However, the expansion in powers of $\frac{m^2}{k^2}$ in $I^\mathcal{T}$ leaves only scaleless integrals which vanish in dimensional regularization. We therefore find

$$\begin{aligned} \Delta I(m, M) &= \mu^{2\epsilon} \int \frac{d^D k}{(2\pi)^D} \frac{1}{[k^2 - M^2]} \left(\frac{1}{k^2} + \frac{m^2}{k^4} + \dots \right) \\ &= \text{---}\circ\text{---} \circ \mathcal{T}(\text{---}\bigcirc\text{---}) \end{aligned} \quad (4.6)$$

where again $\mathcal{T}(G)$ stands for Taylor expanding the integrand in powers of the external momenta and small masses. We can compute this integral too

$$\Delta I(m, M) = \frac{i}{(4\pi)^2} \left[\frac{1}{\epsilon} + 1 + \ln \left(\frac{\bar{\mu}^2}{M^2} \right) \right] \cdot \left(1 + \frac{m^2}{M^2} + \dots \right) \quad (4.7)$$

and confirm, that $I^\mathcal{T}$ and ΔI indeed add up to give I . The original integral can therefore be expressed diagrammatically as

$$\begin{array}{c} \text{---} \bigcirc \text{---} \end{array} = \begin{array}{c} \text{---} \bigcirc \text{---} \end{array} \circ \mathcal{T} \left(\begin{array}{c} \text{---} \bigcirc \text{---} \end{array} \right) + \begin{array}{c} \text{---} \bigcirc \text{---} \end{array} \circ \mathcal{T} \left(\begin{array}{c} \text{---} \text{---} \end{array} \right) \quad (4.8)$$

This result also holds for more general Feynman diagrams and is known as the large mass expansion (LME) [80–82]

Large Mass Expansion

The amplitude \mathcal{F}_G of a Feynman diagram G containing light and heavy internal lines, but only light external lines with small momenta can be written as

$$\mathcal{F}_G = \sum_{g \in \Omega} \mathcal{F}_{G \setminus g} \circ \mathcal{T}(g) \quad (4.9)$$

where Ω denotes the set of subgraphs $g \subset G$ that are one-particle irreducible (1PI) with respect to the light internal lines¹ and contain all of the heavy lines. $G \setminus g$ denotes the graph where g has been shrunk to a point in G and $\mathcal{T}(g)$ denotes the Taylor expansion of the integrand in \mathcal{F}_g with respect to the light masses and external momenta of g , regardless of whether they are loop momenta in G or not.

¹i.e. diagrams which are connected and stay connected if any one of the light internal lines is cut.

4.1.1 One-Loop Examples

Scalar Contributions As a first example, let us look again at the one-loop diagrams in Fig.3.1 for $m_\mu \ll m_S$. Starting with the neutral scalars we find the following diagrammatic expansions

$$p \text{---} \text{---} p' = \text{---} \square \text{---} \circ \mathcal{T} \left(\text{---} \text{---} \right) + \text{---} \bigcirc \text{---} \circ \mathcal{T} \left(\text{---} \text{---} \right) \quad (4.10)$$

where we left a gap in the last effective vertex to clarify that the fermion loop is not closed and no additional factor of -1 has to be included. The amplitude of the one-loop matching diagram is given by

$$\begin{aligned} \mathcal{T} \left(\text{---} \text{---} \right) &= (y_\mu^S)^2 Q_\mu e \mu^{2\epsilon} \int \frac{d^D k}{(2\pi)^D} \frac{(k + (1 + \eta_S)m_\mu)\gamma^\mu (k + (1 + \eta_S)m_\mu)}{(k^2)^2 [k^2 - m_S^2]} \\ &\quad \times \left(1 - \frac{2kp}{k^2} + \frac{4(kp)^2}{(k^2)^2} + \dots \right) \left(1 - \frac{2kp'}{k^2} + \frac{4(kp')^2}{(k^2)^2} + \dots \right) \\ &\simeq i(y_\mu^S)^2 Q_\mu e \left(\eta_S + \left(\frac{\eta_S}{2} - \frac{1}{3} \right) \epsilon \right) \frac{m_\mu}{m_S^4} \mu^{2\epsilon} \int \frac{d^D k}{(2\pi)^D} \frac{\sigma^{\mu\nu} q_\nu}{k^2 - m_S^2} \\ &= -\eta_S \frac{m_\mu^2}{8\pi^2} \frac{(y_\mu^S)^2}{m_S^2} \left(\frac{1}{\epsilon} + \frac{3}{2} - \frac{\eta_S}{3} + \ln \left(\frac{\bar{\mu}^2}{m_S^2} \right) \right) Q_\mu e \frac{\sigma^{\mu\nu}}{2m_\mu} \end{aligned} \quad (4.11)$$

where $\eta_H = +1$, $\eta_A = -1$. In the second step we have dropped all terms not contributing to a_μ using the Gordon identities (2.26). The Taylor expansions of the tree-level diagrams are given by

$$\begin{aligned} \mathcal{T} \left(\text{---}^H \text{---} \right) &= (-iy_\mu^H \delta_{ab}) \frac{i}{k^2 - m_H^2} (-iy_\mu^H \delta_{ij}) \approx i \frac{(y_\mu^H)^2}{m_H^2} \delta_{ab} \delta_{ij} + \dots \\ \mathcal{T} \left(\text{---}^A \text{---} \right) &= (-y_\mu^A \gamma_{ab}^5) \frac{i}{k^2 - m_A^2} (-y_\mu^A \gamma_{ij}^5) \approx -i \frac{(y_\mu^A)^2}{m_A^2} \gamma_{ab}^5 \gamma_{ij}^5 + \dots \end{aligned} \quad (4.12)$$

Note that the γ^5 matrices do not combine to give $\mathbf{1}$ since they are part of distinct Dirac chains. Inserting this expansion in the corresponding diagram, we find

$$\begin{aligned} \text{---} \bigcirc \text{---} &= -\frac{(y_\mu^S)^2}{m_S^2} Q_\mu e \mu^{2\epsilon} \int \frac{d^D k}{(2\pi)^D} \frac{(k + \not{q} + \eta_S m_\mu)\gamma^\mu (k + \eta_S m_\mu)}{[(k + q)^2 - m_\mu^2][k^2 - m_\mu^2]} \\ &\simeq -\eta_S m_\mu \frac{(y_\mu^S)^2}{m_S^2} Q_\mu e \int_0^1 dx \mu^{2\epsilon} \int \frac{d^D k}{(2\pi)^D} \frac{(1-x)\not{q}\gamma^\mu - x\gamma^\mu \not{q}}{[k^2 - m_\mu^2]^2} \\ &\simeq \eta_S \frac{m_\mu^2}{8\pi^2} \frac{(y_\mu^S)^2}{m_S^2} \left(\frac{1}{\epsilon} + \ln \left(\frac{\bar{\mu}^2}{m_\mu^2} \right) \right) Q_\mu e \frac{\sigma^{\mu\nu} q_\nu}{2m_\mu} \end{aligned} \quad (4.13)$$

where we have used the Gordon identities as well as $\gamma^\mu \gamma^\nu = \eta^{\mu\nu} - i\sigma^{\mu\nu}$ and again discarded terms not contributing to a_μ in each step. Adding both contributions we see that the divergences cancel and we recover the result found from the expansion of the loop functions (3.23).

$$\begin{aligned} \Delta a_\mu^H &\approx -\frac{m_\mu^2}{8\pi^2} \frac{(y_\mu^H)^2}{m_H^2} \left(\frac{7}{6} + \ln \left(\frac{m_\mu^2}{m_H^2} \right) + \mathcal{O} \left(\frac{m_\mu^4}{m_H^4} \right) \right) \\ \Delta a_\mu^A &\approx +\frac{m_\mu^2}{8\pi^2} \frac{(y_\mu^A)^2}{m_A^2} \left(\frac{11}{6} + \ln \left(\frac{m_\mu^2}{m_A^2} \right) + \mathcal{O} \left(\frac{m_\mu^4}{m_A^4} \right) \right) \end{aligned} \quad (4.14)$$

For the charged scalar the expansion looks slightly different.

$$\text{Diagram 1} = \text{Diagram 2} \circ \mathcal{T}(\text{Diagram 3}) + \text{Diagram 4} \circ \mathcal{T}(\text{Diagram 5}) \quad (4.15)$$

Note that in the second diagram there is a massless neutrino running in the loop. The corresponding diagram is therefore scaleless and vanishes². As a consequence, the first diagram already reproduces the original result (3.23)

$$\begin{aligned} \mathcal{T}(\text{Diagram 3}) &\simeq e(y_\mu^A)^2 \mu^{2\epsilon} \int \frac{d^D k}{(2\pi)^D} \frac{(\not{k} - m_\mu) 2k^\mu}{k^2 [k^2 - m_{H^\pm}^2]^2} \left(1 + \frac{2kp}{k^2} + \frac{4(kp)^2}{k^4} + \dots \right) \\ &\simeq -\frac{m_\mu^2 (y_\mu^A)^2}{8\pi^2 m_{H^\pm}^2} \left(\frac{1}{6} + \mathcal{O}\left(\frac{m_\mu^2}{m_{H^\pm}^2}\right) \right) Q_\mu e \frac{\sigma^{\mu\nu} q_\nu}{2m_\mu} \end{aligned} \quad (4.16)$$

Or in other words, in this case, the Taylor expansion and loop integration do commute. This explains why the full result for the charged scalar cannot contain any physical logarithms of mass ratios, because no term in the LME is non-analytic in the small mass scale. On the other hand, the one-loop EFT diagram for the neutral scalars does not vanish and consequently we obtain a logarithm in the full result.

Z-boson Contribution In the first example, we have seen how the LME can give an indication of the logarithmic structure of the full result. Let us consider a second example which shows that, still, some care has to be taken in concluding this structure from the diagrammatic expansion. The contribution of the Z-boson is given by

$$\text{Diagram 6} = \text{Diagram 7} \circ \mathcal{T}(\text{Diagram 8}) + \text{Diagram 9} \circ \mathcal{T}(\text{Diagram 10}) \quad (4.17)$$

which looks exactly like the expansion of the neutral scalar contribution (4.10). We might therefore expect the result to contain a leading logarithm $\ln(\frac{m_\mu^2}{m_Z^2})$. Starting with the tree-level matching condition we find (in the notation of [83])

$$\mathcal{T}(\text{Diagram 10}) \approx -i \frac{g_2^2}{c_W^2 m_Z^2} [\gamma^\alpha (g_V^\mu - g_A^\mu \gamma^5)]_{ab} [\gamma_\alpha (g_V^\mu - g_A^\mu \gamma^5)]_{ij} + \dots \quad (4.18)$$

where $g_V^\mu = \frac{1}{2}t_\mu^3 - Q_\mu s_W^2$ and $g_A^\mu = \frac{1}{2}t_\mu^3$. Inserting this expression into the effective vertex of the one-loop EFT diagram gives

$$\begin{aligned} \text{Diagram 9} &= \frac{g_2^2 Q_\mu e}{c_W^2 m_Z^2} \int_k \frac{\gamma^\alpha (g_V^\mu - g_A^\mu \gamma^5) (\not{k} + \not{q} + m_\mu) \gamma^\mu (\not{k} + m_\mu) \gamma_\alpha (g_V^\mu - g_A^\mu \gamma^5)}{[(k+q)^2 - m_\mu^2][k^2 - m_\mu^2]} \\ &\simeq \frac{g_2^2 Q_\mu e}{c_W^2 m_Z^2} m_\mu \int_0^1 dx \int_k \frac{\gamma^\alpha (g_V^\mu - g_A^\mu \gamma^5) \not{q} \gamma^\mu \gamma_\alpha (g_V^\mu - g_A^\mu \gamma^5)}{[k^2 - m^2]} \\ &\simeq \frac{1}{8\pi^2} \frac{g_2^2}{c_W^2} \frac{m_\mu^2}{m_Z^2} [(g_V^\mu)^2 - (g_A^\mu)^2] \left(\frac{\bar{\mu}^2}{m_\mu^2} \right)^\epsilon \frac{4-D}{\epsilon} Q_\mu e \frac{\sigma^{\mu\nu} q_\nu}{2m_\mu^2} \\ &= \frac{1}{4\pi^2} \frac{g_2^2}{c_W^2} \frac{m_\mu^2}{m_Z^2} [(g_V^\mu)^2 - (g_A^\mu)^2] Q_\mu e \frac{\sigma^{\mu\nu} q_\nu}{2m_\mu^2} \end{aligned} \quad (4.19)$$

The diagram does not vanish, but unlike (4.13) it also does not contain any logarithms because, by chance, the $\frac{1}{\epsilon}$ of the diagram is zero. Like in the case of the charged Higgs, this

²If we allow for a small neutrino mass, the diagram is strongly suppressed by $m_\nu^3/m_{H^\pm}^3$.

means that LME of the Z-boson diagram does not contain any terms non-analytic in m_μ and, again, the full result cannot contain any physical logarithms. For completeness, let us also calculate the one-loop matching condition.

$$\begin{aligned}
 \mathcal{T} \left(\text{diagram} \right) &= -\frac{g_2^2}{c_W^2} Q_\mu e \int_k \frac{\gamma^\alpha (g_V^\mu - g_A^\mu \gamma^5) (\not{k} + \not{p}' + m_\mu) \gamma^\mu (\not{k} + \not{p} + m_\mu) \gamma_\alpha (g_V^\mu - g_A^\mu \gamma^5)}{(k^2)^2 [k^2 - m_S^2]} \\
 &\quad \times \left(1 - \frac{2kp}{k^2} + \frac{4(kp)^2}{(k^2)^2} + \dots \right) \left(1 - \frac{2kp'}{k^2} + \frac{4(kp')^2}{(k^2)^2} + \dots \right) \\
 &\simeq i \frac{g_2^2}{c_W^2} \frac{m_\mu}{m_Z^4} \left[(g_V^\mu)^2 + (g_A^\mu)^2 \right] Q_\mu e \sigma^{\mu\nu} q_\nu \frac{16(4-D)}{D(D+2)} \mu^{2\epsilon} \int \frac{d^D k}{(2\pi)^D} \frac{1}{k^2 - m_z^2} \\
 &= -\frac{1}{4\pi^2} \frac{g_2^2}{c_W} \frac{m_\mu^2}{m_Z^2} \frac{2}{3} \left[(g_V^\mu)^2 + (g_A^\mu)^2 \right] Q_\mu e \frac{\sigma^{\mu\nu} q_\nu}{2m_\mu}
 \end{aligned} \tag{4.20}$$

Their sum reproduces the well known result (see for example [17])

$$\Delta a_\mu^{Z,1} = \frac{1}{4\pi^2} \frac{g_2^2}{c_W^2} \frac{m_\mu^2}{m_Z^2} \left[\frac{1}{3} (g_V^\mu)^2 - \frac{5}{3} (g_A^\mu)^2 \right] \tag{4.21}$$

4.1.2 Constructing the EFT

We have seen how the LME exchanges the calculation of complicated integrals involving multiple different scales for a larger number of much simpler single scale integrals³. Beyond the level of loop integrals, the LME has a very elegant and suggestive diagrammatic representation. The original diagram was, of course, obtained from a perturbative calculation in some QFT specified by a Lagrangian density $\mathcal{L}_{\text{full}}$. Similarly, we would like to have a theory \mathcal{L}_{EFT} that reproduces the EFT diagrams in the expansion. In general, such a Lagrangian can be written as

$$\mathcal{L}_{\text{EFT}}(x) = \sum C_i \mathcal{O}_i(x) \tag{4.22}$$

where $\mathcal{O}_i(x)$ denote composite operators whose Feynman rules give the (effective) vertices of the EFT diagrams and the Wilson coefficients C_i denote the corresponding vertex factors. For example, in the previous section we needed a tree-level vertex with the following Feynman rule

$$\text{diagram} \sim \bar{u}(p') \sigma^{\mu\nu} q_\nu u(p) \tilde{A}_\mu^{cl}(q) \tag{4.23}$$

Such a vertex is generated by the following composite operator (we include a factor of $Q_\mu e$ for later convenience), called the magnetic dipole operator

$$\mathcal{O}(x) = -Q_\mu e \bar{\mu}(x) \sigma^{\alpha\beta} \mu(x) F_{\alpha\beta}^{cl}(x) \equiv H_\mu(x) \tag{4.24}$$

where $\mu(x)$ denotes the muon field and $F_{\mu\nu}^{cl} = \partial_\mu A_\nu^{cl} - \partial_\nu A_\mu^{cl}$. The vertex structure and the values of the Wilson coefficients follow from the results of the matching diagrams. The tree-level matching diagrams (4.12), for instance, result in four-fermion vertices

$$\text{diagram} = iC_{\mathcal{O}_\mu^H} (\bar{u}_1 u_2) (\bar{u}_3 u_4), \quad \text{diagram} = iC_{\mathcal{O}_\mu^A} (\bar{u}_1 \gamma^5 u_2) (\bar{u}_3 \gamma^5 u_4) \tag{4.25}$$

³The EFT diagrams may still contain multiple small scales $m_1 \ll m_2 \ll M$ in which case we can apply the LME again to reduce them to single scale diagrams

where the corresponding composite operators are (suppressing the argument)

$$\mathcal{O}_\mu^H = (\bar{\mu}\mu)(\bar{\mu}\mu), \quad \mathcal{O}_\mu^A = (\bar{\mu}\gamma^5\mu)(\bar{\mu}\gamma^5\mu) \quad (4.26)$$

The values of the Wilson coefficients can also be read off from (4.12)

$$C_{\mathcal{O}_\mu^H} = \frac{(y_\mu^H)^2}{m_H^2}, \quad C_{\mathcal{O}_\mu^A} = -\frac{(y_\mu^A)^2}{m_A^2} \quad (4.27)$$

In principle, the value for C_{H_μ} can also be obtained from the corresponding matching diagram (4.11), however, here we encounter an issue. The value of the matching diagram is μ dependent and contains a divergence. The μ dependence is best understood in the context of renormalization where the fields and parameters become μ dependent. In fact, $C_{\mathcal{O}_\mu^H}$ and $C_{\mathcal{O}_\mu^A}$ also depend on μ via the running of the parameters of the full theory. We will discuss this μ dependence in much more detail in section 4.4, as this will be incredibly useful for calculating the logarithmic corrections we are interested in. For now let us just set $\bar{\mu} = m_S$, in which case the logarithm vanishes⁴, and worry about the divergence. We have seen that the full diagram is finite and that the divergences in the expansion cancel in the sum of the tree-level and one-loop EFT diagram. The divergence in (4.11) is therefore best understood as an EFT counterterm to the one-loop diagram and the matching value for C_{H_μ} should only be read off from the finite part

$$C_{H_\mu}(m_S) = -\frac{1}{32\pi^2} \sum_S (y_\mu^S)^2 \frac{m_\mu}{m_S^2} \left(\frac{3}{2}\eta_S - \frac{1}{3} \right) \quad (4.28)$$

In general, we can construct the relevant EFT by expanding the diagrams of interest and finding the operators that give the correct Feynman rules for the effective vertices. The matching conditions of the corresponding Wilson coefficients are then read off from the finite parts of the matching diagrams. If there are multiple remaining mass scales in the EFT we have to iterate this process until there is only one mass scale left in order to correctly capture all logarithms. Finally, two comments about the operator basis are in order. First, the operators we listed so far obviously do not reproduce the complete LME of the full diagram (4.10). If we had included higher orders in the Taylor expansions we would have encountered new vertex structures that would require additional operators in the Lagrange density. The contributions of such operators are, however, suppressed by higher powers of $\frac{1}{M}$ and can for our purposes be ignored. We will also encounter new operators at higher loop orders in the EFT. Their matching conditions are then suppressed by additional loop factors, however the operators themselves can be important for the renormalization group equations of interest via operator mixing. The second point is that once we have chosen a basis of relevant operators we should make sure that this basis is linearly independent in order to avoid ambiguities in the determination of the Wilson coefficients. The choice of basis is, of course, not unique. For instance, we can always rescale operators without changing the results for the physical observables. Also, certain four-fermion operators are related to each other by Fierz identities [84] and more generally, from any given valid basis we can obtain another by linear transformation. We will discuss both of these points in more detail in section 4.4 as well.

A list of all the operators and corresponding Feynman rules relevant for this thesis can be found in Appendix C.

⁴Note that this only works as long as the scalar masses are (approximately) equal. If they are very different from each other, the logarithms in (4.11) cannot all be eliminated by a choice of the renormalization scale and some Wilson coefficients will contain these large logarithmic contributions. We will address this point in more detail later.

4.2 Renormalization

In principle, once we have constructed the effective theory we can forget about the original theory. Predictions for physical observables in the EFT are completely equivalent to those in the full theory. The advantage of using the effective theory is that we automatically obtain results for the observables in the correct $\frac{1}{M}$ expansion. The EFT is therefore particularly useful if higher order terms in this expansion drop off quickly, as is the case for low-energy observables like a_μ . For the calculation of the leading logarithmic corrections we will see that only the lowest order matching conditions are relevant. To construct the EFT, we therefore need to calculate only very few simple matching diagrams. Now, suppose we have found the relevant operator basis $\{\mathcal{O}_i\}$ together with the bare Lagrangian

$$\mathcal{L}_{\text{EFT}}(x) = \sum C_i^0 \mathcal{O}_i^0(x) \quad (4.29)$$

Like in any generic QFT, loop calculations in this theory will, in general, produce divergences. To obtain sensible results for the observables we must therefore first renormalize the EFT. For this, let us briefly introduce some new terminology. First, we are free to include any function $f(e^0, m^0, \dots)$ of the parameters into the definition of the composite operators. In general, we can then write the operators as

$$\mathcal{O}_i^0(x) = f_i(e^0, m^0, \dots) \tilde{\mathcal{O}}_i^0(x) \quad (4.30)$$

where the *composite fields* $\tilde{\mathcal{O}}_i^0(x)$ denote just the field content of the operator. For example

$$H_\mu^0 = -Q_\mu e^0 \bar{\mu}^0 \sigma^{\alpha\beta} \mu^0 F_{\alpha\beta}^{\text{cl},0} \implies \tilde{H}_\mu^0 = \bar{\mu}^0 \sigma^{\alpha\beta} \mu^0 F_{\alpha\beta}^{\text{cl},0}, \quad f_{H_\mu}(e^0) = -Q_\mu e^0 \quad (4.31)$$

A dim- n operator \mathcal{O}_i (i.e. for which $[\tilde{\mathcal{O}}_i] = n$) is called *renormalizable* if $n \leq 4$ and *non-renormalizable* for $n > 4$. Theories with only renormalizable operators, like QED or the SM, require only a finite set of parameters to fully absorb all divergences while theories with non-renormalizable operators will always result in additional new divergences at higher orders in $\frac{1}{M}$. The new operators and Wilson coefficients needed to cancel those divergences can, in principle, then contribute to the observables we are interested in, however, only at these higher orders in $\frac{1}{M}$. For practical purposes, we can therefore fix the order of the $\frac{1}{M}$ expansion and ignore all contributions (divergent or not) at higher orders. In this way, we obtain a finite basis of relevant composite operators.

With this, let us now go on to renormalize the EFT. As in section 2.3.3, we start by introducing field strength renormalization factors for the fundamental fields

$$\mu^0(x) = \sqrt{Z_\mu(\mu)} \mu(x; \mu), \quad A_\mu^0(x) = \sqrt{Z_\gamma(\mu)} A_\mu(\mu), \quad \dots \quad (4.32)$$

and split the parameters of the renormalizable operators (i.e. masses and gauge couplings) into

$$e^0 = \mu^\epsilon Z_e(\mu) e(\mu), \quad m^0 = Z_m(\mu) m(\mu), \quad \dots \quad (4.33)$$

with these definitions, the composite operators are given by

$$\mathcal{O}_i^0 = \mu^{\zeta_i \epsilon} Z_{f_i}(\mu) f_i(e(\mu), m(\mu), \dots) Z_{\tilde{\mathcal{O}}_i}(\mu) \tilde{\mathcal{O}}_i(\mu) \equiv \mu^{\zeta_i \epsilon} Z_{\mathcal{O}_i}(\mu) \mathcal{O}_i(\mu) \quad (4.34)$$

For the dipole operator this means (suppressing the arguments)

$$H_\mu^0 = \mu^\epsilon Z_{H_\mu}(-Q_\mu e) \mu \sigma^{\alpha\beta} \mu F_{\alpha\beta}^{\text{cl}}, \quad Z_{H_\mu} = Z_e Z_\mu \sqrt{Z_A} \quad (4.35)$$

Lastly, we would like to treat the Wilson coefficients just like the parameters of the renormalizable operators. In particular, the renormalized coefficients should also have integer

dimension. For that we need to know the dimensions of the composite operators. Let us write $[\mathcal{O}_i] = n - (2 + \xi_i)\epsilon$, then for \mathcal{L}_{EFT} to have dimension D we need $[C_i] = 4 - n + \xi_i\epsilon$. Note that for $n > 4$, the Wilson coefficients scale like $\frac{1}{M^{n-4}}$ which is precisely what we already found in (4.27) for the dim-6 four-fermion operators: $C_{\mathcal{O}_\mu^{(5)}} \sim \frac{1}{m_S^2}$. For the dim-5 dipole operator we found $C_{H_\mu} \sim \frac{m_\mu}{m_S^2}$ which scales like $\frac{1}{m_S}$ with an extra suppression $\frac{m_\mu}{m_S}$ coming from the fact that the dipole operator is chirality flipping. For this reason, H_μ is often treated as a dim-6 operator by absorbing a factor of the muon mass m_μ into f_{H_μ} . However, since in the Barr-Zee diagrams the chirality flip comes with a factor of the dimensionless coupling y_f^S rather than the muon mass directly, we will continue with the definition given above and leave the suppression factors implicit in the matching condition. In general, we can write the bare coefficients as

$$C_i^0 = \mu^{\xi_i\epsilon} Z_{C_i}(\mu) C_i(\mu) \quad (4.36)$$

4.2.1 Counterterm Structure

In general, the renormalization factors can be written as

$$Z(\mu) = 1 + \sum_{n=0}^{\infty} \frac{Z^{[n]}(\mu)}{\epsilon^n} \quad (4.37)$$

where the $Z^{[n]}$ are dimensionless functions of the parameters of the theory. In particular, we will use the minimal subtraction (MS) scheme, defined by $Z^{[0]} = 0$. To find the general structure of the remaining coefficients, let us rewrite the EFT Lagrangian in terms of the renormalized quantities

$$\mathcal{L}_{\text{EFT}} = \sum \mu^{(\xi_i + \varsigma_i)\epsilon} f_i(e, m, \dots) C_i \tilde{\mathcal{O}}_i + \mathcal{L}_{\text{EFT,ct}} \quad (4.38)$$

The coefficients of the divergences in the (sub-renormalized) Feynman diagrams obtained from this Lagrangian are polynomials in the $f_i C_i$. The general structure of the required counterterms can therefore be obtained by simple dimensional analysis.

$$Z_{C_i} C_i = C_i + \sum_{j_n} \tilde{Z}_{C_i, C_1^{j_1} \dots C_N^{j_N}} (f_1 C_1)^{j_1} \dots (f_N C_N)^{j_N}, \quad \forall \{j_n\} : [C_i] = \sum_{n=1}^N j_n [f_n C_n] \quad (4.39)$$

where N denotes the number of operators in the EFT and the coefficients $\tilde{Z}_{C_i, \dots}$ are purely numerical constants. Similarly, we can write the operator renormalization factors as

$$Z_{\mathcal{O}_i} = 1 + \sum_{j_n} \tilde{Z}_{\mathcal{O}_i, C_1^{j_1} \dots C_N^{j_N}} (f_1 C_1)^{j_1} \dots (f_N C_N)^{j_N}, \quad \forall \{j_n\} : 0 = \sum_{n=1}^N j_n [f_n C_n] \quad (4.40)$$

Example To better understand this slightly cryptic notation, let us consider the one-loop contribution of H_μ to the muon mass renormalization.

$$\begin{aligned} i\Sigma_{H_\mu}(\not{p}) &= \text{diagram 1} + \text{diagram 2} + \text{diagram 3} \\ &= 2iC_{H_\mu}(Q_\mu e)^2 \mu^{2\epsilon} \int \frac{d^D k}{(2\pi)^D} \left(\frac{\sigma^{\alpha\beta} k_\beta (\not{k} + \not{p} + m_\mu) \gamma_\alpha}{[(k+p)^2 - m_\mu^2] k^2} \right. \\ &\quad \left. - \frac{\gamma_\alpha (\not{p} + \not{k} + m_\mu) \sigma^{\alpha\beta} k_\beta}{[(k+p)^2 - m_\mu^2] k^2} + 2iC_{H_\mu} \frac{\sigma^{\alpha\beta} k_\beta (\not{p} + \not{k} + m_\mu) \sigma_{\alpha\rho} k^\rho}{[(k+p)^2 - m_\mu^2] k^2} \right) \\ &= -iC_{H_\mu}(Q_\mu e)^2 \frac{3}{8\pi^2} \left(m_\mu \not{p} + 2m_\mu^2 - p^2 \right) \frac{1}{\epsilon} \\ &\quad - iC_{H_\mu}^2 (Q_\mu e)^2 \frac{1}{8\pi^2} \left(4m_\mu^2 \not{p} + 6m_\mu^3 - \frac{7}{6} p^2 \not{p} + 2m_\mu p^2 \right) \frac{1}{\epsilon} + \dots \end{aligned} \quad (4.41)$$

From this we can directly read off the contribution to the muon field strength renormalization

$$Z_\mu^{[1]} = -\frac{3Q_\mu}{8\pi^2} e m_\mu (-Q_\mu e C_{H_\mu}) + \frac{1}{2\pi^2} m_\mu^2 (-Q_\mu e C_{H_\mu})^2 \quad (4.42)$$

which in the notation of (4.40) gives

$$\tilde{Z}_{\mu, e m C_{H_\mu}} = -\frac{3Q_\mu}{8\pi^2}, \quad \tilde{Z}_{\mu, m^2 C_{H_\mu}^2} = \frac{1}{2\pi^2} \quad (4.43)$$

We also find some unusual p^2 and $\not{p}p^2$ terms in the result. These are exactly the kind of new divergences that require additional operators to be removed. In this case we would need to add operators like

$$\bar{\mu} \partial^2 \mu \quad \text{and} \quad \bar{\mu} \partial^2 \not{p} \mu \quad (4.44)$$

with matching conditions for the corresponding Wilson coefficients from self energy diagrams involving the heavy scalars. However, as discussed before, their contributions to any process will be suppressed by higher orders in $\frac{m_\mu}{m_S}$ with respect to the contributions of the dim-4 kinetic terms.

4.2.2 Renormalized Lagrangian

Having found the structure of the renormalization factors (4.39) and (4.40), we can now express the entire EFT Lagrangian in terms of the renormalized Wilson coefficients and operators as

$$\begin{aligned} \mathcal{L}_{\text{EFT}} &= \sum C_i^0 \mathcal{O}_i^0 = \sum \mu^{(\xi_i + \varsigma_i)\epsilon} \left(C_i + \sum_{j_n} \tilde{Z}_{C_i, C_1^{j_1} \dots C_N^{j_N}} (f_1 C_1)^{j_1} \dots (f_N C_N)^{j_N} \right) \\ &\quad \times \left(1 + \sum_{k_n} \tilde{Z}_{\mathcal{O}_i, C_1^{k_1} \dots C_N^{k_N}} (f_1 C_1)^{k_1} \dots (f_N C_N)^{k_N} \right) \mathcal{O}_i \\ &\equiv \sum \mu^{(\xi_i + \varsigma_i)\epsilon} \left(C_i + \sum_{j_n} \hat{Z}_{\mathcal{O}_i, C_1^{j_1} \dots C_N^{j_N}} (f_1 C_1)^{j_1} \dots (f_N C_N)^{j_N} \right) \mathcal{O}_i \\ &\equiv \sum \mu^{(\xi_i + \varsigma_i)\epsilon} \left(C_i + \sum_{j_n} Z_{\mathcal{O}_i, C_1^{j_1} \dots C_{N'}^{j_{N'}}} C_1^{j_1} \dots C_{N'}^{j_{N'}} \right) \mathcal{O}_i \end{aligned} \quad (4.45)$$

The coefficients $\hat{Z}_{C_i, \dots}$ are obtained by multiplying out the two brackets and the $Z_{C_i, \dots}$ are defined by absorbing all functions f_n and all parameters of the renormalizable operators into $\hat{Z}_{C_i, \dots}$. N' therefore denotes the number of non-renormalizable operators in the EFT. The coefficients defined this way directly correspond to the counterterms that can be read off from the diagrams. For example, the diagram in (4.13) gives

$$Z_{H_\mu, C_{\mathcal{O}_\mu^H}} = Z_{H_\mu, C_{\mathcal{O}_\mu^A}} = -\frac{m_\mu}{32\pi^2} \frac{1}{\epsilon} \quad (4.46)$$

Like (4.37), we can also expand the coefficients in powers of $\frac{1}{\epsilon}$

$$Z_{C_i, C_1^{j_1} \dots C_{N'}^{j_{N'}}} = \sum_{n=1}^{\infty} \frac{1}{\epsilon^n} Z_{C_i, C_1^{j_1} \dots C_{N'}^{j_{N'}}}^{[n]} \quad (4.47)$$

Note that $Z_{\mathcal{O}_i, \dots}^{[l]}$ contains contributions from the $\frac{1}{\epsilon^l}$ poles of all l -loop and higher order diagrams with the same insertions of effective vertices, because we absorbed the coupling parameters of the renormalizable operators into its definition. On the other hand, $\hat{Z}_{C_i, \dots}^{[l]}$ specifies the order in all of the coupling parameters and is therefore given by the $\frac{1}{\epsilon^l}$ pole of only those diagrams with this particular order in the coupling parameters.

4.3 Logarithms, Poles and the Renormalization Scale

Let us now further investigate the connection between the logarithmic terms in the full and effective theory. The main point to stress here is that the physical logarithms in the full result come from asymptotic expansions of the loop functions and are in no way connected to the divergences that may or may not appear in the calculation too. In contrast, the LME splits the diagrams into matching and EFT contributions which are simpler to calculate, but individually cannot produce the physical logarithms as they are non-analytic only in a single scale. Instead, logarithms always appear together with the unphysical renormalization scale and additional divergences that are not present in the original diagram

$$\begin{aligned} G_{\text{EFT}} &\sim \left(\frac{\bar{\mu}^2}{m^2}\right)^{n\epsilon} \frac{1}{\epsilon^n} = \frac{1}{\epsilon^n} + \dots + \frac{n^n}{n!} \ln\left(\frac{\bar{\mu}^2}{m^2}\right)^n \\ G_{\text{match}} &\sim \left(\frac{\bar{\mu}^2}{M^2}\right)^{l\epsilon} \frac{1}{\epsilon^l} = \frac{1}{\epsilon^l} + \dots + \frac{l^l}{l!} \ln\left(\frac{\bar{\mu}^2}{M^2}\right)^l \end{aligned} \quad (4.48)$$

In the sum of all EFT diagrams the μ dependence and additional divergences cancel and give back the original result. At this point we can make the following observation: If we choose $\mu = M$ the logarithms are fully contained in G_{EFT} and if we choose $\mu = m$ they are fully contained in G_{match} . This, of course, drastically reduces the number of diagrams needed to calculate the leading logarithmic terms. To find the optimal approach let us explore both strategies in more detail.

4.3.1 Strategy I: $\mu = M$

If we choose $\mu = M$ all logarithms are contained in the EFT diagrams. To find the leading logarithmic l -loop contributions to some process given at tree-level by the operator \mathcal{O}_i , we need to consider all l -loop diagrams $G_i^{(l)}$ that produce the same vertex structure as \mathcal{O}_i . In particular, let us focus on all EFT diagrams with the same order in the coupling parameters. The sum of their amplitudes can be written as

$$\mathcal{F}_{G_i^{(l)}} = \hat{Z}_{C_i, C_1^{j_1} \dots C_N^{j_N}}^{[l]} (f_1 C_1)^{j_1} \dots (f_N C_N)^{j_N} \left(\frac{M^2}{m^2}\right)^{l\epsilon} \frac{c^{(l)}}{\epsilon^l} (1 + \mathcal{O}(\epsilon)) \langle \mathcal{O}_i \rangle \quad (4.49)$$

where $\langle \mathcal{O}_i \rangle$ denotes the Feynman rule of the operator and $c^{(l)}$ some numerical constant. For example, the diagram in (4.13) gives

$$\begin{aligned} \text{Diagram} &\simeq \underbrace{\frac{-1}{32\pi^2}}_{\hat{Z}_{CH_\mu, m_\mu C_{\mathcal{O}_\mu^A}}^{[1]}} m_\mu^2 C_{\mathcal{O}_\mu^A} \left(\frac{m_A^2}{m_\mu^2}\right)^\epsilon \frac{-1}{\epsilon} \cdot \underbrace{2Q_\mu e \sigma^{\mu\nu} q_\nu}_{\langle H_\mu \rangle} \end{aligned} \quad (4.50)$$

If there were more diagrams of this type, the only thing that could be different are their relative contributions to $c^{(l)}$ in the sum. Similarly, we can write the counterterm diagrams that renormalize the EFT diagram as

$$\mathcal{F}_{G_{i,ct}^{(l_{ct})}} = \hat{Z}_{C_i, C_1^{j_1} \dots C_N^{j_N}}^{[l]} (f_1 C_1)^{j_1} \dots (f_N C_N)^{j_N} \left(\frac{M^2}{m^2}\right)^{l_{ct}\epsilon} \frac{c^{(l_{ct})}}{\epsilon^{l_{ct}}} (1 + \mathcal{O}(\epsilon)) \langle \mathcal{O}_i \rangle \quad (4.51)$$

where l_{ct} denotes the actual number of loops in the counterterm diagram. Of course, due to the counterterm insertions we still find an overall $\frac{1}{\epsilon}$ divergence. In particular, since $\hat{Z}_{C_i, C_1^{j_1} \dots C_N^{j_N}}^{[l]} (f_1 C_1)^{j_1} \dots (f_N C_N)^{j_N}$ denotes the overall tree-level counterterm that has to be

added after sub-renormalization of $\mathcal{F}_{G_i^{(l)}}$ to remove all remaining local divergences, we have by definition $c^{(0_{ct})} = 1$. To obtain the remaining coefficients, we use the fact that in the renormalized amplitude

$$\mathcal{F}_{G_i^{(l)}} + \sum \mathcal{F}_{G_{i,ct}^{(l_{ct})}} \quad (4.52)$$

all (non-analytic) divergences must cancel. If we now expand out the mass ration

$$\left(\frac{M^2}{m^2}\right)^{l_\epsilon} \frac{1}{\epsilon^l} = \frac{1}{\epsilon^l} + \frac{l \ln\left(\frac{M}{m}\right)}{\epsilon^{l-1}} + \frac{l^2 \ln\left(\frac{M}{m}\right)^2}{2\epsilon^{l-2}} + \dots \quad (4.53)$$

we find non-analytic lower order $\frac{1}{\epsilon}$ poles that can only be cancelled by the corresponding expansion in the counterterm diagrams. This results in a system of l equations that determine the coefficients $c^{(l)}$ and $c^{(l_{ct})}$

$$\begin{aligned} c^{(l)} + \sum c^{(l_{ct})} &= 0 \\ l c^{(l)} + \sum l_{ct} c^{(l_{ct})} &= 0 \\ l^2 c^{(l)} + \sum l_{ct}^2 c^{(l_{ct})} &= 0 \\ &\dots \\ l^{l-1} c^{(l)} + \sum l_{ct}^{l-1} c^{(l_{ct})} &= 0 \end{aligned} \quad (4.54)$$

Once we have solved this system and obtained the coefficients, the leading l -loop logarithm produced by these diagrams is given by

$$\begin{aligned} \mathcal{F}_{G_i^{(l)}} + \sum \mathcal{F}_{G_{i,ct}^{(l_{ct})}} &\sim \hat{Z}_{C_i, C_1^{j_1} \dots C_N^{j_N}}^{[l]} (f_1 C_1)^{j_1} \dots (f_N C_N)^{j_N} \\ &\times \left(c^{(l)} \frac{l^l}{l!} + \sum c^{(l_{ct})} \frac{l_{ct}^l}{l!} \right) \ln\left(\frac{M^2}{m^2}\right)^l \langle \mathcal{O}_i \rangle \end{aligned} \quad (4.55)$$

Let us emphasize that the coefficients $c^{(l)}$ and $c^{(l_{ct})}$ are universal for a given loop order l . The leading logarithmic term at l -loop order therefore only depends on the counterterm $\hat{Z}_{C_i, \dots}^{[l]}$. Of course, it seems like we still have to perform the l -loop matching calculation to obtain this counterterm, but we will see in section 4.4 that its value can be obtained in a much simpler way using the renormalization group consistency conditions.

There is one other problem however. The values for the physical observables are related to the amplitudes of diagrams via the LSZ formula. As we have seen in section 2.3.3, this means we need to include normalization factors that cancel the μ dependence to give the physical results. Since these normalization factors are determined from the self-energy corrections of the light fields, setting $\mu = M$ results in additional leading logarithms which are not accounted for in (4.55). For example, in (2.45) we found $a_\mu = R(\mu) F_M(0; \mu)$ where the normalization factor $R(\mu)$ is obtained from the muon self-energy by (2.41). At one-loop the self-energy is given by

$$\Sigma(\not{p}; \mu) = \frac{Q_\mu^2 e^2}{(4\pi)^2} \frac{1}{\epsilon} \int_0^1 dx \left[(D-2)x \not{p} - D m_f \right] \left(\frac{\bar{\mu}^2}{x(1-x)} \right)^\epsilon \frac{1}{[m_\mu^2/x - p^2]^\epsilon} \quad (4.56)$$

which gives for the normalization factor

$$R(M) \approx 1 - \frac{Q_\mu^2 e^2}{16\pi^2} \ln\left(\frac{M^2}{m_\mu^2}\right) + \dots \quad (4.57)$$

To determine the correct l -loop leading logarithm we therefore also need to include contributions from all lower order leading logarithms in $F_M(0; \mu)$ multiplied with the leading terms in $R(\mu)$. Keeping track off all these different terms can quickly become cumbersome. Setting $\mu = m$ obviously avoids this problem and, as we will discuss now, provides us therefore with a more direct way of obtaining the leading logarithms.

4.3.2 Strategy II: $\mu = m$

As we have seen, setting $\mu = m$ means that we do not need to worry about the LSZ normalization factors and the leading logarithms are captured fully in the highest order matching diagrams. This strategy has the major advantage that we do not have to keep track of multiple sources of leading logarithms at every order and is therefore the one used in the literature [12–17]. The logarithmic terms in the matching diagrams arise just like those in the EFT diagrams in the last section and can, in principle, be calculated in the same way. However, we can avoid this calculation using the following idea. In the EFT, we understood the finite parts of the matching diagrams as the vertex factors of the effective vertices. These matching conditions were particularly simple if we evaluated the diagrams at the large scale $\mu = M$. Now, suppose we have a differential equation for the Wilson coefficients

$$\frac{dC_i(\mu)}{d\ln(\mu)} = \beta(C_k) \quad (4.58)$$

where $\beta(C_k)$ will be some function of the coefficients. We can then solve the equation with the initial values given by the matching conditions at the large scale. The leading logarithms at any given loop order are then completely contained in the Wilson coefficient of the operator that produces the process we are interested in at tree-level. For example, the anomalous magnetic moment a_μ is generated at tree-level by the operator H_μ

$$\langle C_{H_\mu} H_\mu \rangle = 2C_{H_\mu} Q_\mu e\sigma^{\mu\nu} q_\nu \quad \implies \quad a_\mu^{\text{tree-level}} = 4m_\mu C_{H_\mu} \quad (4.59)$$

and all leading logarithmic corrections to a_μ are thus contained in $C_{H_\mu}(m_\mu)$.

Our goal now is to find the exact form of (4.58). We can then solve this equation iteratively and directly read off the leading logarithms.

4.4 The EFT Renormalization Group Equation

The main idea behind the renormalization group equation (RGE) is that bare quantities, such as C_i^0 , are independent of the renormalization scale μ . This allows us to directly write down equations like

$$\frac{dC_i^0}{d\ln(\mu)} = 0 \quad (4.60)$$

On the other hand, in section 4.2 we have already written the bare quantities in terms of μ dependent renormalization factors and finite renormalized quantities. Together with (4.60) this lets us deduce the renormalization group equations for all of the μ dependent quantities.

4.4.1 General Renormalization Group Equations

Inserting (4.36) together with the counterterm structure (4.39) into the above equation, we find

$$\begin{aligned} 0 = & \xi_i \epsilon \left(C_i + \sum_{j_n} \tilde{Z}_{C_i, C_1^{j_1} \dots C_N^{j_N}} (f_1 C_1)^{j_1} \dots (f_N C_N)^{j_N} \right) + \frac{dC_i}{d\ln(\mu)} \\ & + \sum_{j_n} \tilde{Z}_{C_i, C_1^{j_1} \dots C_N^{j_N}} \left(\frac{d(f_1 C_1)^{j_1}}{d\ln(\mu)} \dots (f_N C_N)^{j_N} + \dots + (f_1 C_1)^{j_1} \dots \frac{d(f_N C_N)^{j_N}}{d\ln(\mu)} \right) \end{aligned} \quad (4.61)$$

Since f_k depends on μ only via the coupling parameters, we have

$$\frac{d(f_k C_k)^{j_k}}{d \ln(\mu)} = j_k (f_k C_k)^{j_k-1} \left(f_k \frac{dC_k}{d \ln(\mu)} + C_k \sum_r \frac{\partial f_k}{\partial C_r} \frac{dC_r}{d \ln(\mu)} \right) \quad (4.62)$$

We can now look at (4.61) order by order in ϵ . Both the renormalized Wilson coefficients and the functions f_k do not contain any divergences. The coefficients $\tilde{Z}_{C_i, \dots}$, however, start at order $\frac{1}{\epsilon}$ (in the MS scheme). Therefore, to $\mathcal{O}(\epsilon)$ we find

$$0 = \xi_i \epsilon C_i + \frac{dC_i}{d \ln(\mu)} \Big|_{\mathcal{O}(\epsilon)} \quad (4.63)$$

Since C_i is completely finite, this implies

$$\frac{dC_i}{d \ln(\mu)} = -\xi_i \epsilon C_i + \beta(C_i) \quad (4.64)$$

where $\beta(C_i)$ is called the beta function of C_i , which is finite and ϵ independent. With this we can collect the $\mathcal{O}(\epsilon^0)$ terms

$$\begin{aligned} 0 = \xi_i & \left(\sum_{j_n} \tilde{Z}_{C_i, C_1^{j_1} \dots C_N^{j_N}}^{[1]} (f_1 C_1)^{j_1} \dots (f_N C_N)^{j_N} \right) + \beta(C_i) \\ & - \sum_{j_n} \tilde{Z}_{C_i, C_1^{j_1} \dots C_N^{j_N}}^{[1]} (f_1 C_1)^{j_1} \dots (f_N C_N)^{j_N} \sum_k j_k \left(\xi_k + \sum_r \frac{1}{f_k} \frac{\partial f_k}{\partial C_r} \xi_r C_r \right) \end{aligned} \quad (4.65)$$

From this we already obtain the beta function of the Wilson coefficients in the MS scheme

$$\boxed{\beta(C_i) = - \sum_{j_n} \left(\xi_i - \sum_k j_k [\xi_k + \gamma(f_k)] \right) \tilde{Z}_{C_i, C_1^{j_1} \dots C_N^{j_N}}^{[1]} (f_1 C_1)^{j_1} \dots (f_N C_N)^{j_N}} \quad (4.66)$$

where we have introduced the notation

$$\gamma(f_k) = \sum_r \frac{1}{f_k} \frac{\partial f_k}{\partial C_r} \xi_r C_r \quad (4.67)$$

Remarkably, we find that the RGE depends only on the $\frac{1}{\epsilon}$ poles of the renormalization factors and not on the higher order pole terms. Of course, diagrams of any loop order contribute to this coefficient, so one-loop calculations are not sufficient to fully determine the beta functions of the Wilson coefficients. At the same time, higher order diagrams obviously contribute only at higher orders in the coupling constants and can therefore often times be ignored. We could stop here and further examine the RGE, however, if we keep going and look at the higher order poles in (4.61) we find an infinite set of consistency conditions that, rather surprisingly, imply relations between the coefficients of different $\frac{1}{\epsilon}$ poles. In general, at $\mathcal{O}(\frac{1}{\epsilon^l})$ we get the following equation

$$\begin{aligned} 0 = \sum_{j_n} & \left(\xi_i - \sum_k j_k [\xi_k + \gamma(f_k)] \right) \tilde{Z}_{C_i, C_1^{j_1} \dots C_N^{j_N}}^{[l+1]} (f_1 C_1)^{j_1} \dots (f_N C_N)^{j_N} \\ & + \sum_{i_n} \left(\sum_k i_k \left[\frac{\beta(C_k)}{C_k} + \sum_r \frac{1}{f_k} \frac{\partial f_k}{\partial C_r} \beta(C_r) \right] \right) \tilde{Z}_{C_i, C_1^{i_1} \dots C_N^{i_N}}^{[l]} (f_1 C_1)^{i_1} \dots (f_N C_N)^{i_N} \end{aligned} \quad (4.68)$$

This equation holds for each order of the coupling parameters separately and therefore the coefficients $\tilde{Z}_{C_i, \dots}^{[l+1]}$ are already determined by the coefficients $\tilde{Z}_{C_i, \dots}^{[l]}$ and EFT beta functions. In

particular, if we know $Z_{C_i, \dots}^{[1]}$ we can use these equations to obtain all higher order coefficients. This is precisely what we wanted in section 4.3.1 in order to calculate the leading logarithms. However, due to the complicated beta functions, sorting out the correct terms in the second line is quite tedious. In the next section we will make a couple of simplifying assumptions to bring both this equation and the beta functions into a nicer and more useable form. Lastly, in the same way as above we can also obtain a RGE for the operators

$$\frac{d\mathcal{O}_i}{d\ln(\mu)} = -\varsigma_i \mathcal{O}_i + \sum_{j_n} \left(\sum_k j_k [\xi_k + \gamma(f_k)] \right) \tilde{Z}_{\mathcal{O}_i, C_1^{j_1} \dots C_N^{j_N}}^{[1]} (f_1 C_1)^{j_1} \dots (f_N C_N)^{j_N} \mathcal{O}_i \quad (4.69)$$

4.4.2 The Anomalous Dimension Matrix

We now have the general RGE for the Wilson coefficients as well as a set of consistency conditions which can be used to determine the higher order renormalization constants. In their current form, however, applying them in actual calculations is quite complicated for two reasons

- (i) The RGEs are N non-linear coupled differential equations.
- (ii) The coefficients $\tilde{Z}_{C_i, \dots}^{[1]}$ and $\tilde{Z}_{\mathcal{O}_i, \dots}^{[1]}$ cannot be read off from the diagrams directly but have to be reconstructed from the renormalization constants $Z_{C_i, \dots}^{[1]}$ in the Lagrangian.

Let us start with the first point. Integrating (4.64) in the limit $\epsilon \rightarrow 0$ gives the following expression

$$C_i(\mu) = C_i(M) - \int_{\mu}^M \beta(C_i(\mu')) d\ln(\mu') \quad (4.70)$$

In the spirit of perturbation theory, we can iteratively replace the $C_k(\mu)$ in $\beta(C_i)$ by the right hand side which results in an expression involving a mess of nested integrals. The point, however, is that we have expressed the running Wilson coefficients in the integrals by the Wilson coefficients evaluated at the high scale, which are constant. If we stop the expansion at some point and ignore higher order terms, the nested integrals can be evaluated using

$$\int_{\mu}^M \ln^n \left(\frac{M}{\mu'} \right) d\ln(\mu') = \frac{1}{n+1} \ln^{n+1} \left(\frac{M}{\mu} \right) \quad (4.71)$$

and thus give the logarithmic terms we were looking for. To simplify this calculation, we would very much like to decouple and "linearize" the RGEs for the Wilson coefficients. The most straight forward way to achieve this is to ignore all contributions that are of order $\frac{m}{M}$ (or higher) with respect to the leading terms in every expression. For example, in (4.41) we have seen that the dipole operator H_μ contributes to the one-loop muon self-energy in the EFT. However, from the matching condition (4.28) we see that this contribution is suppressed by a factor of $(\frac{m_\mu}{m_S})^2$ (and, in this case, a matching condition of one-loop order). By dimensional analysis, the same is also true for any other contribution of the non-renormalizable operators to the renormalization constants of the mass and gauge parameters. Thus, to good approximation, their RGEs are simply given by the typical expressions in QED or QCD. A similar argument holds also for the dim-5 Wilson coefficients. Terms quadratic in dim-5 or linear in higher order coefficients are suppressed by at least $\frac{m}{M}$ and can be ignored. For dim-6 operators this argument fails, because quadratic terms in dim-5 coefficients have the same mass suppression as terms linear in the dim-6 coefficients. However, in our case the matching condition for the dim-6 four-fermion operators came from tree-level diagrams while the matching condition for the dim-5 dipole operator was of one-loop order. In this way we can again discard the quadratic terms. In general, one must be careful to check these

assumptions and, in some cases, include higher order terms in the RGE [85]. Luckily, for all calculations in this thesis these arguments hold and we only need to consider terms linear in the dim-5 and dim-6 Wilson coefficients. With this, the operator renormalization factors depend only on the dimensionless coupling parameters and the renormalization factor in the Lagrangian can be written as a simple matrix (adopting the notation in [42]) $Z_{\mathcal{O}_i, C_j} \equiv Z_{ji}$. We can now write in simplified notation

$$\begin{aligned} \mathcal{L}_{\text{EFT}} &= \sum \mu^{(\xi_i + \varsigma_i)\epsilon} C_j(\mu) Z_{ji}(\mu) \mathcal{O}_i(\mu) \\ Z_{\mathcal{O}_i}(\mu) &= 1 + \sum_{n=0}^{\infty} \frac{1}{\epsilon^n} Z_{\mathcal{O}_i}^{[n]}(\mu), \quad Z_{ji}(\mu) = \delta_{ji} + \sum_{n=0}^{\infty} \frac{1}{\epsilon^n} Z_{ji}^{[n]}(\mu) \end{aligned} \quad (4.72)$$

where we have absorbed all parameters of the renormalizable operators into $Z_{\mathcal{O}_i}^{[n]}(\mu)$. Z_{ji} corresponds the counterterms subtracting divergences in form of $\langle \mathcal{O}_i \rangle$ that appear in diagrams with insertions of the effective vertex generated by \mathcal{O}_j . The RGEs now drastically simplify. In the MS scheme, where $Z_{\mathcal{O}_i}^{[0]} = Z_{ji}^{[0]} = 0$, the RGEs for the operators become

$$\frac{d\mathcal{O}_i}{d\ln(\mu)} = -\varsigma_i \epsilon \mathcal{O}_i + \sum_k \frac{\partial Z_{\mathcal{O}_i}^{[1]}}{\partial C_k} \xi_k C_k \quad (4.73)$$

The consistency equations (4.68) become

$$Z_{ji}^{[l+1]}(\xi_j - \xi_i) + \sum_k \frac{\partial Z_{ji}^{[l+1]}}{\partial C_k} \xi_k C_k = \sum_k \left(\gamma_{jk} Z_{ki}^{[l]} + Z_{ji}^{[l]} \frac{\partial Z_{\mathcal{O}_i}^{[1]}}{\partial C_k} \xi_k C_k + \frac{\partial Z_{ji}^{[l]}}{\partial C_k} \xi_k C_k \right) \quad (4.74)$$

and, finally, the RGEs for the Wilson coefficients of the non-renormalizable operators can be written as

$$\frac{dC_i}{d\ln(\mu)} = -\xi_i \epsilon C_i + C_j \gamma_{ji} \quad (4.75)$$

where γ_{ji} is called the *anomalous dimension matrix* (ADM) and can be written in terms of the Z_{ji} as

$$\boxed{\gamma_{ji} = Z_{ji}^{[1]}(\xi_j - \xi_i) + \sum_k \frac{\partial Z_{ji}^{[1]}}{\partial C_k} \xi_k C_k - \sum_k \delta_{ji} \frac{\partial Z_{\mathcal{O}_i}^{[1]}}{\partial C_k} \xi_k C_k} \quad (4.76)$$

With this simplified RGE for the Wilson coefficients (4.70) can now be written in a closed form as

$$\begin{aligned} C_i(\mu) &\approx C_i(M) - C_j(M) \int_{\mu}^M d\ln(\mu') \gamma_{ji}(\mu') \\ &\quad + C_j(M) \int_{\mu}^M d\ln(\mu') \int_{\mu'}^M d\ln(\mu'') \gamma_{jk}(\mu'') \gamma_{ki}(\mu') \\ &\quad - \dots \\ &\equiv T_{\mu} \exp \left(- \int_{\mu}^M \gamma_{ji}(\mu') d\ln(\mu') \right) C_j(M) \end{aligned} \quad (4.77)$$

where T_{μ} denotes ordering of the matrix exponential with respect to μ as implied by the expansion. This formula gives us a second way to understand the logarithmic structure of any diagram: the loop order of the logarithms generated by these integrals is given by the loop

order of the matching condition for the Wilson coefficient together with the loop order of the individual ADM entries in each term. For example, if some $C_j(M)$ with a tree-level matching condition mixes into $C_i(\mu)$ via l one-loop ADM entries, the leading l -loop logarithm in C_i will be $\sim \ln(\mu)^l$. Any coefficient with a one-loop matching condition can then only contribute to the *next-to-leading-order* (NLO) logarithms. Of course, something like in the case of the Z-boson can happen, where the lowest order matching condition is tree-level, but there is no one-loop $\ln(\mu)$ in C_{H_μ} , because the corresponding four-fermion operator does not mix into H_μ at one-loop. In general, we can therefore, like in the case of the LME, deduce only the largest possible exponent from the order of the matching conditions.

As a last comment, in the $\overline{\text{MS}}$ scheme we have always written the logarithms in terms of $\bar{\mu}$ which is related to μ by $\bar{\mu}^2 = 4\pi e^{-\gamma_E} \mu^2$. Splitting the logarithms then results in additional terms $\ln(4\pi) - \gamma_E$. These can either be explicitly included in (4.77) by integrating from $\ln(\bar{\mu})$ to $\ln(\bar{M})$ or implicitly in the matching conditions by integrating to $\ln(M)$. In the $\overline{\text{MS}}$ scheme, these terms are absorbed into renormalization factors together with the $\frac{1}{\epsilon}$ poles. In any case, in observables these additional terms cancel together with the unphysical μ dependence and can therefore be ignored.

Example Let us, once again, consider the one-loop result from (4.13). In the simplified notation we have

$$Z_{\mathcal{O}_\mu^H H_\mu}^{[1]} = Z_{\mathcal{O}_\mu^A H_\mu}^{[1]} = -\frac{m_\mu}{32\pi^2} \quad (4.78)$$

To calculate the corresponding ADM entries we also need the factors ξ_{H_μ} , $\xi_{\mathcal{O}_\mu^S} = \xi_{\mathcal{O}_\mu^{S5}}$ and ξ_m , which were defined by $[\mathcal{O}_i] = n - (2 + \xi_i)\epsilon$. For example for the mass term we have

$$[\bar{\mu}\mu] = D - 1 = 3 - 2\epsilon \quad \implies \quad \xi_m = 0 \quad (4.79)$$

The ξ values for the relevant operators are listed in Appendix C. With this, we find the ADM entries

$$\gamma_{\mathcal{O}_\mu^H H_\mu} = \gamma_{\mathcal{O}_\mu^A H_\mu} = -\frac{m_\mu}{32\pi^2}(2 - 0) + 0 - 0 = -\frac{m_\mu}{16\pi^2} \quad (4.80)$$

The one-loop logarithms can then be recovered from

$$\begin{aligned} C_{H_\mu}(m_\mu) &= C_{H_\mu}(m_S) - \int_{m_\mu}^{m_S} \left(C_{\mathcal{O}_\mu^H}(m_S) + C_{\mathcal{O}_\mu^A}(m_S) \right) \left(-\frac{m_\mu(\mu')}{16\pi^2} \right) d\ln(\mu') + \dots \\ &\approx C_{H_\mu}(m_S) + \frac{m_\mu}{16\pi^2} \left(C_{\mathcal{O}_\mu^H}(m_S) + C_{\mathcal{O}_\mu^A}(m_S) \right) \ln\left(\frac{m_S}{m_\mu}\right) \end{aligned} \quad (4.81)$$

Using the matching conditions (4.27) and (4.28) this gives

$$\Delta a_\mu = \frac{m_\mu^2}{8\pi^2} \frac{(y_\mu^A)^2}{m_A^2} \left(\frac{11}{6} + \ln\left(\frac{m_\mu^2}{m_A^2}\right) \right) - \frac{m_\mu^2}{8\pi^2} \frac{(y_\mu^H)^2}{m_H^2} \left(\frac{7}{6} + \ln\left(\frac{m_\mu^2}{m_H^2}\right) \right) \quad (4.82)$$

which gives back exactly (4.14). Unfortunately, this perfect agreement is accidental because, by chance, the one-loop diagram in (4.13) does not contain any finite analytic contributions. In general, the RGE reproduces only the logarithms correctly and in order to recover the full result one must still add up all EFT diagrams of the desired order. Of course, using the RGE to calculate the one-loop logarithms is completely pointless, since the one-loop calculations needed to obtain the ADM also already give these logarithms. This example therefore serves more as an illustration of the method. However, we could now include the next integral in the expansion and in this way obtain the leading 2-loop logarithms, which are not given by the explicit one-loop calculation! For this, we need to evaluate the $\gamma_{kj}\gamma_{ji}$ term in (4.77) which requires further entries in the ADM. We will calculate these in the next two chapters.

4.4.3 Change of Operator Basis

Lastly, let us address a point made early about the choice of operator basis. Specifically, we want to find out how the ADM transforms under a change of the operator basis. This will be particularly useful for comparing results with the literature, since everyone usually uses different conventions for the definition of the operators. Suppose we have two equivalent operator bases $\{\mathcal{O}_i^0\}$ and $\{\hat{\mathcal{O}}_i^0\}$ related by some (invertible) linear transformation. Using the Einstein summation convention, we can write

$$\mathcal{O}_i^0 = M_{i\hat{j}}^0 \hat{\mathcal{O}}_j^0 \quad (4.83)$$

Since we want the bare Lagrangian to stay invariant under this transformation, the Wilson coefficients must be related by

$$C_i^0 M_{i\hat{j}}^0 = \hat{C}_j^0 \quad (4.84)$$

In general, $M_{i\hat{j}}^0$ can be some arbitrary function of the C_i^0 . In terms of the renormalized parameters

$$M_{i\hat{j}}^0 = Z_{M_{ij}} \mu^{\kappa_{ij}} M_{i\hat{j}}, \quad Z_{M_{ij}} = 1 + \sum_{n=0}^{\infty} \frac{1}{\epsilon^n} Z_{M_{ij}}^{[n]} \quad (4.85)$$

where $M_{i\hat{j}}$ depends on the renormalized parameters and both $Z_{M_{ij}}$ and $\mu^{\kappa_{ij}}$ are, in general, different for each of the entries. To obtain the relation between the renormalized Wilson coefficients, we can insert this expression into (4.84) and compare the finite parts. This gives

$$\mu^{(\xi_i + \kappa_{ij})\epsilon} C_i M_{i\hat{j}} = \mu^{\hat{\xi}_j \epsilon} \hat{C}_j \quad (4.86)$$

Since C_i , \hat{C}_j and $M_{i\hat{j}}$ have integer mass dimension $\xi_i + \kappa_{ij} = \hat{\xi}_j$ must hold for all i, j . We can therefore cancel the μ factors on both sides. Then, taking the derivative with respect to $\ln(\mu)$, we find

$$\frac{dC_i}{d\ln(\mu)} M_{i\hat{j}} + C_i \frac{dM_{i\hat{j}}}{d\ln(\mu)} = C_k \gamma_{ki} M_{i\hat{j}} + C_i \frac{\partial M_{i\hat{j}}}{\partial C_k} \beta(C_k) = \frac{d\hat{C}_j}{d\ln(\mu)} = \hat{C}_k \hat{\gamma}_{kj} \quad (4.87)$$

which implies the following relation between the ADM in the two operator bases

$$\boxed{\hat{\gamma}_{sr} = M_{\hat{s}k}^{-1} \gamma_{kl} M_{l\hat{r}} + M_{\hat{s}l}^{-1} \frac{\partial M_{l\hat{r}}}{\partial C_k} \beta(C_k)} \quad (4.88)$$

Example As a simple example, let us look at the different conventions for H_μ . We use

$$H_\mu = -Q_\mu e \bar{\mu} \sigma^{\alpha\beta} \mu F_{\alpha\beta} \quad (4.89)$$

In our case, the ADM (which we will calculate in the next chapter) is given by

$$\gamma_{H_\mu H_\mu} = \frac{5e^2}{8\pi^2} \quad (4.90)$$

In the literature, sometimes a factor of m_μ is included in the definition. For example in [12]

$$\hat{H}_\mu = -\frac{m_\mu e}{4\pi} \bar{\mu} \sigma^{\alpha\beta} \mu F_{\alpha\beta} \quad \implies \quad \hat{\gamma}_{H_\mu H_\mu} = \frac{e^2}{\pi^2} \quad (4.91)$$

The transformation matrix in this case is given by

$$M_{H_\mu \hat{H}_\mu} = \frac{4\pi Q_\mu}{m_\mu} \quad (4.92)$$

Using (4.88) and the one loop result for $\beta(m_\mu)$ [37] we find

$$\hat{\gamma}_{H_\mu H_\mu} \stackrel{!}{=} \gamma_{H_\mu H_\mu} - \frac{1}{m_\mu} \beta(m_\mu) = \frac{5e^2}{8\pi^2} + \frac{3e^2}{\pi^2} = \frac{e^2}{\pi^2} \quad (4.93)$$

Now consider the one-loop logarithm generated by this ADM in both bases. In our case we have

$$C_{H_\mu}(\mu) = C_{H_\mu}(M) \left(1 - \gamma_{H_\mu H_\mu} \ln\left(\frac{M}{\mu}\right) + \dots \right) = C_{H_\mu}(M) \left(1 - \frac{5e^2}{8\pi^2} \ln\left(\frac{M}{\mu}\right) + \dots \right) \quad (4.94)$$

On the other hand, using the second convention gives

$$\hat{C}_{H_\mu}(\mu) = \hat{C}_{H_\mu}(M) \left(1 - \hat{\gamma}_{H_\mu H_\mu} \ln\left(\frac{M}{\mu}\right) + \dots \right) = \hat{C}_{H_\mu}(M) \left(1 - \frac{e^2}{\pi^2} \ln\left(\frac{M}{\mu}\right) + \dots \right) \quad (4.95)$$

At first, it looks like the two results disagree, however, one has to keep in mind that the Wilson coefficients also have to be transformed according to (4.86).

$$\frac{4\pi Q_\mu}{m_\mu(\mu)} C_{H_\mu}(\mu) = \hat{C}_{H_\mu}(\mu) \quad (4.96)$$

The difference between both results then comes precisely from

$$\frac{m_\mu(\mu)}{m_\mu(M)} \approx 1 + \frac{3e^2}{8\pi^2} \ln\left(\frac{M}{\mu}\right) + \dots \quad (4.97)$$

This is a point we will have to keep in mind. In general, all parameters in the matching conditions are evaluated at the large scale. Low-energy parameters, like the electromagnetic coupling e or the muon mass m_μ are, however, more naturally defined at the low scale. Expanding the parameters in the matching conditions in terms of those at the low scale then leads to additional large logarithms which, in some cases, we want to include explicitly.

5 Corrections for Heavy Fermion Loop

We now have all necessary tools to calculate the higher order leading logarithmic corrections to a_μ in the 2HDM. In particular, we are interested in the 3-loop corrections to the Barr-Zee diagrams with scalar and pseudoscalar Higgs which we discussed in section 3.3. The different scales that are relevant to this calculation are

$$m_\mu \ll m_\tau \approx m_b \ll m_S \ll m_t \quad (5.1)$$

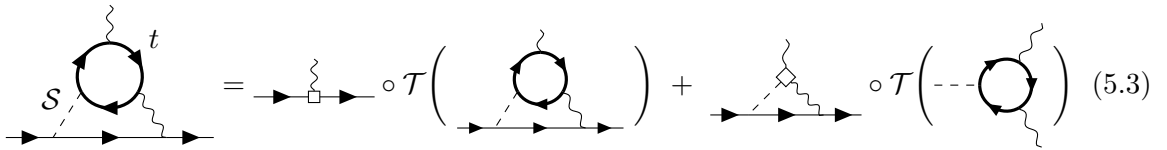
In principle, logarithms of all possible ratios between these masses can appear in the result. As we have discussed, in order to correctly capture these logarithms we need to iteratively expand out the different scales one after the other, starting with the largest. In each step we obtain a new EFT and matching conditions for the Wilson coefficients. Using (4.77) we then run down to the next smaller scale to obtain the matching conditions for the next EFT and in the process pick up all relevant leading logarithmic terms. In this chapter, we therefore start with the case of a heavy fermion $m_t \gg m_S$ running in the loop of the Barr-Zee diagram. In section 3.3 we found from the explicit expansion of the loop functions

$$\Delta a_\mu^{2\text{HDM},2,t} \approx N_c^t \frac{Q_t^2 e^2}{16\pi^4} \frac{m_\mu}{m_t} \left(y_\mu^A y_t^A \ln\left(\frac{m_t}{m_A}\right) - \frac{2}{3} y_\mu^H y_t^H \ln\left(\frac{m_t}{m_H}\right) \right) \quad (5.2)$$

We will rediscover these logarithms in the process of calculating the 3-loop corrections and in this way, at least partially, confirm the validity of our results. With this, we can now begin to construct the EFT.

5.1 Operators and Matching Conditions

As in our previous examples, in order to find the relevant operators we use the LME. The expansion of the Barr-Zee diagram with a heavy fermion loop is given by



$$= \text{tree-level matching} \circ \mathcal{T} \left(\text{loop diagram} \right) + \text{tree-level matching} \circ \mathcal{T} \left(\text{loop diagram} \right) \quad (5.3)$$

We find a two-loop matching diagram for the dipole operator and a one-loop matching diagram for a new operator describing the process $\mathcal{S} \rightarrow \gamma\gamma$ at tree-level. The fact that there is no vertex with a tree-level matching condition explains why we only found a $\ln(\frac{m_t}{m_S})$ term in (5.2) and, as we have argued in section 4.4.2, implies that the 3-loop correction will at most contain a $\ln(\frac{m_t}{m_S})^2$ term. With this, let us now go on to calculate the matching diagrams.

5.1.1 One-Loop Matching Diagrams

To obtain the one-loop matching conditions we can use our previous results from section 3.3.1, where we essentially already calculated the matching diagram. The only difference was that we did not Taylor expand the integrand, but instead evaluated the full diagram. However, we found that the result was completely analytic in the external momenta q and q' . This must be the case, because all of the internal lines are from the heavy fermions. The Taylor expansion therefore does not introduce any divergences and simply commutes with

the integration. We can then obtain our matching conditions directly from expanding (3.36) and (3.39). For the CP-even scalars this gives

$$\mathcal{T}\left(H \text{ --- } \text{[Bubble with two internal lines and two external wavy lines]}\right) \approx iN_c^2 \frac{Q_t^2 e^2}{6\pi^2} \frac{y_t^H}{m_t} [\eta^{\mu\nu} q q' - q'^\mu q^\nu] + \dots \quad (5.4)$$

where, as before, q denotes the momentum of the incoming external photon and q' that of the outgoing virtual photon. The operator describing this vertex and the corresponding matching condition are given by

$$\mathcal{O}_{H\gamma\gamma} = \frac{e^2}{4} F_{\mu\nu} F^{\mu\nu} H, \quad C_{\mathcal{O}_{H\gamma\gamma}}(m_t) = N_c^t \frac{Q_t^2}{6\pi^2} \frac{y_t^H}{m_t} \quad (5.5)$$

For the CP-odd scalar we get

$$\mathcal{T}\left(A \text{---} \text{---} \text{---} \begin{array}{c} \circlearrowright \\ \circlearrowleft \end{array} \text{---} \right) \approx -iN_c^t \frac{Q_t^2 e^2}{4\pi^2} \frac{y_t^A}{m_t} \epsilon^{\mu\nu\alpha\beta} q_\alpha q'_\beta + \dots \quad (5.6)$$

The operator describing this vertex and the corresponding matching condition are given by

$$\mathcal{O}_{A\gamma\gamma} = \frac{e^2}{4} F_{\mu\nu} \tilde{F}^{\mu\nu} A, \quad C_{\mathcal{O}_{A\gamma\gamma}}(m_t) = N_c^t \frac{Q_t^2}{4\pi^2} \frac{y_t^A}{m_t} \quad (5.7)$$

where $\tilde{F}^{\mu\nu} = \frac{1}{2}\epsilon^{\mu\nu\alpha\beta}F_{\alpha\beta}$ is the dual field strength tensor.

5.1.2 Two-Loop Matching Diagrams

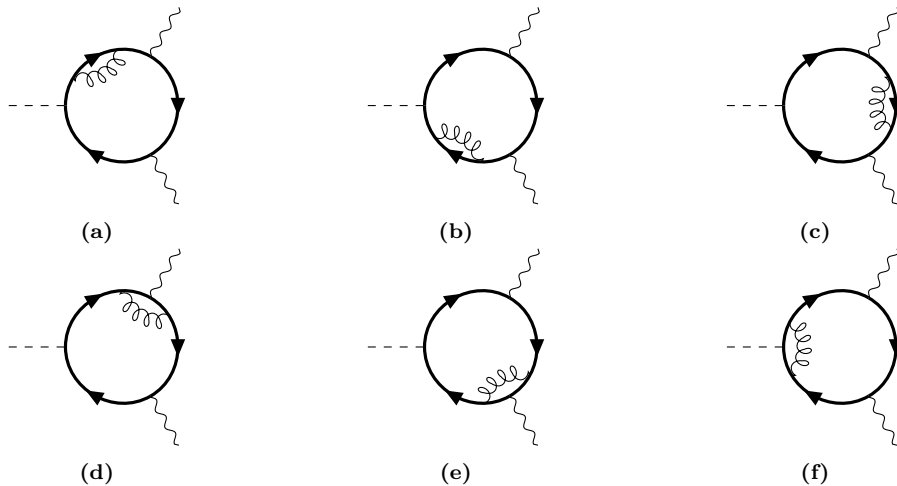


Figure 5.1: Two-loop matching diagrams for $C_{\mathcal{O}_{H\gamma\gamma}}$ and $C_{\mathcal{O}_{A\gamma\gamma}}$.

For the top quark, we expect the dominant 3-loop corrections to the Barr-Zee diagram to come from the QCD corrections to the fermion loop shown in Fig.5.1. These corrections will not be captured by the renormalization group running and must instead be included in the matching condition. In this way, these diagrams only contribute to the next-to-leading-order (NLO) logarithms. However, the large QCD coupling α_s can easily overcome this suppression and these corrections should therefore be included. Fortunately, the process $\mathcal{S} \rightarrow \gamma\gamma$ has been studied extensively in the past and in particular, the two-loop QCD corrections are well known [86–89]. Surprisingly, the two-loop results can be derived without explicitly calculating

the diagrams. The corrections for the CP-even scalar follow from the fact, that the trace of the QCD corrected energy-momentum tensor can be written as [90]

$$\theta_\mu^\mu = \left(1 + \frac{3g_s^2 C_F}{8\pi^2} + \dots\right) m_t \bar{t}t + \frac{e^2 Q_t^2}{2\pi^2} \left(1 + \frac{3g_s^2 C_F}{16\pi^2} + \dots\right) \frac{1}{4} F^{\mu\nu} F_{\mu\nu} \quad (5.8)$$

Since the matrix element

$$\langle \Omega | \theta_\mu^\mu | q', \sigma; q, \lambda \rangle \sim \epsilon_\mu^\lambda(q) \epsilon_\nu^\sigma(q') [\eta^{\mu\nu} q q' - q'^\mu q^\nu] (q + q')^2 \quad (5.9)$$

vanishes for $(q + q')^2 \rightarrow 0$ [91], the amplitudes



$$(5.10)$$

are related to each other in the low energy limit. Since the CP-even Higgs can couple to the vertices on both sides, we obtain the following relation between the two operators

$$-y_t^H H \bar{t}t = \frac{y_t^H}{m_t} \frac{Q_t^2}{2\pi^2} \left(1 - \frac{3g_s^2 C_F}{16\pi^2} + \dots\right) \frac{e^2}{4} H F_{\mu\nu} F^{\mu\nu} \quad (5.11)$$

from which we immediately rediscover the one-loop matching condition (5.4), but also the two-loop QCD correction. We therefore have

$$C_{O_{H\gamma\gamma}}(m_t) = N_c^t \frac{Q_t^2}{6\pi^2} \frac{y_t^H}{m_t} \left(1 - \frac{3g_s^2 C_F}{16\pi^2}\right) \quad (5.12)$$

An explicit calculation of this result can be found in [87]. For the CP-odd Higgs it has been shown [89], using the Ward identity and by explicit calculation, that the radiative corrections in Fig.5.1 do not contribute to the matching condition. In the following we want to confirm this result by an independent calculation of the two-loop amplitudes.

One-loop Subdivergences The simplest approach is to first obtain expressions for the divergent (off-shell) one-loop sub-diagrams which can then be inserted into the two-loop amplitude. In our case these are the QCD quark self-energy correction, the photon vertex correction and corrections to the CP-even and CP-odd vertex. In the full theory, these divergences are subtracted by appropriate counterterm diagrams which also have to be included in the two-loop matching calculation. Starting with the self-energy diagram we have

$$\begin{aligned} \text{Diagram} &= i\Sigma(p) = -g_s^2 C_F \int_0^1 dx \int_k \frac{\gamma^\alpha (\not{k} + x\not{p} + m_t) \gamma_\alpha}{[k^2 - (1-x)m_t^2 + p^2 x(1-x)]^2} \\ &= \frac{ig_s^2 C_F}{(4\pi)^2} \frac{1}{\epsilon} \int_0^1 dx \left(\frac{\bar{\mu}^2}{x(1-x)} \right)^\epsilon \left[(D-2)x\not{p} - Dm_t \right] \frac{1}{[m_t^2/x - p^2]^\epsilon} \end{aligned} \quad (5.13)$$

The photon vertex correction is given by (only including terms up to $\mathcal{O}(\epsilon^0)$)

$$\begin{aligned} \text{Diagram} &= i\Gamma^\mu(p, q) = -g_s^2 C_F Q_t e \int_k \frac{\gamma^\alpha (\not{k} + \not{q} + m_t) \gamma^\mu (\not{k} + m_t) \gamma_\alpha}{[k^2 - m_t^2][(k+q)^2 - m_t^2](k-p)^2} \\ &= -iQ_t e \frac{2g_s^2 C_F}{(4\pi)^2} \int_0^1 dx \int_0^{1-x} dz \left(\frac{\bar{\mu}^2}{\Delta} \right)^\epsilon \left\{ \gamma^\mu \left(\frac{1}{\epsilon} - 2 + \frac{m_t^2 - z^2 p^2}{\Delta} \right) \right. \\ &\quad \left. + \frac{2z}{\Delta} p^\mu (z\not{p} - 2m_t) + \frac{1}{\Delta} z(1-x) \not{p} \gamma^\mu \not{q} - \frac{1}{\Delta} xz \not{q} \gamma^\mu \not{p} \right\} \end{aligned} \quad (5.14)$$

where $\Delta(x, y) = (1 - z)m_t^2 - q^2x(1 - x) - p^2z(1 - z) - 2xypq$. Lastly, in the vertex correction for the CP-odd Higgs it is convenient to already expand in the external momentum q before integration¹. The amplitude is then given by

$$\begin{aligned}
 \text{Diagram} &= i\Gamma_A(p, q) = ig_s^2 C_F y_t^A \gamma^5 \int_k \frac{\gamma^\alpha (\not{k} + \not{q} - m_t)(\not{k} + m_t) \gamma_\alpha}{[k^2 - m_t^2][(k + q)^2 - m_t^2](k - p)^2} \\
 &\simeq -y_t^A \gamma^5 \frac{g_s^2 C_F}{(4\pi)^2} \int_0^1 dx \left(\frac{\bar{\mu}^2}{x(1-x)} \right)^\epsilon \left\{ \frac{4}{\epsilon} - 2 + \frac{4pq + \frac{2}{x}m_t \not{q}}{m_t^2/x - p^2} \right\} \frac{1}{[m_t^2/x - p^2]^\epsilon} + \mathcal{O}(q^2)
 \end{aligned} \tag{5.15}$$

With this we can move on to the two-loop amplitudes.

$A\gamma\gamma$ Two-Loop Diagrams We have to be careful about the treatment of γ^5 in this calculation. We will follow the approach in [92] and simplify the Dirac algebra without assuming any properties of γ^5 except

$$\begin{aligned}
 \text{Tr}\{\gamma^\mu \gamma^\nu \gamma^5\} &= 0, \quad \text{and} \\
 \text{Tr}\{\gamma^{\mu_1} \dots \gamma^{\mu_{2k+1}} \gamma^5\} &= 0
 \end{aligned} \tag{5.16}$$

which allow us to neglect terms with two or an odd number of gamma matrices. Additionally, in anticipation of the gauge-invariant structure of the vertex, we can neglect all terms $\sim q^\mu, q^\nu, q'^\mu, q'^\nu$. Once we have evaluated the (counterterm) diagrams we take the limit $D \rightarrow 4$ and can evaluate the trace

$$\text{Tr}\{\gamma^\mu \gamma^\nu \gamma^\alpha \gamma^\beta\} = -4i\epsilon^{\mu\nu\alpha\beta} \tag{5.17}$$

Let us start with the self-energy insertions. Expanding to lowest order in the external momenta gives (we already include the factor -1 for the trace)

$$\begin{aligned}
 \mathcal{T}(i\Gamma_{(a)}^{\mu\nu}) &= -iN_c^t Q_t^2 e^2 y_t^A \frac{g_s^2 C_F}{(4\pi)^2} \frac{1}{\epsilon} \int_0^1 dx \left(\frac{\bar{\mu}^2}{x(1-x)} \right)^\epsilon \int_k \frac{1}{[k^2 - m_t^2]^4 [m_t^2/x - k^2]^\epsilon} \\
 &\quad \left((\not{k} - \not{p} + m_t) \gamma^\nu (\not{k} + \not{q} + m_t) \gamma^\mu (\not{k} + m_t) ([D-2]x\not{k} - Dm_t)(\not{k} + m_t) \right) \gamma^5 \\
 &\quad \left(1 + \frac{2kp}{k^2 - m_t^2} + \dots \right) \left(1 - \frac{2kq}{k^2 - m_t^2} + \dots \right) \\
 &= \mathcal{T}(i\Gamma_{(b)}^{\mu\nu}) = \mathcal{T}(i\Gamma_{(c)}^{\mu\nu}) = \mathcal{T}(i\bar{\Gamma}_{(b)}^{\mu\nu}) = \mathcal{T}(i\bar{\Gamma}_{(c)}^{\mu\nu})
 \end{aligned} \tag{5.18}$$

where $\bar{\Gamma}$ indicates the diagrams with the fermions running in the opposite direction. The equality for all diagrams is not obvious and has been checked by explicit calculation. We now use

$$\begin{aligned}
 (\not{k} + m_t) ([D-2]x\not{k} - Dm_t)(\not{k} + m_t) &= \not{k} \left((D-2)xk^2 - [2D + (2-D)x]m_t^2 \right) \\
 &\quad - m_t \left((D - (2D-4)x)k^2 + Dm_t^2 \right)
 \end{aligned} \tag{5.19}$$

¹We should have done this also in case of the photon vertex correction. However, for these one-loop diagrams Taylor expansion and integration commute and expanding after integration gives a nicer expression in case of the photon vertex.

With this, the amplitude simplifies to

$$\mathcal{T}(i\Gamma_{(a)}^{\mu\nu}) = -iN_c^t Q_t^2 e^2 y_t^A \frac{g_s^2 C_F}{(4\pi)^2} \frac{1}{\epsilon} \int_0^1 dx \left(\frac{\bar{\mu}^2}{x(1-x)} \right)^\epsilon \int_k \frac{m_t \not{p} \gamma^\nu \not{q} \gamma^\mu \gamma^5}{[k^2 - m_t^2]^3 [m_t^2/x - k^2]^\epsilon} \left([-2\epsilon - (2-3\epsilon)x] + \frac{m_t^2}{k^2 - m_t^2} [4 - 4\epsilon - (2-3\epsilon)x] \right) \quad (5.20)$$

To further simplify we introduce another Feynman parameter

$$\begin{aligned} \int_k \frac{1}{[m_t^2 - k^2]^n [m_t^2/x - k^2]^\epsilon} &= \frac{\Gamma(n+\epsilon)}{\Gamma(n)\Gamma(\epsilon)} \int_k \int_0^1 dy \frac{(1-y)^{n-1} y^{\epsilon-1}}{[(1-y+y/x)m_t^2 - k^2]^{n+\epsilon}} \\ &= \frac{\Gamma(n-2+2\epsilon)}{\Gamma(n)\Gamma(\epsilon)} \frac{i(m_f^2)^{2-n}}{(4\pi)^{D/2}} \left(\frac{\mu^2}{m_f^2} \right)^\epsilon \int_0^1 dy \frac{y^{n-1} (1-y)^{\epsilon-1} x^{n-2+2\epsilon}}{[1-y(1-x)]^{n-2+2\epsilon}} \end{aligned} \quad (5.21)$$

to get the following expression

$$\begin{aligned} \mathcal{T}(i\Gamma_{(a)}^{\mu\nu}) &= N_c^t Q_t^2 e^2 \frac{y_t^A}{m_t} \frac{g_s^2 C_F}{(4\pi)^4} \not{p} \gamma^\nu \not{q} \gamma^\mu \gamma^5 \left(\frac{\bar{\mu}^2}{m_f^2} \right)^{2\epsilon} \frac{\Gamma(1+2\epsilon)}{2\Gamma(1+\epsilon)^2} \int_0^1 dx \left(\frac{1}{x(1-x)} \right)^\epsilon \\ &\quad \int_0^1 dy \frac{y^2 (1-y)^{\epsilon-1} x^{1+2\epsilon}}{[1-y(1-x)]^{1+2\epsilon}} \left([2\epsilon + (2-3\epsilon)x] + \frac{yx}{1-y(1-x)} \right. \\ &\quad \left. \frac{1+2\epsilon}{3} [4 - 4\epsilon - (2-3\epsilon)x] \right) \end{aligned} \quad (5.22)$$

The $\frac{1}{\epsilon}$ pole is now contained in the y -integral which diverges at $y = 1$ for $\epsilon \rightarrow 0$. We can extract this divergence by splitting the integral into a divergent and a regular part using the following formula

$$\int_0^1 dx \int_0^1 dy \frac{f_\epsilon(x, 1)}{(1-y)^{1-\epsilon}} = \frac{1}{\epsilon} \int_0^1 dx f_\epsilon(x, 1) + \int_0^1 dx \int_0^1 dy \frac{[f_0(x, y) - f_0(x, 1)]}{1-y} + \mathcal{O}(\epsilon) \quad (5.23)$$

Since $f_\epsilon(x, y) - f_\epsilon(x, 0) \sim (1-y)$ the subtracted integral is finite and we can set $\epsilon = 0$. This gives

$$\begin{aligned} \mathcal{T}(i\Gamma_{(a)}^{\mu\nu}) &= N_c^t Q_t^2 e^2 \frac{y_t^A}{m_t} \frac{g_s^2 C_F}{(4\pi)^4} \not{p} \gamma^\nu \not{q} \gamma^\mu \gamma^5 \left(\frac{\bar{\mu}^2}{m_t^2} \right)^{2\epsilon} \frac{\Gamma(1+2\epsilon)}{2\Gamma(1+\epsilon)^2} \left(-\frac{13}{3} + \right. \\ &\quad \left. \frac{2}{3\epsilon} [(2+5\epsilon)B(1-\epsilon, 1-\epsilon) + (2-5\epsilon)B(2-\epsilon, 1-\epsilon)] \right) \\ &= N_c^t Q_t^2 e^2 \frac{y_t^A}{m_t} \frac{g_s^2 C_F}{(4\pi)^4} \not{p} \gamma^\nu \not{q} \gamma^\mu \gamma^5 \left(\frac{\bar{\mu}^2}{m_t^2} \right)^{2\epsilon} \left(\frac{1}{\epsilon} + \frac{2}{3} \right) \end{aligned} \quad (5.24)$$

The calculation of the counterterm is completely analogous. We find

$$\mathcal{T}(i\Gamma_{(a),ct}^{\mu\nu}) = -N_c^t Q_t^2 e^2 \frac{y_t^A}{m_t} \frac{g_s^2 C_F}{(4\pi)^4} \not{p} \gamma^\nu \not{q} \gamma^\mu \gamma^5 \left(\frac{\bar{\mu}^2}{m_t^2} \right)^\epsilon \left(\frac{1}{\epsilon} + 1 \right) \quad (5.25)$$

which cancels the divergence from the two-loop diagram and allows us to take the trace. In total (including opposite fermion loops), we get

$$\text{Tr } \mathcal{T}(i\Gamma_{(a+b+c)}^{\mu\nu}) = 4iN_c^t Q_t^2 e^2 \frac{y_t^A}{m_t} \frac{g_s^2 C_F}{(4\pi)^4} \left(-2 + 6 \ln \left(\frac{\bar{\mu}^2}{m_t^2} \right) \right) \epsilon^{\mu\nu\alpha\beta} q_\alpha q'_\beta \quad (5.26)$$

Next, we consider the diagrams with photon vertex corrections.

$$\begin{aligned}
 \mathcal{T} \left(i\Gamma_{(d)}^{\mu\nu} \right) &= 2iN_c^t Q_t^2 e^2 y_t^A \frac{g_s^2 C_F}{(4\pi)^2} \int_0^1 dx \int_0^{1-x} dz \int_k \frac{1}{[k^2 - m_t^2]^3 [m_t^2/z - k^2]^\epsilon} \\
 &\quad \left(\frac{\bar{\mu}^2}{z(1-z)} \right)^\epsilon \left(1 + \frac{2kp}{k^2 - m_t^2} \right) \left(1 - \frac{2kq}{k^2 - m_t^2} + \frac{x\epsilon}{1-z} \frac{2kq}{m_t^2/z - k^2} \right) \\
 &\quad \left\{ (\not{k} - \not{p} + m_t) \gamma^\nu (\not{k} + \not{q} + m_t) \left[\gamma^\mu \left(\frac{1}{\epsilon} - 2 \right) \right. \right. \\
 &\quad \left. \left. + \left(\gamma^\mu [m_t^2 - z^2 k^2] + 2zk^\mu (z\not{k} - 2m_t) + (1-x)z\not{k} \gamma^\mu \not{q} - xz\not{q} \gamma^\mu \not{k} \right) \right. \right. \\
 &\quad \left. \left. \frac{1}{z(1-z)} \frac{1}{m_t^2/z - k^2} \left(1 + \frac{x}{1-z} \frac{2kq}{m_t^2/z - k^2} \right) \right] (\not{k} + m_t) \right\} \gamma^5 \\
 &= \mathcal{T} \left(i\Gamma_{(e)}^{\mu\nu} \right) = \mathcal{T} \left(i\bar{\Gamma}_{(d)}^{\mu\nu} \right) = \mathcal{T} \left(i\bar{\Gamma}_{(e)}^{\mu\nu} \right)
 \end{aligned} \tag{5.27}$$

In this case, we can significantly simplify the calculation by taking the limit $\epsilon \rightarrow 0$ in all terms except those with the explicit $\frac{1}{\epsilon}$ pole. We can then immediately evaluate the trace and obtain finite Feynman parameter integrals. We find

$$\begin{aligned}
 \text{Tr } \mathcal{T} \left(i\Gamma_{(d)}^{\mu\nu} \right) \Big|_{\text{reg}} &= -4m_t N_c^t Q_t^2 e^2 y_t^A \frac{g_s^2 C_F}{(4\pi)^2} \epsilon^{\mu\nu\alpha\beta} q_\alpha q'_\beta \int_0^1 \frac{dz}{z} \\
 &\quad \int_k \frac{1}{[m_t^2/z - k^2]} \left(\frac{z(3+z)}{[k^2 - m_t^2]^2} + \frac{m_t^2(z^2 + 3z - 2)}{[k^2 - m_t^2]^3} \right) \\
 &= -4iN_c^t Q_t^2 e^2 \frac{y_t^A}{m_t} \frac{g_s^2 C_F}{(4\pi)^4} \epsilon^{\mu\nu\alpha\beta} q_\alpha q'_\beta \int_0^1 dz \int_0^1 dy \\
 &\quad \left(\frac{y(z^2 + 3z)}{1 - y(1-z)} - \frac{1}{2} \frac{(z^2 + 3z - 2)y^2 z}{[1 - y(1-z)]^2} \right) \\
 &= -4iN_c^t Q_t^2 e^2 \frac{y_t^A}{m_t} \frac{g_s^2 C_F}{(4\pi)^4} \epsilon^{\mu\nu\alpha\beta} q_\alpha q'_\beta \left(\frac{\pi^2}{6} - \frac{7}{4} \right)
 \end{aligned} \tag{5.28}$$

The divergent part can again be evaluated using (5.23)

$$\begin{aligned}
 \mathcal{T} \left(i\Gamma_{(d)}^{\mu\nu} \right) \Big|_{\frac{1}{\epsilon}} &= -N_c^t Q_t^2 e^2 \frac{y_t^A}{m_t} \frac{g_s^2 C_F}{(4\pi)^4} \left(\frac{\bar{\mu}^2}{m_t^2} \right)^{2\epsilon} \not{p} \gamma^\nu \not{q} \gamma^\mu \gamma^5 (1 - 2\epsilon) \frac{\Gamma(1 + 2\epsilon)}{\Gamma(1 + \epsilon)^2} \\
 &\quad \int_0^1 dz \int_0^1 dy \frac{1-z}{(z(1-z))^\epsilon} \frac{(1-y)^{\epsilon-1} y^2 z^{1+2\epsilon}}{[1 - y(1-z)]^{1+2\epsilon}} \\
 &= -N_c^t Q_t^2 e^2 \frac{y_t^A}{m_t} \frac{g_s^2 C_F}{(4\pi)^4} \left(\frac{\bar{\mu}^2}{m_t^2} \right)^{2\epsilon} \not{p} \gamma^\nu \not{q} \gamma^\mu \gamma^5 \left(\frac{1}{2\epsilon} + \frac{3 - \pi^2}{6} \right)
 \end{aligned} \tag{5.29}$$

The counterterm is given by

$$\mathcal{T} \left(i\Gamma_{(d)}^\mu \right) = N_c^t Q_t^2 e^2 \frac{y_t^A}{m_t} \frac{g_s^2 C_F}{(4\pi)^4} \left(\frac{\bar{\mu}^2}{m_t^2} \right)^{2\epsilon} \not{p} \gamma^\nu \not{q} \gamma^\mu \gamma^5 \frac{1}{2\epsilon} \tag{5.30}$$

and this time only subtracts the divergence such that in total we have

$$\text{Tr } \mathcal{T} \left(i\Gamma_{(d+e)}^{\mu\nu} \right) = 4iN_c^t Q_t^2 e^2 \frac{y_t^A}{m_t} \frac{g_s^2 C_F}{(4\pi)^4} \left(5 - 2 \ln \left(\frac{\bar{\mu}^2}{m_t^2} \right) \right) \epsilon^{\mu\nu\alpha\beta} q_\alpha q'_\beta \tag{5.31}$$

Finally, the insertion of the Higgs vertex correction gives

$$\begin{aligned}
 \mathcal{T} \left(i\Gamma_{(f)}^{\mu\nu} \right) &= iN_c^t Q_t^2 e^2 y_t^A \frac{g_s^2 C_F}{(4\pi)^2} \int_0^1 dx \left(\frac{\bar{\mu}^2}{x(1-x)} \right)^\epsilon \int_k \frac{1}{[k^2 - m_t^2]^3 [m_t^2/z - k^2]^\epsilon} \\
 &\quad \gamma^5 \left\{ \frac{4}{\epsilon} - 2 + \frac{4kp + \frac{2}{x} m_t \not{p}}{m_t^2/x - k^2} \right\} (\not{k} + m_t) \gamma^\nu (\not{k} + \not{q}' + m_t) \gamma^\mu (\not{k} + \not{p} + m_t) \\
 &\quad \left(1 - \frac{2kq'}{k^2 - m_t^2} \right) \left(1 - \frac{2kp}{k^2 - m_t^2} \right) \\
 &= \mathcal{T} \left(i\bar{\Gamma}_{(f)}^{\mu\nu} \right)
 \end{aligned} \tag{5.32}$$

Analogous to above, we find for the regular part

$$\begin{aligned}
 \text{Tr } \mathcal{T} \left(i\Gamma_{(f)}^{\mu\nu} \right) \Big|_{reg} &= 8m_t^3 N_c^t Q_t^2 e^2 y_t^A \frac{g_s^2 C_F}{(4\pi)^2} \epsilon^{\mu\nu\alpha\beta} q_\alpha q'_\beta \int_0^1 \frac{dx}{x} \int_k \frac{1}{[m_t^2/z - k^2][m_t^2 - k^2]^3} \\
 &= 4iN_c^t Q_t^2 e^2 \frac{y_t^A}{m_t} \frac{g_s^2 C_F}{(4\pi)^4} \epsilon^{\mu\nu\alpha\beta} q_\alpha q'_\beta \int_0^1 dz \int_0^1 dy \frac{y^2 x}{[1 - y(1-x)]^2} \\
 &= 4iN_c^t Q_t^2 e^2 \frac{y_t^A}{m_t} \frac{g_s^2 C_F}{(4\pi)^4} \epsilon^{\mu\nu\alpha\beta} q_\alpha q'_\beta \frac{1}{2}
 \end{aligned} \tag{5.33}$$

and for the divergent part

$$\begin{aligned}
 \mathcal{T} \left(i\Gamma_{(f)}^{\mu\nu} \right) \Big|_{\frac{1}{\epsilon}} &= -N_c^t Q_t^2 e^2 \frac{y_t^A}{m_t} \frac{g_s^2 C_F}{(4\pi)^4} \gamma^\nu \not{q}' \gamma^\mu \not{p} \gamma^5 (4 - 2\epsilon) \left(\frac{\bar{\mu}^2}{m_t^2} \right)^{2\epsilon} \frac{\Gamma(1 + 2\epsilon)}{2\Gamma(1 + \epsilon)^2} \\
 &\quad \int_0^1 dx \int_0^1 dy \left(\frac{1}{x(1-x)} \right)^\epsilon \frac{(1-y)^{\epsilon-1} y^2 x^{1+2\epsilon}}{[1 - y(1-z)]^{1+2\epsilon}} \\
 &= N_c^t Q_t^2 e^2 \frac{y_t^A}{m_t} \frac{g_s^2 C_F}{(4\pi)^4} \left(\frac{\bar{\mu}^2}{m_t^2} \right)^{2\epsilon} \gamma^\nu \not{q}' \gamma^\mu \not{p} \gamma^5 \left(\frac{2}{\epsilon} + 2 \right)
 \end{aligned} \tag{5.34}$$

Again, the counterterm only subtracts the divergence

$$\mathcal{T} \left(i\Gamma_{(f),ct}^\mu \right) = -N_c^t Q_t^2 e^2 \frac{y_t^A}{m_t} \frac{g_s^2 C_F}{(4\pi)^4} \left(\frac{\bar{\mu}^2}{m_t^2} \right)^{2\epsilon} \gamma^\nu \not{q}' \gamma^\mu \not{p} \gamma^5 \frac{2}{\epsilon} \tag{5.35}$$

and we find (including the opposite fermion loop)

$$\text{Tr } \mathcal{T} \left(i\Gamma_{(f)}^{\mu\nu} \right) = 4iN_c^t Q_t^2 e^2 \frac{y_t^A}{m_t} \frac{g_s^2 C_F}{(4\pi)^4} \left(-3 - 4 \ln \left(\frac{\bar{\mu}^2}{m_t^2} \right) \right) \epsilon^{\mu\nu\alpha\beta} q_\alpha q'_\beta \tag{5.36}$$

Finally, adding up all contributions we find

$$\text{Tr } \mathcal{T} \left(i\Gamma_{(a+b+c+d+e+f)}^{\mu\nu} \right) = 0 \tag{5.37}$$

As expected, in the sum the contributions cancel exactly and we therefore can confirm the results in [89].

Matching Conditions Together with the one-loop results from the previous section, the matching conditions for the operators are

$$\begin{aligned}
 C_{\mathcal{O}_{A\gamma\gamma}}(m_t) &= N_c^t \frac{Q_t^2}{4\pi^2} \frac{y_t^A}{m_t} \\
 C_{\mathcal{O}_{H\gamma\gamma}}(m_t) &= N_c^t \frac{Q_t^2}{6\pi^2} \frac{y_t^H}{m_t} \left(1 - \frac{3g_s^2 C_F}{16\pi^2} \right)
 \end{aligned} \tag{5.38}$$

5.2 Operator Mixing

In the previous section we have found the relevant operator basis for the EFT

$$\begin{aligned}
H_\mu &= -Q_\mu e \bar{\mu} \sigma^{\alpha\beta} \mu F_{\alpha\beta} \\
\mathcal{O}_{A\gamma\gamma} &= \frac{e^2}{4} F_{\alpha\beta} \tilde{F}^{\alpha\beta} A \\
\mathcal{O}_{H\gamma\gamma} &= \frac{e^2}{4} F_{\alpha\beta} F^{\alpha\beta} H
\end{aligned} \tag{5.39}$$

We now need to calculate all possible one-loop mixing diagrams between these operators.

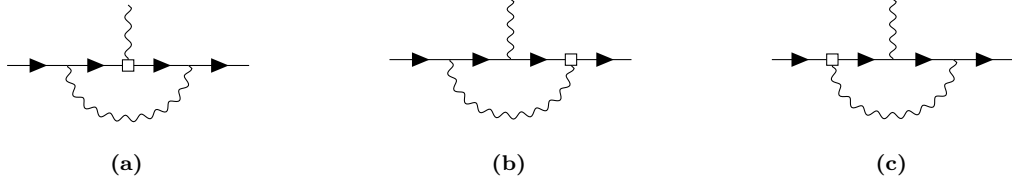


Figure 5.2: One-loop diagrams contributing to $\gamma_{H_\mu H_\mu}$.

$H_\mu H_\mu$ Mixing The diagrams contributing to $Z_{H_\mu H_\mu}$ at one-loop are shown in Fig.5.2. Their respective amplitudes are given by

$$\begin{aligned}
i\Gamma_{(a)}^\mu &= -2iC_{H_\mu} Q_\mu^3 e^3 \mu^{2\epsilon} \int \frac{d^D k}{(2\pi)^D} \frac{\gamma^\alpha (\not{k} + \not{p}' + m_\mu) \sigma^{\mu\nu} q_\nu (\not{k} + \not{p} + m_\mu) \gamma_\alpha}{[(k+p')^2 - m_\mu^2][(k+p)^2 - m_\mu^2]k^2} \\
i\Gamma_{(b)}^\mu &= +2iC_{H_\mu} Q_\mu^3 e^3 \mu^{2\epsilon} \int \frac{d^D k}{(2\pi)^D} \frac{\sigma^{\alpha\nu} k_\nu (\not{k} + \not{p}' + m_\mu) \gamma^\mu (\not{k} + \not{p} + m_\mu) \gamma_\alpha}{[(k+p')^2 - m_\mu^2][(k+p)^2 - m_\mu^2]k^2} \\
i\Gamma_{(c)}^\mu &= -2iC_{H_\mu} Q_\mu^3 e^3 \mu^{2\epsilon} \int \frac{d^D k}{(2\pi)^D} \frac{\gamma_\alpha (\not{k} + \not{p}' + m_\mu) \gamma^\mu (\not{k} + \not{p} + m_\mu) \sigma^{\alpha\nu} k_\nu}{[(k+p')^2 - m_\mu^2][(k+p)^2 - m_\mu^2]k^2}
\end{aligned} \tag{5.40}$$

We only need the divergent part of these integrals. The first amplitude is finite, because $\gamma^\alpha \gamma^\beta \sigma^{\mu\nu} \gamma_\beta \gamma_\alpha = (D-4)^2 \sigma^{\mu\nu}$ in D -dimensions. For the other two integrals, we introduce Feynman parameters

$$\frac{1}{[(k+p)^2 - m_\mu^2][(k+p')^2 - m_\mu^2]k^2} = \int_0^1 dx \int_0^{1-x} dy \frac{2!}{[(k+xp'+yp) - \Delta]^3} \tag{5.41}$$

where $\Delta = (x+y)m_\mu^2 + (xp' + yp)^2 - xp'^2 - yp^2$. The sum of the two amplitudes can then be written as

$$\begin{aligned}
i\Gamma_{(b+c)}^\mu &= 4iC_{H_\mu} Q_\mu^3 e^3 \int_k \int_0^1 dx \int_0^{1-x} dy \frac{k_\nu - xp'_\nu - yp_\nu}{[k^2 - \Delta]^3} \\
&\quad \left(\sigma^{\alpha\nu} (\not{k} + \not{p}_1 + m_\mu) \gamma^\mu (\not{k} + \not{p}_2 + m_\mu) \gamma_\alpha \right. \\
&\quad \left. - \gamma_\alpha (\not{k} + \not{p}_1 + m_\mu) \gamma^\mu (\not{k} + \not{p}_2 + m_\mu) \sigma^{\alpha\nu} \right) \\
&\simeq 4iC_{H_\mu} Q_\mu^3 e^3 \int_k \int_0^1 dx \int_0^{1-x} dy \frac{k^2/D}{[k^2 - \Delta]^3} \\
&\quad \left(\sigma^{\alpha\nu} [\gamma_\nu \gamma^\mu \not{p}_2 + \not{p}_1 \gamma^\mu \gamma_\nu] \gamma_\alpha - \gamma_\alpha [\gamma_\nu \gamma^\mu \not{p}_2 + \not{p}_1 \gamma^\mu \gamma_\nu] \sigma^{\alpha\nu} \right. \\
&\quad \left. - (xp'_\nu + yp_\nu) [\sigma^{\alpha\nu} \gamma^\beta \gamma^\mu \gamma_\beta \gamma_\alpha - \gamma_\alpha \gamma_\beta \gamma^\mu \gamma^\beta \sigma^{\alpha\nu}] \right)
\end{aligned} \tag{5.42}$$

where $p_1 = (1-x)p' - yp$ and $p_2 = (1-y)p - xp'$ and we used (B.3) to eliminate all odd terms in the loop momentum k as well as those that contribute only to the photon vertex renormalization. The tensor structure can be simplified using

Dirac Algebra

$$\gamma^\mu \gamma_\mu = D \quad (5.43)$$

$$\sigma^{\mu\alpha} \gamma_\alpha = i(D-1)\gamma^\mu \quad (5.44)$$

$$\gamma^\mu \gamma^\alpha \gamma_\mu = (2-D)\gamma^\alpha \quad (5.45)$$

$$\gamma^\mu \sigma^{\alpha\beta} \gamma_\mu = -(4-D)\sigma^{\alpha\beta} \quad (5.46)$$

$$\gamma^\mu \gamma^\alpha \gamma^\beta \gamma_\mu = 4\eta^{\alpha\beta} - (4-D)\gamma^\alpha \gamma^\beta \quad (5.47)$$

$$\gamma^\mu \gamma^\alpha \gamma^\beta \gamma^\sigma \gamma_\mu = -2\gamma^\sigma \gamma^\beta \gamma^\alpha + (4-D)\gamma^\alpha \gamma^\beta \gamma^\sigma \quad (5.48)$$

In particular, to find the coefficient of the $\frac{1}{\epsilon}$ pole we can set $D = 4$ and obtain

$$\begin{aligned} i\Gamma_{(b+c)}^\mu \Big|_{\frac{1}{\epsilon}} &\simeq -iC_{H_\mu} \frac{Q_\mu^3 e^3}{4\pi^2} \frac{1}{\epsilon} \int_0^1 dx \int_0^{1-x} dy \left(\gamma^\mu \not{p}_1 + \not{p}_2 \gamma^\mu + 5(p_1^\mu + p_2^\mu) + \frac{3}{2}(x+y)P^\mu \right) \\ &\simeq -C_{H_\mu} \frac{Q_\mu^3 e^3}{4\pi^2} \frac{1}{\epsilon} \int_0^1 dx \int_0^{1-x} dy \left(7 - \frac{9}{2}(x+y) \right) \sigma^{\mu\nu} q_\nu \\ &= -C_{H_\mu} \frac{Q_\mu^2 e^2}{4\pi^2} \frac{1}{\epsilon} \left(2Q_\mu e \sigma^{\mu\nu} q_\nu \right) \end{aligned} \quad (5.49)$$

From this, we can directly read off the required counterterm

$$Z_{H_\mu H_\mu}^{[1]} = \frac{Q_\mu^2 e^2}{4\pi^2} \quad (5.50)$$

$\mathcal{O}_{S\gamma\gamma} H_\mu$ Mixing At one-loop order, $\mathcal{O}_{S\gamma\gamma}$ mixes into the dipole operator through the following two diagrams



Figure 5.3: One-loop diagrams contributing to $\gamma_{\mathcal{O}_{S\gamma\gamma} H_\mu}$.

The corresponding amplitude for the CP-odd scalar is given by

$$\begin{aligned} i\Gamma_{(a+b)}^\mu &= iC_{\mathcal{O}_{A\gamma\gamma}} Q_\mu e^3 y_\mu^A \epsilon^{\mu\nu\alpha\beta} q_\alpha \mu^{2\epsilon} \int \frac{d^D k}{(2\pi)^D} \frac{\gamma_\nu (\not{p}' - \not{k} + m_\mu) \gamma^5 k_\beta}{[(k-p')^2 - m_\mu^2][(k-q)^2 - m_A^2]k^2} \\ &\quad + \frac{\gamma^5 (\not{k} + \not{p} + m_\mu) \gamma_\nu k_\beta}{[(k+p)^2 - m_\mu^2][(k-q)^2 - m_A^2]k^2} \\ &= C_{\mathcal{O}_{A\gamma\gamma}} \frac{y_\mu^A e^2}{32\pi^2} \left(\frac{1}{\epsilon} + \frac{3}{2} \right) \left(\frac{\bar{\mu}^2}{m_A^2} \right)^\epsilon (2eQ_\mu \sigma^{\mu\alpha} q_\alpha) \end{aligned} \quad (5.51)$$

where we set $m_\mu^2 = 0$ in the denominator and used the two identities

$$\begin{aligned} i\epsilon^{\alpha\beta\mu\nu} \gamma_\alpha \gamma^5 &= \gamma^\beta \gamma^\mu \gamma^\nu - \gamma^\beta \eta^{\mu\nu} + \gamma^\mu \eta^{\beta\nu} - \gamma^\nu \eta^{\beta\mu} \\ \epsilon^{\alpha\beta\mu\nu} \gamma_\alpha \gamma_\beta \gamma^5 &= 2\sigma^{\mu\nu} \end{aligned} \quad (5.52)$$

to simplify the gamma structure. The finite part, together with the full result for the Barr-Zee diagram, can be used to easily obtain the two-loop matching condition for the dipole operator,

which is however not needed in the calculation of the leading logarithms. Similarly, for the CP-even scalar we have

$$\begin{aligned}
 i\Gamma_{\mathcal{O}_{H\gamma\gamma}H_\mu}^\mu &= C_{\mathcal{O}_{H\gamma\gamma}} Q_\mu e^3 y_\mu^H \mu^{2\epsilon} \int \frac{d^D k}{(2\pi)^D} \frac{[\gamma^\mu q k - k^\mu \not{q}][\not{p}' - \not{k} + m_\mu]}{[(k-p')^2 - m_\mu^2][(k-q)^2 - m_H^2]k^2} \\
 &\quad - \frac{[\not{k} + \not{p} + m_\mu][\gamma^\mu q k - k^\mu \not{q}]}{[(k+p)^2 - m_\mu^2][(k-q)^2 - m_H^2]k^2} \\
 &= -C_{\mathcal{O}_{H\gamma\gamma}} \frac{y_\mu^H e^2}{32\pi^2} \left(\frac{1}{\epsilon} + \frac{3}{2} \right) \left(\frac{\bar{\mu}^2}{m_H^2} \right)^\epsilon (2Q_\mu e \sigma^{\mu\nu} q_\nu)
 \end{aligned} \tag{5.53}$$

The counterterms are therefore

$$Z_{\mathcal{O}_{A\gamma\gamma}H_\mu}^{[1]} = -\frac{y_\mu^A e^2}{32\pi^2}, \quad Z_{\mathcal{O}_{H\gamma\gamma}H_\mu}^{[1]} = \frac{y_\mu^H e^2}{32\pi^2} \tag{5.54}$$

$H_\mu \mathcal{O}_{S\gamma\gamma}$ Mixing In principle, the dipole operator can mix into $\mathcal{O}_{A\gamma\gamma}$ and $\mathcal{O}_{H\gamma\gamma}$ through light fermion loops.

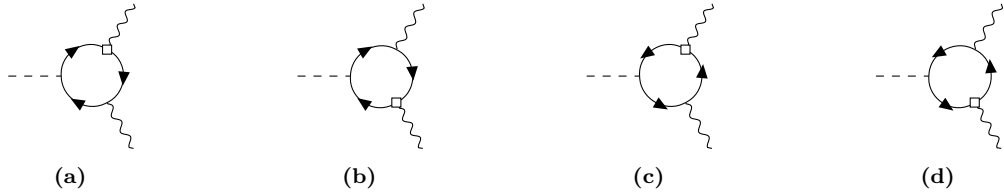


Figure 5.4: One-loop diagrams contributing to $\gamma_{H_\mu \mathcal{O}_{S\gamma\gamma}}$.

The corresponding amplitudes are however of $\mathcal{O}(y_f^S)$ and can, for our purposes, be neglected.

$$Z_{H_\mu \mathcal{O}_{A\gamma\gamma}}^{[1]} \approx 0, \quad Z_{H_\mu \mathcal{O}_{H\gamma\gamma}}^{[1]} \approx 0 \tag{5.55}$$

Even if we include them, they contribute to the leading logarithms first at 4-loop order.

$\mathcal{O}_{S\gamma\gamma} \mathcal{O}_{S\gamma\gamma}$ Mixing The operators $\mathcal{O}_{S\gamma\gamma}$ do not mix into each other at one-loop order.

$$Z_{\mathcal{O}_{A\gamma\gamma} \mathcal{O}_{A\gamma\gamma}}^{[1]} = Z_{\mathcal{O}_{A\gamma\gamma} \mathcal{O}_{H\gamma\gamma}}^{[1]} = Z_{\mathcal{O}_{H\gamma\gamma} \mathcal{O}_{A\gamma\gamma}}^{[1]} = Z_{\mathcal{O}_{H\gamma\gamma} \mathcal{O}_{H\gamma\gamma}}^{[1]} = 0 \tag{5.56}$$

5.3 Running Wilson Coefficients

We now have all counterterms from the operator mixing diagrams. In order to calculate the ADM entries we also need the operator renormalization constants. In section 4.4.2 we argued that the field strength renormalization should be given by the usual expressions in QED and QCD. At one-loop these are [93]

$$\begin{aligned}
 Z_\gamma &= 1 - \frac{1}{12\pi^2} \left(\sum N_c^f Q_f^2 e^2 \right) \frac{1}{\epsilon} + \dots \\
 Z_\mu &= 1 - \frac{1}{16\pi^2} Q_\mu^2 e^2 \frac{1}{\epsilon} + \dots \\
 Z_q &= 1 - \frac{1}{16\pi^2} \left(Q_q^2 e^2 + C_F g_s^2 \right) \frac{1}{\epsilon} + \dots
 \end{aligned} \tag{5.57}$$

The sum in photon renormalization factor Z_γ runs over all fermions in the EFT. The scalar field strength renormalization Z_S depends on the Yukawa couplings and parameters of the Higgs potential and should, in principle, be included as it contributes to the leading logarithms

through the diagonal ADM entries $\gamma_{\mathcal{O}_{S\gamma\gamma}\mathcal{O}_{S\gamma\gamma}}$. Here, we will focus only on the QED and QCD corrections and ignore this contribution. Since the composite operators are gauge invariant, the Ward-Takahashi identity holds also in the EFT and implies $Z_e\sqrt{Z_\gamma} = 1$. The operator renormalization factors therefore take the simple form

$$Z_{H_\mu} = Z_\mu, \quad Z_{\mathcal{O}_{S\gamma\gamma}} = 1 + \mathcal{O}(y_f^S, \lambda_i) \quad (5.58)$$

We will also need the one-loop QED and QCD beta functions, which can be obtained from the renormalization factors using (4.58)

$$\begin{aligned} \beta(e) &= +\frac{e^3}{12\pi^2} \sum N_c^f Q_f^2 \equiv \beta_e e^3 \\ \beta(g_s) &= -\frac{g_s^3}{16\pi^2} \left(11 - \frac{2n_f}{3} \right) \equiv -\beta_s g_s^3 \\ \beta(m_f) &= -\frac{3m_f}{8\pi^2} \left(Q_f^2 e^2 + C_F g_s^2 \right) \equiv -(\gamma_e e^2 + \gamma_s g_s^2) m_f \end{aligned} \quad (5.59)$$

where n_f denotes the number of quark flavours in the EFT and the sum, again, runs over all fermions in the EFT. These equations can be solved exactly to express the running coupling parameters in terms of their values at some fixed reference scale Q

$$\begin{aligned} e^2(\mu) &= \frac{e^2(Q)}{1 + 2\beta_e e^2(Q) \ln\left(\frac{Q}{\mu}\right)} \\ &\approx e^2(Q) \left(1 - 2\beta_e e^2(Q) \ln\left(\frac{Q}{\mu}\right) + \dots \right) \\ g_s^2(\mu) &= \frac{g_s^2(Q)}{1 - 2\beta_s g_s^2(Q) \ln\left(\frac{Q}{\mu}\right)} \\ &\approx g_s^2(Q) \left(1 + 2\beta_s g_s^2(Q) \ln\left(\frac{Q}{\mu}\right) + \dots \right) \\ m_f(\mu) &= m_f(Q) \left(\frac{e^2(Q)}{e^2(\mu)} \right)^{\frac{\gamma_e}{2\beta_e}} \left(\frac{g_s^2(Q)}{g_s^2(\mu)} \right)^{-\frac{\gamma_s}{2\beta_s}} \\ &\approx m_f(Q) \left(1 + \gamma_e e^2(Q) \ln\left(\frac{Q}{\mu}\right) + \gamma_s g_s^2(Q) \ln\left(\frac{Q}{\mu}\right) + \dots \right) \end{aligned} \quad (5.60)$$

The natural choice for the reference scale is different for the different parameters. For example, $\frac{e^2(m_e)}{4\pi} = \alpha(m_e) \approx \frac{1}{137}$, while $\alpha_s(m_Z) \approx 0.12$. Similarly, the running lepton masses are approximately equal to their pole masses at the small scale, while the quark masses are defined at different large scales. All physical values are taken from [67].

Finally, using (4.76) and the counterterms calculated in the last section, we obtain the one-loop ADM

$Z_{ij}^{[1]}$	H_μ	$\mathcal{O}_{A\gamma\gamma}$	$\mathcal{O}_{H\gamma\gamma}$
H_μ	$\frac{Q_\mu^2 e^2}{4\pi^2}$	0	0
$\mathcal{O}_{A\gamma\gamma}$	$-\frac{y_\mu^A e^2}{32\pi^2}$	0	0
$\mathcal{O}_{H\gamma\gamma}$	$\frac{y_\mu^H e^2}{32\pi^2}$	0	0

γ_{ij}	H_μ	$\mathcal{O}_{A\gamma\gamma}$	$\mathcal{O}_{H\gamma\gamma}$
H_μ	$\frac{5Q_\mu^2 e^2}{8\pi^2}$	0	0
$\mathcal{O}_{A\gamma\gamma}$	$-\frac{y_\mu^A e^2}{16\pi^2}$	0	0
$\mathcal{O}_{H\gamma\gamma}$	$\frac{y_\mu^H e^2}{16\pi^2}$	0	0

Figure 5.5: One-loop renormalization factors (left) and anomalous dimension matrix (right).

We now have everything we need to run the Wilson coefficients down to scale m_S . Due to the one-loop matching conditions for $C_{\mathcal{O}_{S\gamma\gamma}}$, in order to collect the 3-loop leading logarithms we need to expand (4.77) only up to the double integral. For C_{H_μ} we find

$$C_{H_\mu}(m_S) \approx C_{H_\mu}(m_t) - \int_{m_S}^{m_t} d\ln(\mu) \left\{ \sum_S C_{\mathcal{O}_{S\gamma\gamma}}(m_t) \gamma_{\mathcal{O}_{S\gamma\gamma}H_\mu}(\mu) - \int_{\mu}^{m_t} d\ln(\mu') \left(\sum_S C_{\mathcal{O}_{S\gamma\gamma}}(m_t) \gamma_{\mathcal{O}_{S\gamma\gamma}H_\mu}(\mu') \gamma_{H_\mu H_\mu}(\mu) + \dots \right) \right\} \quad (5.61)$$

From the Barr-Zee diagrams we found a two-loop matching condition for $C_{H_\mu}(m_t)$ which is irrelevant for the leading logarithms. However, if there were contributions from particles heavier than m_t their leading logarithmic terms would be captured in $C_{H_\mu}(m_t)$. For example, typically $m_H \approx m_{H^\pm} \gtrsim m_t$ is assumed in which case the one-loop logarithms found in section 4.1.1 would be included in the matching condition

$$C_{H_\mu}(m_t) = \frac{(y_\mu^H)^2}{16\pi^2} \frac{m_\mu}{m_H^2} \ln\left(\frac{m_H}{m_t}\right) + \dots \quad (5.62)$$

together with the two-loop logarithms from running in the previous EFT. In (5.61) we would then have to include the expression in (4.94) and obtain leading logarithms of the form

$$C_{H_\mu}(m_S) \sim \ln\left(\frac{m_H}{m_t}\right) \ln\left(\frac{m_t}{m_S}\right) \quad (5.63)$$

We will focus on the Barr-Zee logarithms for $m_S \gg m_f$ (for $f = \tau, b$) in the next chapter, but do not include them here and instead continue with $m_A, m_H \ll m_t$. To obtain the correct 3-loop logarithms, we need to include the running of the coupling parameters in $\gamma_{\mathcal{O}_{S\gamma\gamma}H_\mu}(\mu)$ in the first integral. This can be done by either substituting $d\ln(\mu) = \frac{de}{\beta(e)}$ or, as we will do, by expanding (5.60) and obtaining the logarithms explicitly from the integrals. Using $y_\mu^S \propto m_\mu$ we have

$$\gamma_{\mathcal{O}_{S\gamma\gamma}H_\mu}(\mu) \approx \gamma_{\mathcal{O}_{S\gamma\gamma}H_\mu}(m_S) \left(1 - (2\beta_e - \gamma_e) e^2(m_S) \ln\left(\frac{m_S}{\mu}\right) + \dots \right) \quad (5.64)$$

We can ignore this running in the double integral, because the leading result is already of 3-loop order. With this, we find

$$C_{H_\mu}(m_S) \approx C_{H_\mu}(m_t) - \sum_S C_{\mathcal{O}_{S\gamma\gamma}}(m_t) \gamma_{\mathcal{O}_{S\gamma\gamma}H_\mu}(m_S) \int_{m_S}^{m_t} d\ln(\mu) \left\{ \left(1 - (2\beta_e - \gamma_e) e^2(m_S) \ln\left(\frac{m_S}{\mu}\right) - \gamma_{H_\mu H_\mu}(m_S) \int_{\mu}^{m_t} d\ln(\mu') + \dots \right) \right\} \quad (5.65)$$

Using the matching conditions (5.38) we can write the result explicitly in terms of the coupling parameters

$$\begin{aligned} C_{H_\mu}(m_S) \approx C_{H_\mu}(m_t) &+ N_c^t \frac{Q_t^2 \tilde{e}^2}{64\pi^4} \frac{1}{m_t} \left(\hat{y}_t^A \tilde{y}_\mu^A \left[\ln\left(\frac{m_t}{m_A}\right) \right. \right. \\ &+ \left. \left(\frac{\tilde{e}^2}{6\pi^2} \sum N_c^f Q_f^2 - \frac{Q_\mu^2 \tilde{e}^2}{\pi^2} \right) \frac{1}{2} \ln^2\left(\frac{m_t}{m_A}\right) \right] \\ &- \frac{2}{3} \hat{y}_t^H \tilde{y}_\mu^H \left(1 - \frac{3\hat{g}_s^2 C_F}{(4\pi)^2} \right) \left[\ln\left(\frac{m_t}{m_H}\right) \right. \\ &+ \left. \left. \left(\frac{\tilde{e}^2}{6\pi^2} \sum N_c^f Q_f^2 - \frac{Q_\mu^2 \tilde{e}^2}{\pi^2} \right) \frac{1}{2} \ln^2\left(\frac{m_t}{m_H}\right) \right] + \dots \right) \end{aligned} \quad (5.66)$$

where the parameters \hat{g}_s and \hat{y}_t^S are evaluated at $\mu = m_t$, while the parameters \tilde{e} and \tilde{y}_μ^S are evaluated at $\mu = m_S$. The mass parameters are evaluated already at their respective defining scales and therefore correspond directly to the pole masses. The sums run over all fermions of the EFT, i.e. all except the top-quark. As promised, this expression contains the two-loop logarithms we found in the explicit expansion of the Barr-Zee result (5.2) (using our convention $\Delta a_\mu = 4m_\mu C_{H_\mu}$), but now we also have obtained the leading 3-loop logarithms from QED and QCD corrections to the Barr-Zee diagram! Finally, the coefficients $C_{\mathcal{O}_{S\gamma\gamma}}$ do not receive any QED or QCD corrections at one-loop order and are, therefore, approximately constant.

In the next step we want to expand out the scalars to obtain the logarithmic corrections generated by Barr-Zee diagrams with light fermion loops. As before, we will use the LME to find the relevant operators, except that we now start from the EFT we have constructed in this chapter. In principle, in addition to the Barr-Zee diagrams with light fermions, we also need to expand all other EFT diagrams containing scalars. However, at the matching scale m_S these do not contain any of the leading logarithms we are interested in and can therefore be ignored. The only new operators therefore come from the expansion of the remaining Barr-Zee diagrams, which we will calculate in the following chapter.

6 Corrections for Light Fermion Loop

We now move on to calculate the leading logarithmic corrections to the Barr-Zee diagrams with fermion loops at the intermediate scale.

$$m_\mu \ll m_f \ll m_S \quad (6.1)$$

In section 3.3 we found the following correction to a_μ from the explicit expansion of the loop functions

$$\Delta a_\mu^{2\text{HDM},2,f} \approx \frac{m_\mu e^2}{8\pi^4} \sum_f N_c^f Q_f^2 m_f \left(\frac{y_\mu^A y_f^A}{m_A^2} \ln^2 \left(\frac{m_A}{m_f} \right) - \frac{y_\mu^H y_f^H}{m_H^2} \ln^2 \left(\frac{m_H}{m_f} \right) \right) \quad (6.2)$$

where the τ lepton and b quark give the most significant contributions. Like in the previous chapter, we will use this result as a reference for the logarithms obtained from the renormalization group running.

6.1 Operators and Matching Condition

At the end of the last chapter we argued that the relevant operators in this EFT follow from the matching diagrams obtained from the LME of the remaining Barr-Zee diagrams. Again, only the lowest order matching conditions will be important for the leading logarithms, except this time we also have a tree-level matching condition for the dipole operator that contains the two- and 3-loop leading logarithms from the top quark loop. We will come back to this at the end when we calculate the logarithms. For now, let us consider the LME of the Barr-Zee diagrams with a light fermion loop given by

$$\begin{aligned} \text{Barr-Zee diagram} &= \text{Tree-level matching diagram} \circ \mathcal{T} \left(\text{Feynman diagram} \right) + \text{Tree-level matching diagram} \circ \mathcal{T} \left(\text{Feynman diagram} \right) \\ &+ \text{Tree-level matching diagram} \circ \mathcal{T} \left(\text{Feynman diagram} \right) + \text{Tree-level matching diagram} \circ \mathcal{T} \left(\text{Feynman diagram} \right) \end{aligned} \quad (6.3)$$

In contrast to the LME of the Barr-Zee diagram with a heavy fermion loop, this time we find a tree-level matching diagram at lowest order. In fact, this matching diagram is basically the same as the one we found in the one-loop example (4.12), except that we now get one such diagram for each of the light fermions.

$$\begin{aligned} \mathcal{T} \left(\text{Feynman diagram} \right) &= (-iy_\mu^H \delta_{ab}) \frac{i}{k^2 - m_H^2} (-iy_f^H \delta_{ij}) \approx i \frac{y_\mu^H y_f^H}{m_H^2} \delta_{ab} \delta_{ij} + \dots \\ \mathcal{T} \left(\text{Feynman diagram} \right) &= (-y_\mu^A \gamma_{ab}^5) \frac{i}{k^2 - m_A^2} (-y_f^A \gamma_{ij}^5) \approx -i \frac{y_\mu^A y_f^A}{m_A^2} \gamma_{ab}^5 \gamma_{ij}^5 + \dots \end{aligned} \quad (6.4)$$

As in section 4.1.2 these diagrams are described by four-fermion operators.

$$\mathcal{O}_f^H = (\bar{\mu}\mu)(\bar{f}f), \quad \mathcal{O}_f^A = (\bar{\mu}\gamma^5\mu)(\bar{f}\gamma^5f) \quad (6.5)$$

with corresponding matching conditions

$$C_{\mathcal{O}_\mu^H}(m_H) = \frac{y_\mu^H y_f^H}{m_H^2}, \quad C_{\mathcal{O}_\mu^A}(m_A) = -\frac{y_\mu^A y_f^A}{m_A^2} \quad (6.6)$$

With this, we can directly move on to the mixing diagrams.

6.2 Operator Mixing

Like in the previous chapter, we now need to calculate all possible mixing diagrams between the dipole and four-fermion operators. We start with the four-fermion mixing.

$\mathcal{O}_f^S \mathcal{O}_f^S$ Mixing There are four different types of mixing diagrams between the four fermion operators

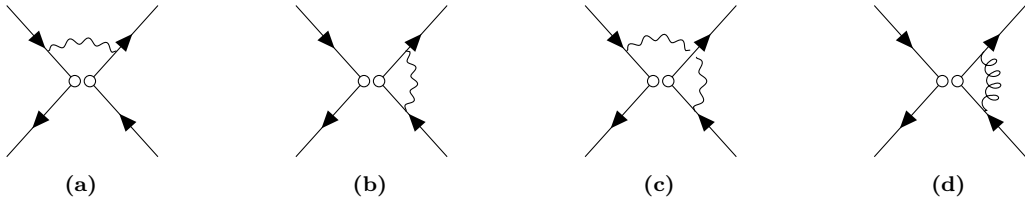


Figure 6.1: Diagrams contributing to the four-fermion operator mixing at one-loop order.

When calculating the diagrams, we must be careful to keep the different Dirac chains separate. The divergences can be easily read off from the amplitudes given by (including all equivalent diagrams)

$$\begin{aligned} i\Gamma_{(a)} &= C_{\mathcal{O}_f^S} Q_\mu Q_f e^2 \int_k \left(\frac{[\gamma^\mathcal{O}(\not{k} + \not{p} + m_\mu)\gamma^\alpha]_{ab} [\gamma_\alpha(\not{k} + \not{q}' + m_f)\gamma^\mathcal{O}]_{ij}}{[(k+p)^2 - m_\mu^2][(k+q')^2 - m_f^2]k^2} \right. \\ &\quad \left. + \frac{[\gamma^\alpha(\not{k} + \not{p}' + m_\mu)\gamma^\mathcal{O}]_{ab} [\gamma^\mathcal{O}(\not{k} + \not{q}' + m_f)\gamma_\alpha]_{ij}}{[(k+p)^2 - m_\mu^2][(k+q')^2 - m_f^2]k^2} \right) \\ &\simeq iC_{\mathcal{O}_f^S} \frac{Q_f Q_\mu e^2}{4(4\pi)^2} \frac{1}{\epsilon} \left([\gamma^\mathcal{O}\gamma^\beta\gamma^\alpha]_{ab} [\gamma_\alpha\gamma_\beta\gamma^\mathcal{O}]_{ij} + [\gamma^\alpha\gamma^\beta\gamma^\mathcal{O}]_{ab} [\gamma^\mathcal{O}\gamma_\beta\gamma_\alpha]_{ij} \right) \end{aligned} \quad (6.7)$$

where $\gamma^\mathcal{O} = 1$ for \mathcal{O}_f^H and $\gamma^\mathcal{O} = \gamma^5$ for \mathcal{O}_f^A . Similarly, for the other diagrams we find

$$\begin{aligned} i\Gamma_{(b)} &\simeq +iC_{\mathcal{O}_f^S} \frac{e^2}{4(4\pi)^2} \frac{1}{\epsilon} \left(Q_\mu^2 [\gamma_\beta\gamma_\alpha\gamma^\mathcal{O}\gamma^\alpha\gamma^\beta]_{ab} \gamma_{ij}^\mathcal{O} + Q_f^2 \gamma_{ab}^\mathcal{O} [\gamma_\beta\gamma_\alpha\gamma^\mathcal{O}\gamma^\alpha\gamma^\beta]_{ij} \right) \\ i\Gamma_{(c)} &\simeq -iC_{\mathcal{O}_f^S} \frac{Q_f Q_\mu e^2}{4(4\pi)^2} \frac{1}{\epsilon} \left([\gamma^\mathcal{O}\gamma^\beta\gamma^\alpha]_{ab} [\gamma^\mathcal{O}\gamma_\beta\gamma_\alpha]_{ij} + [\gamma^\alpha\gamma^\beta\gamma^\mathcal{O}]_{ab} [\gamma_\alpha\gamma_\beta\gamma^\mathcal{O}]_{ij} \right) \\ i\Gamma_{(d)} &\simeq +iC_{\mathcal{O}_f^S} \frac{g_s^2 C_F}{4(4\pi)^2} \frac{1}{\epsilon} \gamma_{ab}^\mathcal{O} [\gamma_\beta\gamma_\alpha\gamma^\mathcal{O}\gamma^\alpha\gamma^\beta]_{ij} \end{aligned} \quad (6.8)$$

To bring this vertex structure back into the form of our original four-fermion operators we can use the two identities

$$\begin{aligned} \gamma^\alpha\gamma^\beta &= \eta^{\mu\nu} - i\sigma^{\alpha\beta} \\ \gamma^5\sigma^{\alpha\beta} &= \frac{i}{2}\epsilon^{\alpha\beta\mu\nu}\sigma_{\mu\nu} \end{aligned} \quad (6.9)$$

With this, the vertex structure simplifies to

$$i\Gamma_{(a+b+c+d)} = iC_{\mathcal{O}_f^S} \left(\left[\frac{e^2}{4\pi^2} (Q_\mu^2 + Q_f^2) + \frac{g_s^2 C_F}{4\pi^2} \right] \gamma_{ab}^{\mathcal{O}} \gamma_{ij}^{\mathcal{O}} + \frac{e^2 Q_\mu Q_f}{(4\pi)^2} [\sigma^{\alpha\beta}]_{ab} [\sigma_{\alpha\beta}]_{ij} \right) \quad (6.10)$$

and we obtain the self-mixing counterterms

$$Z_{\mathcal{O}_f^H \mathcal{O}_f^H}^{[1]} = Z_{\mathcal{O}_f^A \mathcal{O}_f^A}^{[1]} = -\frac{e^2}{4\pi^2} (Q_\mu^2 + Q_f^2) - \frac{g_s^2 C_F}{4\pi^2} \quad (6.11)$$

However, we also find a term that requires a new operator

$$\mathcal{O}_f^T = (\bar{\mu} \sigma^{\alpha\beta} \mu) (\bar{f} \sigma_{\alpha\beta} f) \quad (6.12)$$

in order to remove all of the divergences.

The original four-fermion operators mix into \mathcal{O}_f^T with the counterterm

$$Z_{\mathcal{O}_f^H \mathcal{O}_f^T}^{[1]} = Z_{\mathcal{O}_f^A \mathcal{O}_f^T}^{[1]} = -\frac{e^2}{(4\pi)^2} Q_\mu Q_f \quad (6.13)$$

Finally, we will also need the counterterms for \mathcal{O}_f^T mixing into other four-fermion operators. The corresponding amplitudes are also given by (6.7) and (6.8) with $\gamma^{\mathcal{O}} = \sigma^{\mu\nu}$. To simplify the vertex structure we can use (5.52) together with the identities given above. After some algebraic manipulation we find

$$i\Gamma_{(a+b+c+d)} = iC_{\mathcal{O}_f^T} \frac{3e^2}{2\pi^2} Q_\mu Q_f (\gamma_{ab}^5 \gamma_{ij}^5 + \delta_{ab} \delta_{ij}) \quad (6.14)$$

which gives

$$Z_{\mathcal{O}_f^T \mathcal{O}_f^T}^{[1]} = 0, \quad Z_{\mathcal{O}_f^T \mathcal{O}_f^H}^{[1]} Z_{\mathcal{O}_f^T \mathcal{O}_f^A}^{[1]} = -\frac{3e^2}{2\pi^2} Q_\mu Q_f \quad (6.15)$$

$\mathcal{O}_f^{S,T}$ H_μ Mixing The four-fermion operators can mix into H_μ via the one-loop diagrams¹



Figure 6.2: One-loop diagrams contributing to the mixing of the four-fermion operators into the dipole operator.

Diagram (a) only contributes for $f = \mu$. The matching condition of the corresponding Wilson coefficients is of $\mathcal{O}((y_\mu^S)^2)$ and the diagram can therefore be ignored. The amplitude of diagram (b) can be written as

$$\begin{aligned} i\Gamma_{(b)}^\mu &= \gamma^{\mathcal{O}} C_{\mathcal{O}} N_c^f Q_f e \int_k \frac{\text{Tr}\{\gamma^{\mathcal{O}}(\not{k} + \not{q} + m_f) \gamma^\mu (\not{k} + m_f)\}}{[(k+q)^2 - m_f^2][k^2 - m_f^2]} \\ &= \gamma^{\mathcal{O}} C_{\mathcal{O}} N_c^f Q_f e \int_0^1 dx \int_k \frac{\text{Tr}\{\gamma^{\mathcal{O}}(\not{k} + (1-x)\not{q} + m_f) \gamma^\mu (\not{k} - x\not{q} + m_f)\}}{[k^2 - m_f^2]^2} \end{aligned} \quad (6.16)$$

¹In the full calculation there was also a contribution from the Barr-Zee diagram with opposite fermion loop. In the EFT the diagrams with opposite fermion direction are the same only one must be included. Instead, the additional factor of 2 is contained in the matching condition of the four-fermion operators.

For $\gamma^O = \gamma^5$ the trace already vanishes and for $\gamma^O = \mathbb{1}$ the trace gives

$$\text{Tr}\{(\not{k} + (1-x)\not{q} + m_f)\gamma^\mu(\not{k} - x\not{q} + m_f)\} = 4m_f(2k^\mu - (1-2x)q^\mu) \quad (6.17)$$

The k^μ term drops out in the momentum integral and the q^μ term drops out in the Feynman parameter integral. For $\gamma^O = \sigma_{\alpha\beta}$ the trace gives

$$\text{Tr}\{\sigma_{\alpha\beta}(\not{k} + (1-x)\not{q} + m_f)\gamma^\mu(\not{k} - x\not{q} + m_f)\} = 4im_f(\delta_\alpha^\mu q_\beta - \delta_\beta^\mu q_\alpha) \quad (6.18)$$

With this, the amplitude becomes

$$\begin{aligned} i\Gamma_{(b)}^\mu &= -8C_{\mathcal{O}_f^T} N_f m_f \frac{Q_f e}{(4\pi)^2} \sigma^{\mu\beta} q_\beta \int_k \frac{1}{[k^2 - m_f^2]^2} \\ &= -C_{\mathcal{O}_f^T} \frac{Q_f}{Q_\mu} \frac{N_c^f m_f}{4\pi^2} \frac{1}{\epsilon} (2Q_\mu e \sigma^{\mu\nu} q_\nu) + \dots \end{aligned} \quad (6.19)$$

Therefore, only \mathcal{O}_f^T mixes into H_μ at one-loop

$$Z_{\mathcal{O}_f^H H_\mu}^{[1]} = Z_{\mathcal{O}_f^A H_\mu}^{[1]} = 0, \quad Z_{\mathcal{O}_f^T H_\mu}^{[1]} = \frac{Q_f}{Q_\mu} \frac{N_c^f m_f}{4\pi^2} \quad (6.20)$$

$H_\mu \mathcal{O}_f^{S,T}$ Mixing H_μ can mix into the four-fermion operators over box diagrams like



Figure 6.3: One-loop diagrams contributing to the mixing of the dipole operator into four-fermion operators.

However, from our power counting argument in section 4.2.1 we expect no mixing of the dim-5 dipole operator into the dim-6 four-fermion operators at $\mathcal{O}(C_{H_\mu})$. This is confirmed explicitly by the above diagrams, because (a) is finite and (b) is divergent but of $\mathcal{O}(C_{H_\mu}^2)$ and can therefore be ignored. Thus, to good approximation, the dipole operator does not mix into the four-fermion operators.

$$Z_{H_\mu \mathcal{O}_f^H}^{[1]} = Z_{H_\mu \mathcal{O}_f^A}^{[1]} = Z_{H_\mu \mathcal{O}_f^T}^{[1]} = 0 \quad (6.21)$$

6.3 Running Wilson Coefficients

We have now evaluated all of the mixing diagrams and can move on to calculate the ADM. Like in the last chapter, we need the operator renormalization factors. Using (5.57) we find

$$Z_{\mathcal{O}_f^S} = Z_\mu Z_f = 1 - \frac{1}{16\pi^2} \left((Q_\mu^2 + Q_f^2) e^2 + C_F g_s^2 \right) \frac{1}{\epsilon} \quad (6.22)$$

From the one-loop renormalization constants

$Z_{ij}^{[1]}$	H_μ	\mathcal{O}_f^H	\mathcal{O}_f^A	\mathcal{O}_f^T
H_μ	$\frac{Q_\mu^2 e^2}{4\pi^2}$	0	0	0
\mathcal{O}_f^H	0	$-\frac{e^2(Q_\mu^2+Q_f^2)}{4\pi^2} - \frac{g_s^2 C_F}{4\pi^2}$	0	$-\frac{e^2}{16\pi^2} Q_\mu Q_f$
\mathcal{O}_f^A	0	0	$-\frac{e^2(Q_\mu^2+Q_f^2)}{4\pi^2} - \frac{g_s^2 C_F}{4\pi^2}$	$-\frac{e^2}{16\pi^2} Q_\mu Q_f$
\mathcal{O}_f^T	$\frac{Q_f}{Q_\mu} \frac{N_c^f m_f}{4\pi^2}$	$-\frac{3e^2}{2\pi^2} Q_\mu Q_f$	$-\frac{3e^2}{2\pi^2} Q_\mu Q_f$	0

Figure 6.4: One-loop Renormalization Constants.

and (4.76) we obtain the following ADM

γ_{ij}	H_μ	\mathcal{O}_f^H	\mathcal{O}_f^A	\mathcal{O}_f^T
H_μ	$\frac{5Q_\mu^2 e^2}{8\pi^2}$	0	0	0
\mathcal{O}_f^H	0	$-\frac{3e^2(Q_\mu^2+Q_f^2)}{8\pi^2} - \frac{3C_F g_s^2}{8\pi^2}$	0	$-\frac{e^2}{8\pi^2} Q_\mu Q_f$
\mathcal{O}_f^A	0	0	$-\frac{3e^2(Q_\mu^2+Q_f^2)}{8\pi^2} - \frac{3C_F g_s^2}{8\pi^2}$	$-\frac{e^2}{8\pi^2} Q_\mu Q_f$
\mathcal{O}_f^T	$\frac{Q_f}{Q_\mu} \frac{N_c^f m_f}{2\pi^2}$	$-\frac{3e^2}{\pi^2} Q_\mu Q_f$	$-\frac{3e^2}{\pi^2} Q_\mu Q_f$	$\frac{e^2(Q_\mu^2+Q_f^2)}{8\pi^2} + \frac{C_F g_s^2}{8\pi^2}$

Figure 6.5: One-loop Anomalous Dimension Matrix.

Because of the tree-level matching conditions (6.6) we need to expand (4.77) up to the triple integral in order to obtain the leading 3-loop logarithms.

$$\begin{aligned}
C_{H_\mu}(m_\tau) &\approx C_{H_\mu}(m_S) - C_{H_\mu}(m_S) \int_{m_\tau}^{m_S} d\ln(\mu) \left(\gamma_{H_\mu H_\mu}(m_f) + \dots \right) \\
&+ \sum_{f,S} C_{\mathcal{O}_f^S}(m_S) \int_{m_\tau}^{m_S} d\ln(\mu) \int_\mu^{m_S} d\ln(\mu') \left\{ \gamma_{\mathcal{O}_f^S \mathcal{O}_f^T}(\mu') \gamma_{\mathcal{O}_f^T H_\mu}(\mu) \right. \\
&- \int_{\mu'}^{m_S} d\ln(\mu'') \left(\gamma_{\mathcal{O}_f^S \mathcal{O}_f^S}(m_f) \gamma_{\mathcal{O}_f^S \mathcal{O}_f^T}(m_f) \gamma_{\mathcal{O}_f^T H_\mu}(m_f) \right. \\
&\quad + \gamma_{\mathcal{O}_f^S \mathcal{O}_f^T}(m_f) \gamma_{\mathcal{O}_f^T \mathcal{O}_f^T}(m_f) \gamma_{\mathcal{O}_f^T H_\mu}(m_f) \\
&\quad \left. \left. + \gamma_{\mathcal{O}_f^S \mathcal{O}_f^T}(m_f) \gamma_{\mathcal{O}_f^T H_\mu}(m_f) \gamma_{H_\mu H_\mu}(m_f) + \dots \right) \right\}
\end{aligned} \tag{6.23}$$

Besides the two-loop matching condition from the LME of the Barr-Zee diagram, $C_{H_\mu}(m_S)$ also contains the relevant leading logarithms from the previous chapter given by (5.66). In particular, the leading two-loop logarithms in $C_{H_\mu}(m_S)$ now produce additional 3-loop logarithms through the integral in the first line. We can again ignore the running of the ADM entries in the highest order of this expansion, but need to include it everywhere else. Using the expressions for the running coupling parameters (5.60) we have

$$\begin{aligned}
\gamma_{\mathcal{O}_f^S \mathcal{O}_f^T}(\mu') \gamma_{\mathcal{O}_f^T H_\mu}(\mu) &= \gamma_{\mathcal{O}_f^S \mathcal{O}_f^T}(m_f) \gamma_{\mathcal{O}_f^T H_\mu}(m_f) \left(1 - 2\beta_e e^2(m_f) \ln\left(\frac{m_f}{\mu'}\right) \right. \\
&\quad \left. + \left[\gamma_e e^2(m_f) + \gamma_s g_s^2(m_f) \right] \ln\left(\frac{m_f}{\mu}\right) + \dots \right)
\end{aligned} \tag{6.24}$$

Both logarithmic terms in the expansion will produce leading 3-loop logarithms, but we must be careful about the order of integration as it leads to different prefactors in both terms.

$$\begin{aligned} \int_{m_f}^{m_S} d\ln(\mu) \int_{\mu}^{m_S} d\ln(\mu') \ln\left(\frac{m_f}{\mu'}\right) &= -\frac{1}{3} \ln^3\left(\frac{m_S}{m_f}\right) \\ \int_{m_f}^{m_S} d\ln(\mu) \int_{\mu}^{m_S} d\ln(\mu') \ln\left(\frac{m_f}{\mu}\right) &= -\frac{1}{6} \ln^3\left(\frac{m_S}{m_f}\right) \end{aligned} \quad (6.25)$$

With this we can evaluate the integrals and find

$$\begin{aligned} C_{H_\mu}(m_\tau) \approx C_{H_\mu}(m_S) &\left(1 - \frac{5Q_\mu^2 \bar{e}^2}{8\pi^2} \ln\left(\frac{m_S}{m_\tau}\right)\right) - \sum_{f,S} \eta_S \frac{\tilde{y}_\mu^S \tilde{y}_f^S}{m_S^2} \left\{ N_c^f m_f \frac{Q_f^2 \bar{e}^2}{16\pi^4} \left(\right. \right. \\ &\frac{1}{2} \ln^2\left(\frac{m_S}{m_f}\right) + \left[\frac{2}{3} \beta_e \bar{e}^2 - \frac{Q_f^2 \bar{e}^2 + C_F \bar{g}_s^2}{16\pi^2} \right] \ln^3\left(\frac{m_S}{m_f}\right) \Bigg) \\ &\left. - N_c^f m_f Q_f^2 \frac{\bar{e}^2}{3\pi^2} \frac{(2Q_f^2 - 3Q_\mu^2) \bar{e}^2 + 2C_F \bar{g}_s^2}{(4\pi)^4} \ln^3\left(\frac{m_S}{m_f}\right) + \dots \right\} \end{aligned} \quad (6.26)$$

Again, we find the two-loop logarithms from the explicit expansion (6.2). The parameters \tilde{y}_μ^S and \tilde{y}_f^S come from the matching conditions and are evaluated at $\mu = m_S$, while the parameters \bar{e} and \bar{g}_s come from the RGE running and are evaluated at $\mu = m_\tau$. In the first sum only the contributions from $f \in \{b, \tau\}$ are relevant, but the sum over f' must include all fermions in the EFT. The mass parameters should again be understood as the pole masses. Before we insert the explicit expression for $C_{H_\mu}(m_f)$ and express the parameters in terms of their appropriate scales, let us go one step further and integrate the RGE all the way down to m_μ . For this, we should construct a third EFT where all but the light fermions with $m_f \leq m_\mu$ are removed. However, the only relevant matching condition is that of the dipole operator given by the expression above. We therefore obtain just a very simple additional logarithm

$$C_{H_\mu}(m_\mu) \approx C_{H_\mu}(m_\tau) \left(1 - \frac{5Q_\mu^2 e^2}{8\pi^2} \ln\left(\frac{m_\tau}{m_\mu}\right) + \dots\right) \quad (6.27)$$

Finally, we can substitute all matching conditions and expand the results in terms of on-shell parameters, which generates additional 3-loop logarithms. After collecting all terms, our result for the leading logarithmic 3-loop corrections from QED and QCD to a_μ in the 2HDM is

$$\begin{aligned} \Delta a_\mu^{\text{2HDM,3,LL}} &= N_c^t \frac{Q_t^2 e^2}{16\pi^4} \frac{m_\mu}{m_t} \left\{ \hat{y}_t^A y_\mu^A \left[\left(2\beta_e - \frac{Q_\mu^2}{\pi^2} \right) \frac{e^2}{2} \ln\left(\frac{m_A m_t}{m_\mu^2}\right) \right] \ln\left(\frac{m_t}{m_A}\right) \right. \\ &- \frac{2}{3} \hat{y}_t^H y_\mu^H \left[\left(2\beta_e - \frac{Q_\mu^2}{\pi^2} \right) \frac{e^2}{2} \ln\left(\frac{m_H m_t}{m_\mu^2}\right) - \frac{3\hat{g}_s^2 C_F}{(4\pi)^2} \right] \ln\left(\frac{m_t}{m_H}\right) \Bigg\} \\ &- \sum_{f,S} \eta_S N_c^f \frac{Q_f^2 e^2}{8\pi^4} \frac{m_f m_\mu}{m_S^2} y_\mu^S \tilde{y}_f^S \left\{ \left(2\beta_e - \frac{Q_\mu^2}{\pi^2} \right) \frac{e^2}{3} \ln\left(\frac{m_f m_S^2}{m_\mu^3}\right) \right. \\ &\left. - \frac{7\bar{g}_s^2 C_F + (7Q_f^2 - 5Q_\mu^2) e^2}{12\pi^2} \ln\left(\frac{m_S}{m_f}\right) \right\} \ln^2\left(\frac{m_S}{m_f}\right) \end{aligned} \quad (6.28)$$

where $\beta_e = \sum_{f \neq t} N_c^f Q_f^2$. The parameters y_μ^S and e are evaluated at $\mu = m_\mu$, \bar{y}_f^S and \bar{g}_s at $\mu = m_f$ and \hat{y}_t^S and \hat{g}_s at $\mu = m_t$, which corresponds to the on-shell parametrization. With this result we have also fixed the two-loop expression (3.46) in terms of on-shell parameters. We can now revisit the plots from section 3.3.3 to decide which of the schemes best captures these 3-loop corrections.

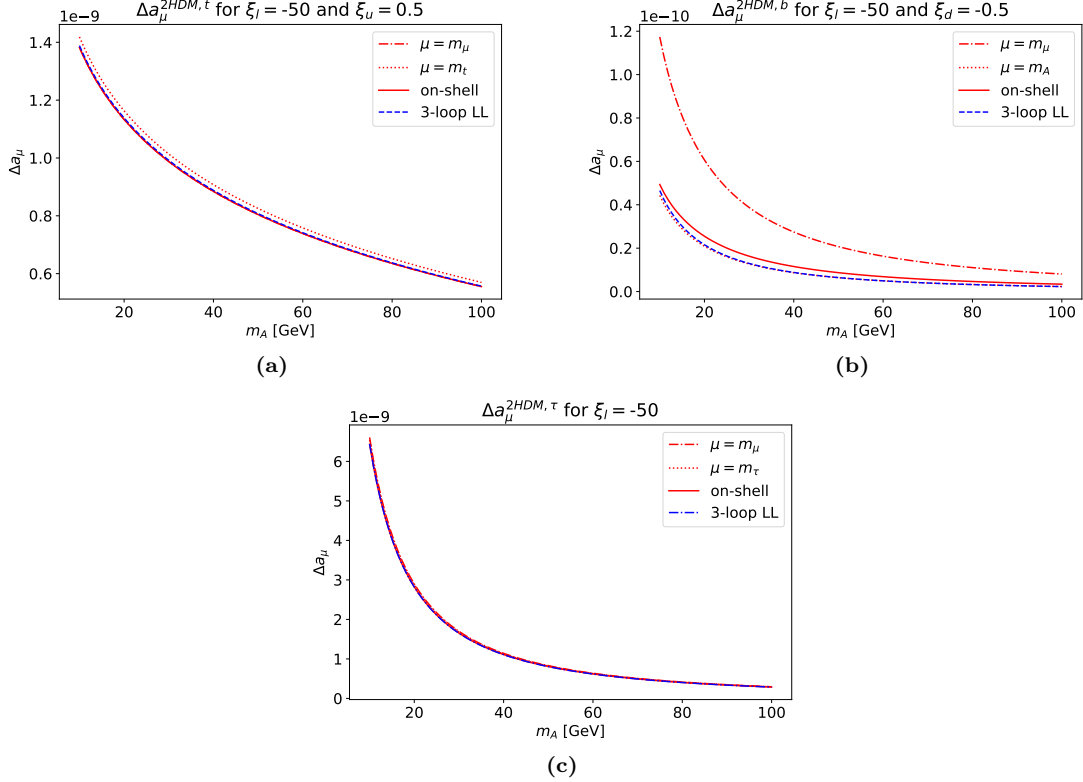


Figure 6.6: Contributions to $\Delta a_\mu^{2\text{HDM},2}$ from the Barr-Zee diagram with CP-odd Higgs and t-quark (a), b-quark (b) and tau-lepton (c) loop as a function of m_A for representative values of the alignment parameters $\xi_l = -50$, $\xi_u = 0.5$ and $\xi_d = -0.5$ and different choices of the renormalization scale μ . The blue lines show the on-shell results including the 3-loop leading logarithms.

Fig.6.6 again shows the same plots as Fig.3.5, but this time including the 3-loop leading logarithms. We can clearly see that the on-shell parametrization results in smallest 3-loop correction in each case. To understand this result, as promised, we now compare the different parametrizations using the expressions (5.60) for the running couplings. Starting with the top contribution we find

$$\Delta a_\mu^{2\text{HDM},t}(\mu = m_t) \approx \Delta a_\mu^{2\text{HDM},t,\text{OS}} \cdot \underbrace{\left(1 + 2 \left(\beta_e - \frac{3Q_\mu^2}{8\pi^2} \right) e^2 \ln \left(\frac{m_t}{m_\mu} \right) + \dots \right)}_{\approx 0.03} \quad (6.29)$$

On the other hand, the low scale ($\mu = m_\mu$) parametrization already corresponds to the on-shell parametrization because the QCD running cancels in $\Delta a_\mu^{2\text{HDM},t} \propto \frac{y_t^S}{m_t}$. We therefore find a $\sim 3\%$ difference between both schemes. The actual leading logarithmic correction is given by

$$\Delta a_\mu^{2\text{HDM},3,\text{LL},t} = \Delta a_\mu^{2\text{HDM},2,\text{LL},t} \cdot \underbrace{\left(2\beta_e - \frac{Q_\mu^2}{\pi^2} \right) \frac{e^2}{2} \ln \left(\frac{m_A m_t}{m_\mu^2} \right)}_{\approx 0.01} \quad (6.30)$$

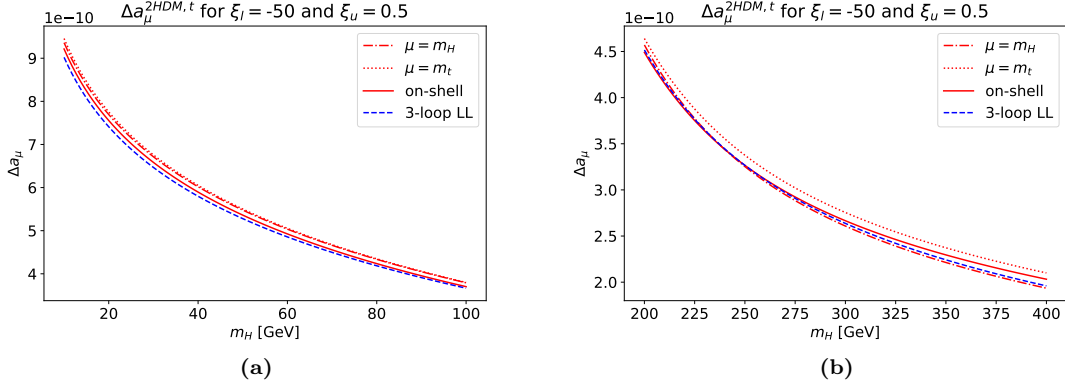


Figure 6.7: Top contribution to $\Delta a_\mu^{2\text{HDM},2}$ from the Barr-Zee diagram with light (a) and heavy (b) CP-even Higgs in the SM limit $\beta - \alpha = \frac{\pi}{2}$ as a function of m_H with $\xi_l = -50$, $\xi_u = 0.5$ and different choices of the renormalization scale μ . The blue lines show the on-shell results including the 3-loop leading logarithms.

which is smaller than the leading logarithms produced by the high scale parametrization. In addition, the high scale parametrization also produces NLO logarithms and includes the higher order leading logarithms resummed in $e^2(m_t)$. The on-shell parametrization is therefore much closer to the 3-loop result. However, it is worth pointing out that the 3-loop contribution is small only because in case of the CP-odd Higgs we found no QCD corrections to the matching condition. For the CP-even Higgs the QCD logarithm leads to a larger correction to the on-shell result that cannot not be captured by any of these simple parametrizations. This is illustrated in Fig.6.7 where the top contributions are shown for both heavy and light CP-even Higgs masses m_H . For light Higgs masses we see the negative correction coming from the large QCD logarithm which, as expected, deviates from all parametrizations, while for (very) heavy Higgs masses the parametrization at $\mu = m_H$ agrees very well with the actual correction. This agreement comes from the fact that running m_t to a smaller scale correctly captures the sign of the QCD logarithms in (6.28). And while the parametrization does not reproduce the leading logarithms exactly, the remaining terms are rather small

$$\Delta a_\mu^{2\text{HDM},t}(m_H) - \Delta a_\mu^{2\text{HDM},3,\text{LL},t} \approx \Delta a_\mu^{2\text{HDM},t,\text{OS}} \left\{ 1 - \underbrace{\frac{Q_f^2 e^2 + C_F g_s^2}{6\pi^2} \ln\left(\frac{m_H}{m_t}\right)}_{\approx 0.005 \dots 0.03} + \underbrace{\left(2\beta_e + \frac{Q_\mu^2}{4\pi^2}\right) \frac{e^2}{3} \ln\left(\frac{m_H}{m_t}\right) + \frac{Q_\mu^2 e^2}{4\pi^2} \ln\left(\frac{m_H}{m_\mu}\right)}_{\approx 0.02} \right\} \quad (6.31)$$

Before we move on, we should note that taking into account experimental constraints, contributions from the CP-even Higgs are strongly suppressed [5]. For the remaining discussion we will therefore focus only on the CP-odd Higgs.

Continuing with the light quark contributions, the reason why the different parametrizations deviate so strongly from the actual 3-loop corrections is that for light fermions $\Delta a_\mu^{2\text{HDM},f} \propto y_f^S m_f$. The QCD running therefore does not cancel and leads to large leading logarithms. Like in the case of the top-quark contribution for large m_H , choosing $\mu = m_A$ reproduces the correct signs of the logarithms and therefore leads to the smallest deviation

from the actual 3-loop correction. On the other hand, choosing $\mu = m_b$ or $\mu = m_\mu$ results in

$$\begin{aligned}\Delta a_\mu^{2\text{HDM},b}(\mu = m_b) &\approx \Delta a_\mu^{2\text{HDM},t,\text{OS}} \cdot \underbrace{\left(1 + 2 \left(\beta_e - \frac{3Q_\mu^2}{8\pi^2}\right) e^2 \ln\left(\frac{m_b}{m_\mu}\right) + \dots\right)}_{\approx 0.01} \\ \Delta a_\mu^{2\text{HDM},b}(\mu = m_\mu) &\approx \Delta a_\mu^{2\text{HDM},t,\text{OS}} \cdot \underbrace{\left(1 + 2 \left(\frac{3Q_b^2}{8\pi^2} \tilde{e}^2 + \frac{3C_F}{8\pi^2} \tilde{g}_s^2\right) \ln\left(\frac{m_b}{m_\mu}\right) + \dots\right)}_{\approx 0.80}\end{aligned}\quad (6.32)$$

In contrast to the top contributions with light m_A , in this case the low scale parametrization produces very large leading QCD logarithms with the opposite sign to those in (6.28) and therefore deviates a lot from the actual correction. For $\mu = m_b$ the expansion does not contain any QCD logarithms and is numerically quite close to the on-shell two-loop result. We can again compare these expansions to the actual 3-loop leading logarithms

$$\begin{aligned}\Delta a_\mu^{2\text{HDM},3,\text{LL},b} &= \Delta a_\mu^{2\text{HDM},2,\text{LL},b} \cdot \left\{ \left(2\beta_e - \frac{Q_\mu^2}{\pi^2}\right) \frac{e^2}{3} \ln\left(\frac{m_b m_A^2}{m_\mu^3}\right) \right. \\ &\quad \left. - \frac{7\tilde{g}_s^2 C_F + (7Q_f^2 - 5Q_\mu^2)e^2}{12\pi^2} \ln\left(\frac{m_A}{m_b}\right) \right\} \\ &\approx -(0.20 \dots 0.35) \cdot \Delta a_\mu^{2\text{HDM},2,\text{LL},b}\end{aligned}\quad (6.33)$$

The low scale parametrization completely fails to reproduce this correction and therefore deviates strongly from the actual result. Choosing $\mu = m_b$ roughly gives the right QED logarithm, but still deviates by up to $\sim 50\%$ (at large scalar masses) from the actual correction due to the missing QCD terms. In any case, the light quark contributions are quite small and, taking into account experimental constraints, can essentially be ignored. Lastly, as evident from Fig.6.6, the parametrizations of the τ contribution only result in very small numerical differences

$$\begin{aligned}\Delta a_\mu^{2\text{HDM},\tau}(\mu = m_\tau) &\approx \Delta a_\mu^{2\text{HDM},\tau,\text{OS}} \cdot \underbrace{\left(1 + 2 \left(\beta_e - \frac{3Q_\mu^2}{8\pi^2}\right) e^2 \ln\left(\frac{m_\tau}{m_\mu}\right) + \dots\right)}_{\approx 0.01} \\ \Delta a_\mu^{2\text{HDM},\tau}(\mu = m_\mu) &\approx \Delta a_\mu^{2\text{HDM},\tau,\text{OS}} \cdot \underbrace{\left(1 + \frac{3Q_\tau^2}{4\pi^2} e^2 \ln\left(\frac{m_\tau}{m_\mu}\right) + \dots\right)}_{\approx 0.02}\end{aligned}\quad (6.34)$$

Due to the absence of QCD correction, the actual 3-loop result is also very small

$$\begin{aligned}\Delta a_\mu^{2\text{HDM},3,\text{LL},\tau} &= \Delta a_\mu^{2\text{HDM},2,\text{LL},\tau} \cdot \left\{ \left(2\beta_e - \frac{Q_\mu^2}{\pi^2}\right) \frac{e^2}{3} \ln\left(\frac{m_\tau m_A^2}{m_\mu^3}\right) \right. \\ &\quad \left. - \frac{(7Q_\tau^2 - 5Q_\mu^2)e^2}{12\pi^2} \ln\left(\frac{m_A}{m_\tau}\right) \right\} \\ &\approx -0.01 \cdot \Delta a_\mu^{2\text{HDM},2,\text{LL},\tau}\end{aligned}\quad (6.35)$$

The on-shell parametrization is therefore, again, closest to the actual result.

7 Summary

The Two-Higgs-Doublet Model (2HDM) has been known for a long time as a potential explanation for the deviation of the measurement of the anomalous magnetic moment of the muon a_μ from the Standard Model (SM) prediction. As an extension to the SM Higgs sector, the 2HDM introduces an additional CP-even Higgs H , a CP-odd Higgs A and a charged Higgs H^\pm . In this thesis we focused on the aligned 2HDM, which contains the usual Type X, Y, I and II 2HDM as special cases. The dominant contributions to a_μ in the 2HDM arise at the two-loop level through Barr-Zee diagrams with the light pseudoscalar A ($m_A \sim 20 \dots 100$ GeV) and heavy fermion loops. The goal of this thesis was to reduce the theoretical uncertainty of these two-loop results by calculating the leading logarithmic 3-loop corrections to the Barr-Zee diagrams. Due to the multiple different mass scales involved in the calculation, these logarithmic contributions can become very large and in this way provide a good approximation of the higher order corrections.

Since a direct computation of the 3-loop amplitudes is rather tedious, we instead made use of a well known effective field theory (EFT) approach. The basis of this method was the large mass expansion, which allowed us to split complicated integrals with multiple mass scales into multiple simpler integrals with only a single scale. In this process, physical logarithms of ratios of these masses were also split up into unphysical μ dependent terms. This renormalization scale dependence then cancelled in the sum of all diagrams and reproduced the original result. As discussed in detail in chapter 4, since the μ dependence is governed by the renormalization group equations (RGEs), the logarithmic corrections to any physical process can be obtained in a straight forward way once the EFT renormalization group equations and matching conditions are known. In particular, to calculate the leading logarithmic corrections it was sufficient to know the RGEs only to the lowest order. In this way we only had to calculate simple one-loop integrals.

In chapter 5 we applied this method in the case of the top quark contributions $m_t \gg m_A$ and in chapter 6 to light quark and lepton contributions $m_b, m_\tau \ll m_A$ to a_μ . In both cases we calculated the one-loop renormalization group equations and solved them to obtain the values of the running Wilson coefficients. In particular, we were interested in the leading logarithmic contributions to a_μ , which are contained in the Wilson coefficient of the dipole operator $C_{H_\mu}(m_\mu)$. Using (4.77) we were able to directly read off these logarithms from the expansion. Our result for the leading logarithmic QED and QCD 3-loop corrections to a_μ in the aligned 2HDM is given in (6.28).

The Barr-Zee diagram with a top-quark loop and CP-odd Higgs ($m_t \gg m_A$) receives no QCD corrections at 3-loop order. If the two-loop result is evaluated in terms of on-shell parameters, the QED contribution results only in a $\sim 1\%$ correction. The other parametrization schemes lead to slightly larger 3-loop corrections and included incorrect higher order leading logarithms through the resummation in $e(m_t)$ and $m_\mu(m_t)$. However, the parametrizations differed only by small QED logarithms because, due to the Yukawa alignment, the QCD running in the $\Delta a_\mu^{2\text{HDM},t}$ cancelled between y_t^A and m_t . For the light quarks we found a much larger differences between the parametrizations since the QCD running did not cancel and instead produced very large logarithmic corrections. We found that choosing the parametrization at $\mu = m_A$ captured the correct sign of the actual 3-loop QCD logarithms and therefore lead to the smallest correction. The other parametrizations resulted in large negative 3-loop corrections. Overall, the light quark contributions to Δa_μ remain insignificant. Lastly, we discussed the correction to the τ contribution. In this case we found a negligible parametrization

dependence, which was explained by the small scale difference and absent QCD contributions in the running of e^2 and m_τ . For the on-shell parametrization the 3-loop leading logs resulted in a $\sim 1\%$ correction. With this we have successfully calculated the leading logarithmic 3-loop correction to a_μ in the 2HDM. We have seen that in most cases the corrections are captured by some specific parametrization of the two-loop result. In particular, for the dominant contributions, coming from the Barr-Zee diagram with CP-odd Higgs and top-quark or τ lepton loop, the on-shell parametrization resulted in the smallest higher order corrections. Lastly, it is worth emphasizing again that the EFT method used for the calculation of the leading logarithmic correction to a_μ can also be applied to other processes and thus provides an efficient and general way to improve the accuracy of theoretical predictions without immense computational efforts.

A Conventions

Units Throughout the thesis natural units $c = \hbar = \epsilon_0 = 1$ are used. All physical constants are taken from [67]

Sign Conventions The metric tensor is given by

$$(\eta^{\mu\nu}) = (\eta_{\mu\nu}) = \text{diag}(1, -1, -1, -1) \quad (\text{A.1})$$

The $SU(3)_c \times U(1)_{EM}$ covariant derivative of a generic field ψ is defined as [83]

$$D_\mu \psi = \left(\partial_\mu + ieQ_\psi A_\mu + ig_s G_\mu^a T^a \right) \psi \quad (\text{A.2})$$

where A_μ and G_μ^a denote the photon and gluon field, Q_ψ is the electric charge of ψ ($Q_e = -1$, $Q_u = \frac{2}{3}$, $Q_d = -\frac{1}{3}$) and T^a are the generators of $SU(3)$ in the fundamental representation for which

$$T_{ik}^a T_{kj}^a = C_F \delta_{ij}, \quad C_F = \frac{4}{3} \quad (\text{A.3})$$

Dirac and Pauli Matrices The Pauli matrices are

$$\sigma^0 = \begin{pmatrix} 1 & 0 \\ 0 & 1 \end{pmatrix}, \quad \sigma^1 = \begin{pmatrix} 0 & 1 \\ 1 & 0 \end{pmatrix}, \quad \sigma^2 = \begin{pmatrix} 0 & -i \\ i & 0 \end{pmatrix}, \quad \sigma^3 = \begin{pmatrix} 1 & 0 \\ 0 & -1 \end{pmatrix} \quad (\text{A.4})$$

They obey the following relations ($i, j \in \{1, 2, 3\}$)

$$[\sigma^i, \sigma^j] = 2i\epsilon^{ijk}\sigma^k, \quad \{\sigma^i, \sigma^j\} = 2\delta^{ij}\sigma^0 \quad (\text{A.5})$$

We use the notation $\sigma^\mu = (\sigma^0, \boldsymbol{\sigma})$ and $\bar{\sigma}^\mu = (\sigma^0, -\boldsymbol{\sigma})$. With this, the Dirac matrices in the Weyl basis take the following simple form

$$\gamma^\mu = \begin{pmatrix} 0 & \sigma^\mu \\ \bar{\sigma}^\mu & 0 \end{pmatrix}, \quad \gamma^5 = \begin{pmatrix} -\sigma^0 & 0 \\ 0 & \sigma^0 \end{pmatrix} \quad (\text{A.6})$$

They obey

$$\{\gamma^\mu, \gamma^\nu\} = 2\eta^{\mu\nu}, \quad \{\gamma^\mu, \gamma^5\} = 0 \quad (\text{A.7})$$

Lastly, we define $\sigma^{\mu\nu} = \frac{i}{2}[\gamma^\mu, \gamma^\nu]$ and $P_{R/L} = \frac{1}{2}(1 \pm \gamma^5)$.

Notation We use the following abbreviation for D -dimensional momentum integrals

$$\int_k \equiv \mu^{2\epsilon} \int \frac{d^D k}{(2\pi)^D} \quad (\text{A.8})$$

where $D := 4 - 2\epsilon$ and μ is called the renormalization scale. We further define $\bar{\mu}$ by

$$(4\pi\mu^2)^\epsilon \Gamma(\epsilon) =: \bar{\mu}^{2\epsilon} \frac{1}{\epsilon} \quad (\text{A.9})$$

In the limit $\epsilon \rightarrow 0$ we have $\bar{\mu}^2 \rightarrow 4\pi e^{-\gamma_E} \mu^2$ where γ_E is the Euler-Mascheroni constant.

The bare Lagrangian is written as

$$\mathcal{L}(x) = \sum_i C_i^0 \mathcal{O}_i^0(x) \quad (\text{A.10})$$

We write the mass dimension of the D -dimensional composite operators as $[\mathcal{O}_i^0] = n - (2 + \xi_i)\epsilon$ (the corresponding Wilson coefficients then have $[C_i^0] = 4 - n + \xi_i\epsilon$).

B Loop Integral Techniques

B.1 Feynman Parametrization

For any $\{A_n\} \subset \mathbb{C}$ whose convex hull does not contain 0 and $\{\lambda_n\} \subset \mathbb{C} : \text{Re}\{\lambda_n\} > 0$

$$\prod_n \frac{1}{A_n^{\lambda_n}} = \frac{\Gamma(\sum_n \lambda_n)}{\prod_n \Gamma(\lambda_n)} \int_0^1 dx_1 \dots \int_0^1 dx_n \delta(1 - \sum_n x_n) \frac{\prod_n x_n^{\lambda_n - 1}}{[\sum_n x_n A_n]^{\sum_n \lambda_n}} \quad (\text{B.1})$$

where $\Gamma(z)$ denotes the Gamma function and $\delta(z)$ the Dirac delta distribution.

B.2 Master Formula

The one-loop master formula holds for $\Delta \in \mathbb{R}^+$ and $n \in \mathbb{N}_{>D/2}$

$$\int \frac{d^D k}{(2\pi)^D} \frac{1}{[k^2 - \Delta + i\epsilon]^n} = (-1)^n i(4\pi)^{-\frac{D}{2}} \Delta^{\frac{D}{2} - n} \frac{\Gamma(n - \frac{D}{2})}{\Gamma(n)} \quad (\text{B.2})$$

and can be extended to $n \in \mathbb{R}_{>D/2}$ after factoring $(-1)^n$ from both sides. Tensor integrals can be reduced to the master formula using

$$\int d^D k \frac{\prod_{j=1}^n k^{\mu_j}}{f(k^2)} = \begin{cases} 0 & \text{if } n \text{ odd} \\ \int d^D k \frac{k^n}{f(k^2)} \sum_{\substack{\pi \in S_n \\ \pi \text{ unique}}} \frac{\eta^{\mu_{\pi(1)} \mu_{\pi(2)}} \dots \eta^{\mu_{\pi(n-1)} \mu_{\pi(n)}}}{D(D+2) \dots (D+n-2)} & \text{if } n \text{ even} \end{cases} \quad (\text{B.3})$$

where "unique permutation" means unique with respect to exchange $\eta^{\mu\nu} \rightarrow \eta^{\nu\mu}$ and $\eta^{\mu\nu} \eta^{\alpha\beta} \rightarrow \eta^{\alpha\beta} \eta^{\mu\nu}$. From the $n!$ total permutations there are only $\frac{n!}{(n/2)!2^{n/2}}$ unique permutations in this sense.

Example

$$\int_k \frac{k^\mu k^\nu}{[k^2 - \Delta]^n} = \int_k \frac{\frac{1}{D} k^2 \eta^{\mu\nu}}{[k^2 - \Delta]^n} = i \eta^{\mu\nu} \frac{(-1)^{n-1}}{(4\pi)^{\frac{D}{2}}} \Delta^{\frac{D}{2} + 1 - n} \frac{\Gamma(n - 1 - \frac{D}{2})}{2\Gamma(n)} \quad (\text{B.4})$$

C Operators and Feynman Rules

In the following we list all the (non-)renormalizable composite operators and corresponding Feynman rules relevant to this work. A complete List of Feynman rules of the SM can be found in [83] and for the 2HDM in [72].

C.1 Dim-4 Operators

\mathcal{O}_i	Vertex	Feynman Rule	ξ_i
$-Q_f(\bar{f}\gamma^\mu f)A_\mu$		$-ieQ_f\gamma^\mu$	1
$-g_s(\bar{q}\gamma^\mu T^a q)G_\mu^a$		$-ig_s T_{ji}^a \gamma^\mu$	1
$-H\bar{f}y_f^{H,h}f$		$-i(y_f^{H,h})_{ji}$	1
$iA\bar{f}y_f^A\gamma^5 f$		$-(y_f^A)_{ji}\gamma^5$	1
$-\sqrt{2}H^+\bar{u}(Vy_d^A P_R + y_u^A V P_L)d$		$-i\sqrt{2}(Vy_d^A P_R + y_u^A V P_L)_{ji}$	1
$-\sqrt{2}H^+\bar{\nu}y_l^A P_R e$		$-i\sqrt{2}(y_l^A)_{ji} P_R$	1
$-\sqrt{2}H^-\bar{d}(y_d^A V P_L + Vy_u^A P_R)u$		$-i\sqrt{2}(y_d^A V P_L + Vy_u^A P_R)_{ji}$	1
$-\sqrt{2}H^-\bar{e}y_l^A P_L \nu$		$-i\sqrt{2}(y_l^A)_{ji} P_L$	1

C.2 Dim-5 Operators

\mathcal{O}_i	Vertex	Feynman Rule	ξ_i
$H_\mu = -eQ_\mu(\bar{\mu}\sigma^{\alpha\beta}\mu)F_{\alpha\beta}$		$2C_{H_\mu} eQ_\mu \sigma^{\alpha\beta} q_\alpha$	0
$\mathcal{O}_{A\gamma\gamma} = -\frac{e^2}{8}\epsilon^{\mu\nu\alpha\beta}F_{\nu\beta}F_{\mu\alpha}A$		$-iC_{\mathcal{O}_{A\gamma\gamma}} e^2 \epsilon^{\mu\nu\alpha\beta} q_\alpha q'_\beta$	-1
$\mathcal{O}_{H\gamma\gamma} = \frac{e^2}{4}F_{\mu\nu}F^{\mu\nu}H$		$iC_{\mathcal{O}_{H\gamma\gamma}} e^2 (qq'\eta^{\mu\nu} - q'^\mu q^\nu)$	

C.3 Dim-6 Operators

\mathcal{O}_i	Vertex	Feynman Rule	ξ_i
$\mathcal{O}_f^H = (\bar{\mu}\mu)(\bar{f}f)$		$iC_{\mathcal{O}_f^H} \delta_{ab} \delta_{ij}$	2
$\mathcal{O}_f^A = (\bar{\mu}\gamma^5\mu)(\bar{f}\gamma^5 f)$		$iC_{\mathcal{O}_f^A} \gamma_{ab}^5 \gamma_{ij}^5$	
$\mathcal{O}_f^T = (\bar{\mu}\sigma^{\mu\nu}\mu)(\bar{f}\sigma_{\mu\nu} f)$		$iC_{\mathcal{O}_f^T} \sigma_{ab}^{\mu\nu} (\sigma_{\mu\nu})_{ij}$	

Bibliography

- [1] G. W. Bennett *et al.*, “Final Report of the Muon E821 Anomalous Magnetic Moment Measurement at BNL,” *Phys. Rev. D*, vol. 73, p. 072003, 2006. DOI: 10.1103/PhysRevD.73.072003. arXiv: hep-ex/0602035.
- [2] B. e. a. Abi, “Measurement of the Positive Muon Anomalous Magnetic Moment to 0.46 ppm,” *Phys. Rev. Lett.*, vol. 126, p. 141801, 14 Apr. 2021. DOI: 10.1103/PhysRevLett.126.141801.
- [3] T. Aoyama *et al.*, “The anomalous magnetic moment of the muon in the Standard Model,” *Phys. Rept.*, vol. 887, pp. 1–166, 2020. DOI: 10.1016/j.physrep.2020.07.006. arXiv: 2006.04822 [hep-ph].
- [4] P. Athron, C. Balázs, D. H. J. Jacob, W. Kotlarski, D. Stöckinger, and H. Stöckinger-Kim, “New physics explanations of a_μ in light of the FNAL muon $g - 2$ measurement,” *JHEP*, vol. 09, p. 080, 2021. DOI: 10.1007/JHEP09(2021)080. arXiv: 2104.03691 [hep-ph].
- [5] A. Cherchiglia, D. Stöckinger, and H. Stöckinger-Kim, “Muon $g-2$ in the 2HDM: maximum results and detailed phenomenology,” *Phys. Rev. D*, vol. 98, p. 035001, 2018. DOI: 10.1103/PhysRevD.98.035001. arXiv: 1711.11567 [hep-ph].
- [6] D. Chang, W.-F. Chang, C.-H. Chou, and W.-Y. Keung, “Large two loop contributions to $g-2$ from a generic pseudoscalar boson,” *Phys. Rev. D*, vol. 63, p. 091301, 2001. DOI: 10.1103/PhysRevD.63.091301. arXiv: hep-ph/0009292.
- [7] K.-m. Cheung, C.-H. Chou, and O. C. W. Kong, “Muon anomalous magnetic moment, two Higgs doublet model, and supersymmetry,” *Phys. Rev. D*, vol. 64, p. 111301, 2001. DOI: 10.1103/PhysRevD.64.111301. arXiv: hep-ph/0103183.
- [8] K. Cheung and O. C. W. Kong, “Can the two Higgs doublet model survive the constraint from the muon anomalous magnetic moment as suggested?” *Phys. Rev. D*, vol. 68, p. 053003, 2003. DOI: 10.1103/PhysRevD.68.053003. arXiv: hep-ph/0302111.
- [9] F. Larios, G. Tavares-Velasco, and C. P. Yuan, “A Very light CP odd scalar in the two Higgs doublet model,” *Phys. Rev. D*, vol. 64, p. 055004, 2001. DOI: 10.1103/PhysRevD.64.055004. arXiv: hep-ph/0103292.
- [10] A. Broggio, E. J. Chun, M. Passera, K. M. Patel, and S. K. Vempati, “Limiting two-Higgs-doublet models,” *JHEP*, vol. 11, p. 058, 2014. DOI: 10.1007/JHEP11(2014)058. arXiv: 1409.3199 [hep-ph].
- [11] A. Cherchiglia, P. Kneschke, D. Stöckinger, and H. Stöckinger-Kim, “The muon magnetic moment in the 2HDM: complete two-loop result,” *JHEP*, vol. 01, p. 007, 2017, [Erratum: *JHEP* 10, 242 (2021)]. DOI: 10.1007/JHEP10(2021)242. arXiv: 1607.06292 [hep-ph].
- [12] M. Ciuchini, E. Franco, G. Martinelli, L. Reina, and L. Silvestrini, “Scheme independence of the effective Hamiltonian for $b \rightarrow s$ gamma and $b \rightarrow sg$ decays,” *Phys. Lett. B*, vol. 316, pp. 127–136, 1993. DOI: 10.1016/0370-2693(93)90668-8. arXiv: hep-ph/9307364.
- [13] T. Mannel, W. Kilian, and P. Manakos, “Leading and subleading logarithmic QCD corrections to bilinear heavy quark currents,” *AIP Conference Proceedings*, vol. 272, pp. 610–613, 1992. DOI: <https://doi.org/10.1063/1.43386>.

- [14] G. Cella, G. Curci, G. Ricciardi, and A. Viceré, “QCD corrections to the weak radiative B-meson decay,” *Physics Letters B*, vol. 248, no. 1, pp. 181–187, 1990, ISSN: 0370-2693. DOI: [https://doi.org/10.1016/0370-2693\(90\)90036-6](https://doi.org/10.1016/0370-2693(90)90036-6).
- [15] B. Grinstein, R. P. Springer, and M. B. Wise, “Strong Interaction Effects in Weak Radiative \bar{B} Meson Decay,” *Nucl. Phys. B*, vol. 339, pp. 269–309, 1990. DOI: 10.1016/0550-3213(90)90350-M.
- [16] G. Degrossi and G. F. Giudice, “QED logarithms in the electroweak corrections to the muon anomalous magnetic moment,” *Phys. Rev. D*, vol. 58, p. 053007, 1998. DOI: 10.1103/PhysRevD.58.053007. arXiv: [hep-ph/9803384](https://arxiv.org/abs/hep-ph/9803384).
- [17] A. Czarnecki, W. J. Marciano, and A. Vainshtein, “Refinements in electroweak contributions to the muon anomalous magnetic moment,” *Phys. Rev. D*, vol. 67, p. 073006, 2003. DOI: 10.1103/PhysRevD.67.073006. arXiv: [hep-ph/0212229](https://arxiv.org/abs/hep-ph/0212229).
- [18] R. L. Garwin, L. M. Lederman, and M. Weinrich, “Observations of the Failure of Conservation of Parity and Charge Conjugation in Meson Decays: the Magnetic Moment of the Free Muon,” *Phys. Rev.*, vol. 105, pp. 1415–1417, 4 Feb. 1957. DOI: 10.1103/PhysRev.105.1415.
- [19] C. S. Wu, E. Ambler, R. W. Hayward, D. D. Hoppes, and R. P. Hudson, “Experimental Test of Parity Conservation in Beta Decay,” *Phys. Rev.*, vol. 105, pp. 1413–1415, 4 Feb. 1957. DOI: 10.1103/PhysRev.105.1413.
- [20] T. D. Lee and C. N. Yang, “Question of Parity Conservation in Weak Interactions,” *Phys. Rev.*, vol. 104, pp. 254–258, 1 Oct. 1956. DOI: 10.1103/PhysRev.104.254.
- [21] J. D. Jackson, *Classical Electrodynamics*. Wiley, 1998, ISBN: 978-0-471-30932-1.
- [22] V. Bargmann, L. Michel, and V. L. Telegdi, “Precession of the Polarization of Particles Moving in a Homogeneous Electromagnetic Field,” *Phys. Rev. Lett.*, vol. 2, pp. 435–436, 10 May 1959. DOI: 10.1103/PhysRevLett.2.435.
- [23] S. I. Rubinow and J. B. Keller, “Asymptotic Solution of the Dirac Equation,” *Phys. Rev.*, vol. 131, pp. 2789–2796, 6 Sep. 1963. DOI: 10.1103/PhysRev.131.2789.
- [24] K. Rafanelli and R. Schiller, “Classical Motions of Spin- $\frac{1}{2}$ Particles,” *Phys. Rev.*, vol. 135, B279–B281, 1B Jul. 1964. DOI: 10.1103/PhysRev.135.B279.
- [25] J. Bailey *et al.*, “The Anomalous Magnetic Moment of Positive and Negative Muons,” *Phys. Lett. B*, vol. 67, p. 225, 1977. DOI: 10.1016/0370-2693(77)90199-X.
- [26] B. L. Roberts, “The History of the Muon ($g - 2$) Experiments,” *SciPost Phys. Proc.*, vol. 1, p. 032, 2019. DOI: 10.21468/SciPostPhysProc.1.032. arXiv: [1811.06974](https://arxiv.org/abs/1811.06974) [hep-ex].
- [27] H. E. Habert, *Thomas Precession and the BMT equation*, 2022. [Online]. Available: <http://scipp.ucsc.edu/~haber/ph214/Thomas22.pdf>.
- [28] F. Jegerlehner, *The Anomalous Magnetic Moment of the Muon*. Cham: Springer, 2017, vol. 274. DOI: 10.1007/978-3-319-63577-4.
- [29] T. e. a. Albahri, “Beam dynamics corrections to the Run-1 measurement of the muon anomalous magnetic moment at Fermilab,” *Phys. Rev. Accel. Beams*, vol. 24, p. 044002, 4 Apr. 2021. DOI: 10.1103/PhysRevAccelBeams.24.044002.
- [30] T. e. a. Albahri, “Measurement of the anomalous precession frequency of the muon in the Fermilab Muon $g - 2$ Experiment,” *Phys. Rev. D*, vol. 103, p. 072002, 7 Apr. 2021. DOI: 10.1103/PhysRevD.103.072002.
- [31] T. e. a. Albahri, “Magnetic-field measurement and analysis for the Muon $g - 2$ Experiment at Fermilab,” *Phys. Rev. A*, vol. 103, p. 042208, 4 Apr. 2021. DOI: 10.1103/PhysRevA.103.042208.

- [32] J. Grange *et al.*, “Muon ($g-2$) Technical Design Report,” Jan. 2015. arXiv: 1501.06858 [physics.ins-det].
- [33] P. Girotti, “Status of the Fermilab Muon $g - 2$ Experiment,” *EPJ Web Conf.*, vol. 262, p. 01003, 2022. DOI: 10.1051/epjconf/202226201003. arXiv: 2202.11391 [hep-ex].
- [34] H. Iinuma, “New approach to the muon $g-2$ and EDM experiment at J-PARC,” *J. Phys. Conf. Ser.*, vol. 295, H. Stroher and F. Rathmann, Eds., p. 012032, 2011. DOI: 10.1088/1742-6596/295/1/012032.
- [35] M. Abe *et al.*, “A New Approach for Measuring the Muon Anomalous Magnetic Moment and Electric Dipole Moment,” *PTEP*, vol. 2019, no. 5, p. 053C02, 2019. DOI: 10.1093/ptep/ptz030. arXiv: 1901.03047 [physics.ins-det].
- [36] S. Weinberg, *The Quantum theory of fields. Vol. 1: Foundations*. Cambridge University Press, Jun. 2005, ISBN: 978-0-521-67053-1, 978-0-511-25204-4.
- [37] M. D. Schwartz, *Quantum Field Theory and the Standard Model*. Cambridge University Press, Mar. 2014, ISBN: 978-1-107-03473-0, 978-1-107-03473-0.
- [38] I. B. Zel’dovich, “Electromagnetic Interaction With Parity Violation,” *Soviet Phys. JETP*, vol. Vol: 6, Jun. 1958. [Online]. Available: <https://www.osti.gov/biblio/4309791>.
- [39] A. Gongora and R. G. Stuart, “The Charge Radius and Anapole Moment of a Free Fermion,” *Z. Phys. C*, vol. 55, pp. 101–106, 1992. DOI: 10.1007/BF01558294.
- [40] J. L. Feng, K. T. Matchev, and Y. Shadmi, “Theoretical Expectations for the Muon’s Electric Dipole Moment,” *Nucl. Phys. B*, vol. 613, pp. 366–381, 2001. DOI: 10.1016/S0550-3213(01)00383-2. arXiv: hep-ph/0107182.
- [41] M. E. Peskin and D. V. Schroeder, *An Introduction to quantum field theory*. Reading, USA: Addison-Wesley, 1995, ISBN: 978-0-201-50397-5.
- [42] M. Neubert, “Renormalization Theory and Effective Field Theories,” S. Davidson, P. Gambino, M. Laine, M. Neubert, and C. Salomon, Eds., Jan. 2019. DOI: 10.1093/oso/9780198855743.003.0001. arXiv: 1901.06573 [hep-ph].
- [43] M. Srednicki, *Quantum field theory*. Cambridge University Press, Jan. 2007, ISBN: 978-0-521-86449-7, 978-0-511-26720-8.
- [44] A. Fedotov *et al.*, “Advances in QED with intense background fields,” Feb. 2022. arXiv: 2203.00019 [hep-ph].
- [45] T. Aoyama, M. Hayakawa, T. Kinoshita, and M. Nio, “Complete Tenth-Order QED Contribution to the Muon $g-2$,” *Phys. Rev. Lett.*, vol. 109, p. 111808, 2012. DOI: 10.1103/PhysRevLett.109.111808. arXiv: 1205.5370 [hep-ph].
- [46] T. Aoyama, T. Kinoshita, and M. Nio, “Theory of the anomalous magnetic moment of the electron,” *Atoms*, vol. 7, no. 1, 2019, ISSN: 2218-2004. DOI: 10.3390/atoms7010028. [Online]. Available: <https://www.mdpi.com/2218-2004/7/1/28>.
- [47] C. Gnendiger, D. Stöckinger, and H. Stöckinger-Kim, “The electroweak contributions to $(g - 2)_\mu$ after the Higgs boson mass measurement,” *Phys. Rev. D*, vol. 88, p. 053005, 2013. DOI: 10.1103/PhysRevD.88.053005. arXiv: 1306.5546 [hep-ph].
- [48] J. Ellis, “TikZ-Feynman: Feynman diagrams with TikZ,” *Comput. Phys. Commun.*, vol. 210, pp. 103–123, 2017. DOI: 10.1016/j.cpc.2016.08.019. arXiv: 1601.05437 [hep-ph].
- [49] S. Borsanyi *et al.*, “Leading hadronic contribution to the muon magnetic moment from lattice QCD,” *Nature*, vol. 593, no. 7857, pp. 51–55, 2021. DOI: 10.1038/s41586-021-03418-1. arXiv: 2002.12347 [hep-lat].

- [50] M. Davier, A. Hoecker, B. Malaescu, and Z. Zhang, “Reevaluation of the Hadronic Vacuum Polarisation Contributions to the Standard Model Predictions of the Muon $g - 2$ and $\alpha(m_Z^2)$ using Newest Hadronic Cross-section Data,” *Eur. Phys. J. C*, vol. 77, no. 12, p. 827, 2017. DOI: 10.1140/epjc/s10052-017-5161-6. arXiv: 1706.09436 [hep-ph].
- [51] A. Keshavarzi, D. Nomura, and T. Teubner, “Muon $g - 2$ and $\alpha(M_Z^2)$: a New Data-based Analysis,” *Phys. Rev. D*, vol. 97, no. 11, p. 114 025, 2018. DOI: 10.1103/PhysRevD.97.114025. arXiv: 1802.02995 [hep-ph].
- [52] G. Colangelo, M. Hoferichter, and P. Stoffer, “Two-pion Contribution to Hadronic Vacuum Polarization,” *JHEP*, vol. 02, p. 006, 2019. DOI: 10.1007/JHEP02(2019)006. arXiv: 1810.00007 [hep-ph].
- [53] M. Hoferichter, B.-L. Hoid, and B. Kubis, “Three-pion Contribution to Hadronic Vacuum Polarization,” *JHEP*, vol. 08, p. 137, 2019. DOI: 10.1007/JHEP08(2019)137. arXiv: 1907.01556 [hep-ph].
- [54] M. Davier, A. Hoecker, B. Malaescu, and Z. Zhang, “A new evaluation of the hadronic vacuum polarisation contributions to the muon anomalous magnetic moment and to $\alpha(m_Z^2)$,” *Eur. Phys. J. C*, vol. 80, no. 3, p. 241, 2020, [Erratum: *Eur.Phys.J.C* 80, 410 (2020)]. DOI: 10.1140/epjc/s10052-020-7792-2. arXiv: 1908.00921 [hep-ph].
- [55] A. Keshavarzi, D. Nomura, and T. Teubner, “ $g - 2$ of charged leptons, $\alpha(M_Z^2)$, and the hyperfine splitting of muonium,” *Phys. Rev. D*, vol. 101, no. 1, p. 014 029, 2020. DOI: 10.1103/PhysRevD.101.014029. arXiv: 1911.00367 [hep-ph].
- [56] A. Kurz, T. Liu, P. Marquard, and M. Steinhauser, “Hadronic contribution to the muon anomalous magnetic moment to next-to-next-to-leading order,” *Phys. Lett. B*, vol. 734, pp. 144–147, 2014. DOI: 10.1016/j.physletb.2014.05.043. arXiv: 1403.6400 [hep-ph].
- [57] K. Melnikov and A. Vainshtein, “Hadronic light-by-light scattering contribution to the muon anomalous magnetic moment revisited,” *Phys. Rev. D*, vol. 70, p. 113 006, 2004. DOI: 10.1103/PhysRevD.70.113006. arXiv: hep-ph/0312226.
- [58] P. Masjuan and P. Sanchez-Puertas, “Pseudoscalar-pole contribution to the $(g_\mu - 2)$: a rational approach,” *Phys. Rev. D*, vol. 95, no. 5, p. 054 026, 2017. DOI: 10.1103/PhysRevD.95.054026. arXiv: 1701.05829 [hep-ph].
- [59] G. Colangelo, M. Hoferichter, M. Procura, and P. Stoffer, “Dispersion relation for hadronic light-by-light scattering: two-pion contributions,” *JHEP*, vol. 04, p. 161, 2017. DOI: 10.1007/JHEP04(2017)161. arXiv: 1702.07347 [hep-ph].
- [60] M. Hoferichter, B.-L. Hoid, B. Kubis, S. Leupold, and S. P. Schneider, “Dispersion relation for hadronic light-by-light scattering: pion pole,” *JHEP*, vol. 10, p. 141, 2018. DOI: 10.1007/JHEP10(2018)141. arXiv: 1808.04823 [hep-ph].
- [61] A. Gérardin, H. B. Meyer, and A. Nyffeler, “Lattice calculation of the pion transition form factor with $N_f = 2 + 1$ Wilson quarks,” *Phys. Rev. D*, vol. 100, no. 3, p. 034 520, 2019. DOI: 10.1103/PhysRevD.100.034520. arXiv: 1903.09471 [hep-lat].
- [62] J. Bijnens, N. Hermansson-Truedsson, and A. Rodríguez-Sánchez, “Short-distance constraints for the HLbL contribution to the muon anomalous magnetic moment,” *Phys. Lett. B*, vol. 798, p. 134 994, 2019. DOI: 10.1016/j.physletb.2019.134994. arXiv: 1908.03331 [hep-ph].
- [63] G. Colangelo, F. Hagelstein, M. Hoferichter, L. Laub, and P. Stoffer, “Longitudinal short-distance constraints for the hadronic light-by-light contribution to $(g - 2)_\mu$ with large- N_c Regge models,” *JHEP*, vol. 03, p. 101, 2020. DOI: 10.1007/JHEP03(2020)101. arXiv: 1910.13432 [hep-ph].

- [64] G. Colangelo, M. Hoferichter, A. Nyffeler, M. Passera, and P. Stoffer, “Remarks on higher-order hadronic corrections to the muon $g-2$,” *Phys. Lett. B*, vol. 735, pp. 90–91, 2014. DOI: 10.1016/j.physletb.2014.06.012. arXiv: 1403.7512 [hep-ph].
- [65] T. Blum *et al.*, “Hadronic Light-by-Light Scattering Contribution to the Muon Anomalous Magnetic Moment from Lattice QCD,” *Phys. Rev. Lett.*, vol. 124, no. 13, p. 132 002, 2020. DOI: 10.1103/PhysRevLett.124.132002. arXiv: 1911.08123 [hep-lat].
- [66] J. F. Gunion, H. E. Haber, G. L. Kane, and S. Dawson, *The Higgs Hunter’s Guide*. 2000, vol. 80.
- [67] R. L. Workman *et al.*, “Review of Particle Physics,” *PTEP*, vol. 2022, p. 083C01, 2022. DOI: 10.1093/ptep/ptac097.
- [68] M. Aaboud *et al.*, “Search for flavor-changing neutral currents in top quark decays $t \rightarrow Hc$ and $t \rightarrow Hu$ in multilepton final states in proton-proton collisions at $\sqrt{s} = 13$ TeV with the ATLAS detector,” *Phys. Rev. D*, vol. 98, no. 3, p. 032 002, 2018. DOI: 10.1103/PhysRevD.98.032002. arXiv: 1805.03483 [hep-ex].
- [69] G. Aad *et al.*, “Search for flavour-changing neutral-current interactions of a top quark and a gluon in pp collisions at $\sqrt{s} = 13$ TeV with the ATLAS detector,” *Eur. Phys. J. C*, vol. 82, no. 4, p. 334, 2022. DOI: 10.1140/epjc/s10052-022-10182-7. arXiv: 2112.01302 [hep-ex].
- [70] A. Pich and P. Tuzon, “Yukawa Alignment in the Two-Higgs-Doublet Model,” *Phys. Rev. D*, vol. 80, p. 091 702, 2009. DOI: 10.1103/PhysRevD.80.091702. arXiv: 0908.1554 [hep-ph].
- [71] G. C. Branco, P. M. Ferreira, L. Lavoura, M. N. Rebelo, M. Sher, and J. P. Silva, “Theory and phenomenology of two-Higgs-doublet models,” *Phys. Rept.*, vol. 516, pp. 1–102, 2012. DOI: 10.1016/j.physrep.2012.02.002. arXiv: 1106.0034 [hep-ph].
- [72] L. Altenkamp, “Precise predictions within the Two-Higgs-Doublet Model,” PhD dissertation, Freiburg U., 2017. DOI: 10.6094/UNIFR/11737.
- [73] V. Ilisie, “New Barr-Zee contributions to $(g - 2)_\mu$ in two-Higgs-doublet models,” *JHEP*, vol. 04, p. 077, 2015. DOI: 10.1007/JHEP04(2015)077. arXiv: 1502.04199 [hep-ph].
- [74] S. M. Barr and A. Zee, “Electric dipole moment of the electron and of the neutron,” *Phys. Rev. Lett.*, vol. 65, pp. 21–24, 1 Jul. 1990. DOI: 10.1103/PhysRevLett.65.21. [Online]. Available: <https://link.aps.org/doi/10.1103/PhysRevLett.65.21>.
- [75] K. Cheung, O. C. W. Kong, and J. S. Lee, “Electric and anomalous magnetic dipole moments of the muon in the MSSM,” *JHEP*, vol. 06, p. 020, 2009. DOI: 10.1088/1126-6708/2009/06/020. arXiv: 0904.4352 [hep-ph].
- [76] T. Abe, J. Hisano, T. Kitahara, and K. Tobioka, “Gauge invariant Barr-Zee type contributions to fermionic EDMs in the two-Higgs doublet models,” *JHEP*, vol. 01, p. 106, 2014, [Erratum: JHEP 04, 161 (2016)]. DOI: 10.1007/JHEP01(2014)106. arXiv: 1311.4704 [hep-ph].
- [77] M. S. Chanowitz, M. Furman, and I. Hinchliffe, “The Axial Current in Dimensional Regularization,” *Nucl. Phys. B*, vol. 159, pp. 225–243, 1979. DOI: 10.1016/0550-3213(79)90333-X.
- [78] R. Morris, “The dilogarithm function of a real argument,” *Mathematics of Computation*, vol. 33, no. 146, pp. 778–787, 1979, ISSN: 00255718, 10886842. [Online]. Available: <http://www.jstor.org/stable/2006312> (visited on 09/08/2022).
- [79] A. V. Manohar, “Introduction to Effective Field Theories,” S. Davidson, P. Gambino, M. Laine, M. Neubert, and C. Salomon, Eds., Apr. 2018. DOI: 10.1093/oso/9780198855743.003.0002. arXiv: 1804.05863 [hep-ph].

- [80] V. A. Smirnov, “Large Mass Expansion, Operator Product Expansion, and R^* Operation,” *Mod. Phys. Lett. A*, vol. 3, pp. 381–391, 1988. DOI: 10.1142/S0217732388000477.
- [81] V. A. Smirnov, “Asymptotic expansions in momenta and masses and calculation of Feynman diagrams,” *Mod. Phys. Lett. A*, vol. 10, pp. 1485–1500, 1995. DOI: 10.1142/S0217732395001617. arXiv: hep-th/9412063.
- [82] V. A. Smirnov, “Applied asymptotic expansions in momenta and masses,” *Springer Tracts Mod. Phys.*, vol. 177, pp. 1–262, 2002.
- [83] J. C. Romao and J. P. Silva, “A resource for signs and Feynman diagrams of the Standard Model,” *Int. J. Mod. Phys. A*, vol. 27, p. 1230025, 2012. DOI: 10.1142/S0217751X12300256. arXiv: 1209.6213 [hep-ph].
- [84] C. C. Nishi, “Simple derivation of general Fierz-like identities,” *Am. J. Phys.*, vol. 73, pp. 1160–1163, 2005. DOI: 10.1119/1.2074087. arXiv: hep-ph/0412245.
- [85] E. E. Jenkins, A. V. Manohar, and P. Stoffer, “Low-Energy Effective Field Theory below the Electroweak Scale: Anomalous Dimensions,” *JHEP*, vol. 01, p. 084, 2018. DOI: 10.1007/JHEP01(2018)084. arXiv: 1711.05270 [hep-ph].
- [86] A. Djouadi, M. Spira, and P. M. Zerwas, “Two photon decay widths of Higgs particles,” *Phys. Lett. B*, vol. 311, pp. 255–260, 1993. DOI: 10.1016/0370-2693(93)90564-X. arXiv: hep-ph/9305335.
- [87] H.-q. Zheng and D.-d. Wu, “First-order qcd corrections to the decay of the higgs boson into two photons,” *Phys. Rev. D*, vol. 42, pp. 3760–3763, 11 Dec. 1990. DOI: 10.1103/PhysRevD.42.3760. [Online]. Available: <https://link.aps.org/doi/10.1103/PhysRevD.42.3760>.
- [88] S. Dawson and R. P. Kauffman, “QCD corrections to $H \rightarrow \gamma \gamma$,” *Phys. Rev. D*, vol. 47, pp. 1264–1267, 1993. DOI: 10.1103/PhysRevD.47.1264.
- [89] S. L. Adler and W. A. Bardeen, “Absence of higher-order corrections in the anomalous axial-vector divergence equation,” *Phys. Rev.*, vol. 182, pp. 1517–1536, 5 Jun. 1969. DOI: 10.1103/PhysRev.182.1517. [Online]. Available: <https://link.aps.org/doi/10.1103/PhysRev.182.1517>.
- [90] S. L. Adler, J. C. Collins, and A. Duncan, “Energy-Momentum-Tensor Trace Anomaly in Spin 1/2 Quantum Electrodynamics,” *Phys. Rev. D*, vol. 15, p. 1712, 1977. DOI: 10.1103/PhysRevD.15.1712.
- [91] Y. Iwasaki, “Coupling of the trace of the energy-momentum tensor to two photons,” *Phys. Rev. D*, vol. 15, pp. 1172–1172, 4 Feb. 1977. DOI: 10.1103/PhysRevD.15.1172. [Online]. Available: <https://link.aps.org/doi/10.1103/PhysRevD.15.1172>.
- [92] D. R. T. Jones and J. P. Leveille, “Dimensional Regularization and the Two Loop Axial Anomaly in Abelian, Nonabelian and Supersymmetric Gauge Theories,” *Nucl. Phys. B*, vol. 206, p. 473, 1982, [Erratum: Nucl.Phys.B 222, 517 (1983)]. DOI: 10.1016/0550-3213(83)90549-7.
- [93] A. Grozin, “Lectures on QED and QCD,” in *3rd Dubna International Advanced School of Theoretical Physics*, Aug. 2005. arXiv: hep-ph/0508242.

Acknowledgments

I want to thank Prof. Dominik Stöckinger for his excellent supervision, insightful suggestions and in particular for taking the time to have regular discussions, despite his busy schedule. Many thanks also to Dr. Hyejung Stöckinger-Kim for her helpful comments and regular participation in the discussions. I also want to thank the rest of our working group for the interesting presentations and discussions during our group meetings and the generally welcoming and constructive atmosphere. In particular, I would like to express my gratitude to my parents for enabling me to fully focus on my studies, for their financial support and for proofreading this thesis.

Statement of authorship

I hereby certify that I have authored this document entitled *Leading Logarithmic 3-loop Corrections to $(\mathbf{g} - \mathbf{2})_\mu$ in the Two-Higgs-Doublet Model* independently and without undue assistance from third parties. No other than the resources and references indicated in this document have been used. I have marked both literal and accordingly adopted quotations as such. There were no additional persons involved in the intellectual preparation of the present document. I am aware that violations of this declaration may lead to subsequent withdrawal of the academic degree.

Dresden, 4th October 2022

Kilian Möhling